 © 2015 Russian Academy of Sciences and Turpion Ltd

DOI 10.1070/RCR4493

Ligand-protected gold clusters: the structure, synthesis and applications

D A Pichugina,[a] N E Kuz'menko,[a] A F Shestakov [b]

[a] Department of Chemistry, Lomonosov Moscow State University
Leninskie Gory 1, str. 3, 119991 Moscow, Russian Federation
[b] Institute of Problems of Chemical Physics, Russian Academy of Sciences
Prosp. Akademika Semenova 1, 142400 Chernogolovka, Moscow Region, Russian Federation

Modern concepts of the structure and properties of atomic gold clusters protected by thiolate, selenolate, phosphine and phenylacetylene ligands are analyzed. Within the framework of the superatom theory, the 'divide and protect' approach and the structure rule, the stability and composition of a cluster are determined by the structure of the cluster core, the type of ligands and the total number of valence electrons. Methods of selective synthesis of gold clusters in solution and on the surface of inorganic composites based, in particular, on the reaction of Au_n with RS, RSe, PhC≡C, Hal ligands or functional groups of proteins, on stabilization of clusters in cavities of the α-, β- and γ-cyclodextrin molecules (Au_{15} and Au_{25}) and on anchorage to a support surface (Au_{25}/SiO_2, Au_{20}/C, Au_{10}/FeO_x) are reviewed. Problems in this field are also discussed. Among the methods for cluster structure prediction, particular attention is given to the theoretical approaches based on the density functional theory (DFT). The structures of a number of synthesized clusters are described using the results obtained by X-ray diffraction analysis and DFT calculations. A possible mechanism of formation of the $SR(AuSR)_n$ 'staple' units in the cluster shell is proposed. The structure and properties of bimetallic clusters $M_xAu_nL_m$ (M = Pd, Pt, Ag, Cu) are discussed. The Pd or Pt atom is located at the centre of the cluster, whereas Ag and Cu atoms form bimetallic compounds in which the heteroatom is located on the surface of the cluster core or in the 'staple' units. The optical properties, fluorescence and luminescence of ligand-protected gold clusters originate from the quantum effects of the Au atoms in the cluster core and in the oligomeric $SR(AuSR)_x$ units in the cluster shell. Homogeneous and heterogeneous reactions catalyzed by atomic gold clusters are discussed in the context of the reaction mechanism and the nature of the active sites.
The bibliography includes 345 references.

Contents

I.	Introduction	1114
II.	The structure of $[L_sAu_nX_m]^q$ clusters	1116
III.	Methods of synthesis of atomic gold clusters	1117
IV.	Methods for determination of the structure and properties of clusters	1120
V.	Clusters with strong metal – ligand interaction	1122
VI.	Gold clusters stabilized by phosphine ligands	1129
VII.	Bimetallic clusters $M_xAu_nL_m$ (M = Pd, Pt, Cu, Ag)	1133
VIII.	Properties and applications of $[L_sAu_nX_m]^q$ clusters in nanoelectronics, nanooptics and catalysis	1135
IX.	Conclusion	1139

I. Introduction

A key problem in nanotechnology is to design materials with specified properties.[1 – 3] The quality of such materials is governed by the degree of dispersion of their components (nanoparticles). Nanoparticles prepared by modern chemical methods are characterized by the size distribution function, while their structure, morphology and exact atomic composition remain unknown.[4, 5] As a result, it is impossible to relate the observed physicochemical proper-

D A Pichugina Candidate of Chemical Sciences, Assistant Professor at the Department of Chemistry, MSU.
Telephone: +7(495)939 – 4765, e-mail: daria@phys.chem.msu.ru
N E Kuz'menko Doctor of Physical and Mathematical Sciences, Professor at the same Department.
Telephone: +7(495)939 – 4765, e-mail: nek@educ.chem.msu.ru
Current research interests of authors: gold clusters, quantum chemistry, theoretical simulation of catalytic reactions, molecular spectroscopy.

A F Shestakov Doctor of Chemical Sciences, Leading Researcher at the IPCP RAS. Telephone: +7(496)522 – 5163, e-mail: a.s@icp.ac.ru
Current research interests: chemistry of metal complexes, reactivity, quantum chemical studies.

Received 30 August 2014
Uspekhi Khimii **84** (11) 1114 – 1144 (2015); translated by A M Raevskiy

ties of a species to a particular composition or structure. Therefore, of crucial interest are atomic clusters whose compositions and structures are known with certainty.[6,7] Progress in physicochemical and synthetic methods made it possible to synthesize and study atomic clusters (i) in solutions where they are stabilized by organic ligands or macromolecules and (ii) on the surface of composite materials.[8–11]

Among atomic metal clusters, small gold clusters attract special attention. There is a long history of research into the properties of these systems. Ligand-protected gold clusters were synthesized and studied by X-ray diffraction long before the 'nanotechnology era',[12–17] while theoretical interpretation of their structure in terms of molecular orbitals[18] was done long before high-level quantum chemical calculations were practically implemented. Recently, the number of scientific publications devoted to gold clusters has continuously increased. According to the Scopus bibliographic database, more than 7000 studies containing key words 'gold cluster' were published only in 2014 (Fig. 1). To date, gold clusters protected by thiolate,[9,19,20] phosphine,[12–17,21] selenolate[22–25] and acetylene[26,27] ligands were synthesized and investigated, and the mechanisms of formation of some clusters were studied.[28,29] Ligand-free gold clusters existing in the gas phase also attract the attention of researchers.[30–32] Recently, atomic gold clusters Au_{10}, Au_{20}, Au_{25},[33–35] and Au_{55} (in zeolite cavity)[36] have been detected on the surface of heterogeneous catalysts.

Intensive progress in the chemistry of gold clusters is favoured by the advances in their synthesis, stabilization and structure determination. Among the studies that underlie modern methods of targeted synthesis, there are the synthesis of the $Au_{55}(PPh_3)_{12}Cl_6$ cluster (main component of commercially available reagent Nanogold ®) by Schmid *et al.*[37] and the development of a two-phase method of synthesis of thiol-derivatized gold nanoparticles by Brust, Schiffrin and co-workers.[38] Further development of this method led to the synthesis of various stable clusters containing from 10 to 102 gold atoms. The structures of ten thiolate clusters including $Au_{20}(SC_6H_4Bu^t\text{-}4)_{16}$,[39] $[Au_{23}(SCy)_{16}]^-$ (Cy is cyclohexyl),[40] $Au_{24}(SAd)_{16}$ (Ad is 1-adamantyl),[41] $Au_{24}(SCH_2C_6H_4Bu^t\text{-}4)_{20}$,[42] $[Au_{25}(SCH_2Bn)_{18}]^-$,[43–45] $Au_{28}(SC_6H_4Bu^t\text{-}4)_{20}$,[46] $Au_{30}S(SBu^t)_{18}$,[47,48] $Au_{36}(SC_6H_4Bu^t\text{-}4)_{24}$,[49] $Au_{38}(SCH_2Bn)_{24}$,[50] $Au_{102}(SC_6H_4CO_2H\text{-}4)_{44}$ (Ref. 51); twelve phosphine-containing clusters, *viz.*, $[Au_6(dppp)_4]^{2+}$ (Ref. 52), $[Au_7(dppp)_4]^{3+}$ (Ref. 53), $[Au_8(dppp)_4Cl_2]^{2+}$ [dppp is 1,3-bis(diphenylphosphino)propane)],[54] $Au_{11}(PPh_3)_7(SPy\text{-}4)_3$ (Py is pyridyl),[55] $[Au_{13}(PMe_2Ph)_{10}Cl_2]^{3+}$ (Ref. 56), $Au_{14}(PPh_3)_8(NO_3)_4$,[57] $[Au_{20}\{PPh(2\text{-}Py)_2\}_{10}Cl_4]^{2+}$ (Ref. 58), $[Au_{20}(PP_3)_4]^{4+}$ (PP_3 is tris[2-(diphenylphosphino)ethyl]-phosphine),[59,60] $Au_{22}(PPh_3)_6$,[61] $[Au_{24}(PPh_3)_{10}(SCH_2Bn)_5ClBr]^+$ (Ref. 62), $[Au_{25}(PPh_3)_{10}(SC_nH_{2n+1})_5Cl_2]^{2+}$ (see Ref. 63),† $[Au_{39}(PPh_3)_{14}Cl_6]^-$ (Ref. 17) and a selenium-containing compound $Au_{38}(SeC_{12}H_{25})_{24}$ (Ref. 25) were determined by X-ray diffraction. Methods for the synthesis of ligand-protected gold clusters are available from the literature.[10,64]

A breakthrough in research on gold clusters became possible due to progress in the theoretical methods based on the density functional theory (DFT). Calculations of the molecular structure and studies on the electronic properties of the clusters with known compositions were used to determine their structures and mechanism of formation, to predict the compositions of non-synthesized compounds and to formulate a number of theories and concepts. Using the fundamental 'divide and protect' approach,[65] the 'superatom' theory,[66] and the 'structure rule',[67] one can determine the structure and properties of gold clusters with all types of ligand environment. For instance, the molecular geometry and optical properties of the $Au_{38}(SR)_{24}$ ($R = C_6H_{13}$, $C_{12}H_{25}$) clusters were predicted using these theoretical concepts before crystal structure determination.[67,68] Successful application of quantum chemical methods to investigation of the structure and properties of ligand-protected clusters gives an impetus to research into targeted isolation and crystallization of novel clusters of theoretically predicted composition.

Gold clusters are used as 'building blocks' to design nanomaterials with controllable properties.[69–71] Applications of gold clusters and nanoparticles in catalysis[72] are at least equally promising. Professor Haruta discovered low-temperature catalytic activity of oxide-supported gold nanoparticles in CO oxidation.[73] At present, the range of reactions catalyzed by gold nanoparticles is significantly extended; it includes various reactions used in organic chemistry and petrochemistry; many of them belong to 'green' chemistry.[74–76] The reason for activity of heterogeneous catalysts containing gold nanoparticles remained unclear for long. A modern point of view is as follows: the major contribution to the activity of gold-containing composites comes from atomic clusters containing from 10 to 20 metal atoms and formed on the surface of heterogeneous catalysts along with larger particles.[33] Also, it is assumed that atomic clusters are responsible for transformations in homogeneous catalytic reactions involving formation of subatomic gold clusters from corresponding organic salts.[77] The optical,[78,79] magnetic[80,81] and biochemical[82,83] properties of gold clusters that are due to the 'nano state' (it is also inherent in other metal clusters) and to unique

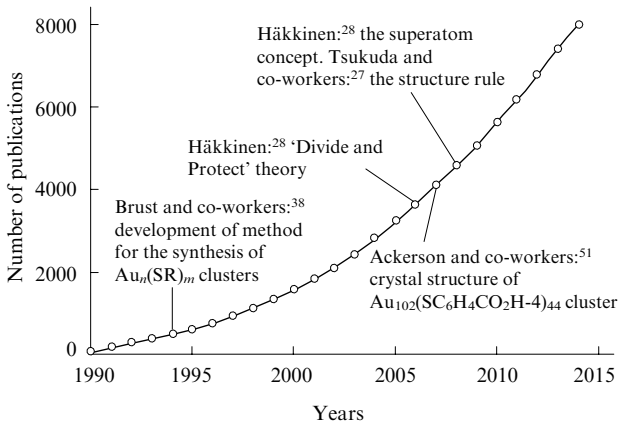


Figure 1. The number of scientific publications containing 'gold cluster' key words since 1990 (according to the data retrieved from the Scopus bibliographic database).
The fundamental studies in chemistry of atomic gold clusters are shown.

† From this point on, the substituents C_nH_{2n+1} have normal structure unless otherwise specified.

electronic structure of this noble metal[84] are no less important than their catalytic properties.

Recently, there has been a considerable increase in the number of original experimental and theoretical studies on the synthesis and separation of individual gold clusters, structure elucidation, diagnostics of optical[11] and biochemical properties[82,85] and on tests of catalysts based on gold clusters in various processes[86–89] including photocatalysis.[90,91] A novel research trend is concerned with doping of gold clusters with atoms of other metals (copper, palladium, silver, platinum).[92–102] The structures of some bimetallic clusters, *e.g.*, $[Ag_6Au_{19}(SCH_2Bn)_{18}]^-$,[103] $[Ag_{32}Au_{12}(SC_6H_4CF_3\text{-}4)_{30}]^{4-}$,[104] $[Cu_nAu_{13}L_{12}]^+$ [n = 2, 4, 8; L = PPh_3, PPh_2(Py-2), SPy-2, $SC_6H_4Bu^t$-4],[105] and $[Cu_{32}Au_{12+n}(SC_6H_4CF_3\text{-}4)_{30+n}]^{4-}$ (n = 0, 2, 4, 6)[106] were determined by X-ray diffraction. The need for systematization and critical analysis of the available experimental and theoretical data on atomic gold clusters gave an impetus to write this review. It concerns the structure, methods of synthesis as well as properties of individual ligand-protected gold clusters. Long experience of the authors in research on the structure of gold clusters and on their adsorption and catalytic properties made it possible to perform a critical analysis and to compare the existing concepts that are used to explain the structure and specific 'magic' compositions of these nanoclusters.

II. The structure of $[L_sAu_nX_m]^q$ clusters

Most ligand-protected gold clusters have core–shell structures (Fig. 2). The cluster core comprises metal atoms only, while the cluster shell is formed by a number of ligand molecules or ions (PR_3, SR, Hal, *etc.*) It is noteworthy that gold atoms can also be constituents of the shell and form so-called 'staple' units $-Au-X-Au-$. The number of atoms in the shell and in the core is fixed.

All thiolate-, selenolate-, phosphine- and halogen-protected gold clusters known to date can be described by the general formula[20] $[L_sAu_nX_m]^q$ which denotes the Au_n cluster bearing the charge q ($q = 0, \pm 1, \pm 2$) and stabilized by m electron-withdrawing ligands X (SR, Hal) and s weakly bound ligands L (PR_3) that provide steric protection for the core.

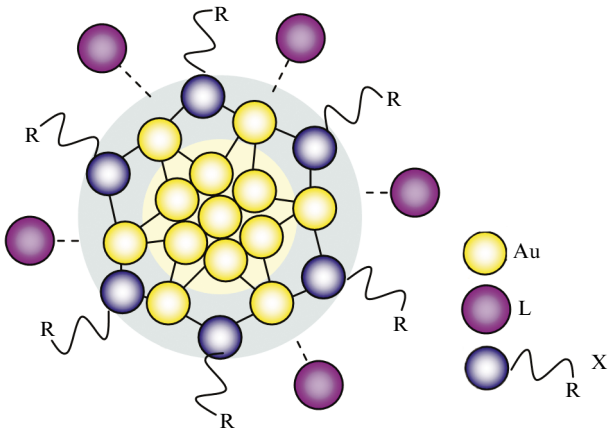


Figure 2. A schematic of $[L_sAu_nX_m]^q$ cluster with the shell containing gold atoms (Au) and two types of ligands (X and L).

Most often, the cluster core represents a highly symmetric polyhedron, *e.g.*, icosahedron. According to the shell model, the central atom of an icosahedron is surrounded by twelve metal atoms of the first coordination sphere; the second coordination sphere includes forty-two atoms. The number of atoms in the nth shell is $(10n^2 + 2)$.[9] This structure is characteristic of the ligand-free clusters Au_{13} (n = 1), Au_{55} (n = 2), Au_{147} (n = 3). The electron shell model predicts high stability for these clusters.

The stability of the $[L_sAu_nX_m]^q$ cluster is governed by not only the type of the polyhedron of the cluster core, but also the total number of valence electrons (n_e). Unlike ligand-free gold clusters whose composition is described by the 'filled electron shell' theory,[107] the superatom concept[66] allows one to predict the stability of a cluster based on the total number of valence electrons, which is determined by the n and m values and by the charge of the cluster:

$$n_e = nv - m - q \quad (1)$$

where v is the formal valence of gold atom equal to unity. Approximation of the interaction between valence electrons and the cluster core by a spherically symmetric potential with allowance for the order of energy levels with different angular momentum (S, P, D, F, G, ...) in the potential well gives the following sequence of filling of delocalized superatomic orbitals of the cluster:

$$1S^2, 1P^6, 1D^{10}, 2S^21F^{14}, 2P^61G^{18} \ldots$$

Stable closed-shell clusters are characterized by particular n_e values corresponding to fully filled levels: n_e = 2, 8, 18, 34 or 58. They are called 'magic', 'noble' or 'superatomic' clusters.[20]

Using the superatom theory and the total number of valence electrons, one can explain the existence of the $Au_{11}(PH_3)_7(SMe)_3$ (n_e = 8), $[Au_{39}Cl_6(PH_3)_{14}]^-$ (n_e = 34) and $Au_{102}(SC_6H_4CO_2H\text{-}4)_{44}$ (n_e = 58) clusters, give a physically correct interpretation of the optical and EPR spectra of the $[L_sAu_nX_m]^q$ clusters, predict the compositions of the doped clusters MAu_nL_m. However, the compositions of some clusters do not obey the 'magic number' rule for valence electrons. For instance, cluster $Au_{32}(SR)_{18}$ has a total of fourteen valence electrons. Deviation from the superatom theory is characteristic of aspherical clusters. Their stability and structure can be explained and predicted within the framework of the ellipsoidal shell model,[108] which treats the electron shell of the cluster as a set of ellipsoidal subshells. As a result, a number of clusters, *e.g.*, $Au_{20}(SR)_{14}$, $Au_{24}(SR)_{20}$ and $Au_{38}(SR)_{24}$), have prolate structures.

The stability and structure of $[L_sAu_nX_m]^q$ clusters are to a great extent determined by the nature of the ligands L and X. For instance, unusual structure of the $Au_{102}(SC_6H_4CO_2H\text{-}4)_{44}$ cluster containing gold atoms in different coordination environment (a rare example of a crystallized cluster) is due to the polydentate nature of 4-sulfanylbenzoic acid.[51] On the one hand, the ligand forms strong Au–S bonds. On the other hand, it forms a shell surrounding the metallic core owing to the coordination potential of carboxylic group. By and large, electron-withdrawing ligands influence the electronic state of the metal atoms in both the core and the shell and thus induce changes in the cluster structure. Changes in the cluster

structure due to metal–ligand interactions can be explained using the 'divide and protect' (or 'stabilization through destruction') concept proposed by Häkkinen,[65] who postulated that ligands play a dual role. Namely, they (i) form a protective layer on the surface to prevent the cluster from growing and (ii) change the composition of the cluster core through transfer of some metal atoms to the ligand shell. The general formula of a cluster can be refined by specifying the number of gold atoms in the ligand shell. For instance, cluster $[Au_{25}(SCH_2Bn)_{18}]^-$ has an icosahedral core, Au_{13}^-, and six $SR(AuSR)_2$ ($R = CH_2Bn$) units in the ligand shell;[43,44] therefore, the composition of the cluster is described by the general formula $[Au_{13}\{SR(AuSR)_2\}_6]^-$ or $[Au_{13+12}(SR)_{18}]^-$. Cluster $Au_{102}(SC_6H_4CO_2H\text{-}4)_{44}$ contains nineteen $-SR-Au-SR-$ units, two $-SR-Au-SR-Au-SR-$ ($R = C_6H_4CO_2H\text{-}4$) units and can be described by the general formula $Au_{79}(RSAuSR)_{19}\{SR(AuSR)_2\}_2$ or $Au_{58+44}(SR)_{44}$.[51]

The $-X-Au-X-$ fragments of the ligand shell are called 'staples'. The arrangement and number of the 'staple' units are determined by balance between the energy of the breaking Au–Au bonds and the energy of the Au–X covalent bonds being formed. The superatom theory predicts the total composition and the charge of the cluster, but the number of metal atoms in the cluster core and in the ligand shell, as well as the composition of 'staple' units remain unknown. To determine the composition of the ligand shell, Tsukuda and co-workers[67] proposed the 'structure rule', *viz.*, the cluster core is a highly symmetric polyhedron and contains a corresponding number of atoms. Other metal atoms are constituents of monomeric, dimeric or polymeric 'staple' units $SR(AuSR)_x$ in the ligand shell,‡ each gold atom in the surface layer being bound to a terminal sulfur atom from the 'staple' unit. As the number of gold atoms in the cluster increases, the curvature of the core surface decreases, which leads to an increase in the number of monomeric motifs $-SR-(Au-SR)-$. The structure of the $Au_{38}(SR)_{24}$ cluster was predicted theoretically based on the structural principles discussed above[67] and then confirmed by X-ray diffraction.[50]

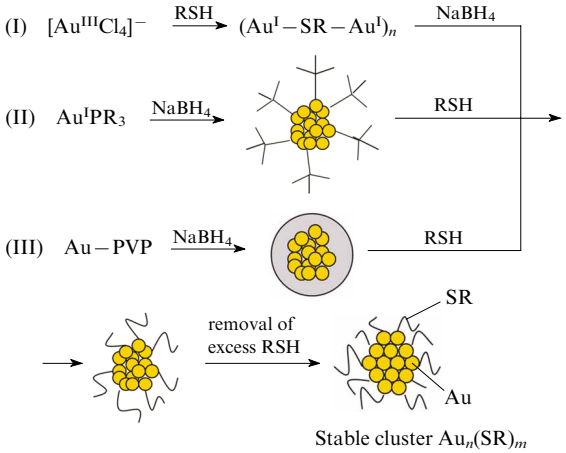
III. Methods of synthesis of atomic gold clusters

The history of synthesis of gold clusters goes hand-in-hand with the synthesis of nanoparticles in solution. The first colloidal solution of gold nanoparticles was prepared by Faraday in 1857. In 1985, Turkevich[109] proposed synthesizing gold particles 7–100 nm in diameter by reduction of gold from chloroauric acid with citrate anions. The chemistry of thiolate-protected gold clusters has been progressing widely owing to the studies by Brust *et al.*[38] In 1994, they proposed a two-phase method for the synthesis of gold particles 2–8 nm in size which involves transfer of the $[AuCl_4]^-$ ion and reducing agent, $NaBH_4$, from aqueous solution to the organic phase by tetraoctylammonium (TOA^+) cation in the presence of dodecanethiol $HSC_{12}H_{25}$. Using this method and controlled variation of the gold-to-thiol ratio, stable gold clusters of different composition were synthesized.

‡ From this point on, '$SR(AuSR)_x$' denotes the ...S(R)–Au–S(R)–Au–S(R)... fragment containing x gold atoms.

The synthesis of $[L_sAu_nX_m]^q$ clusters became possible owing to high skills of experimentalists. The simplest scheme includes synthesis of clusters of different composition in solution and subsequent separation of the clusters. Thiolate clusters $Au_n(SR)_m$ are synthesized following one out of three routes (I–III, Scheme 1) using thiols soluble in water (glutathiones, sulfanylbenzoic acid) or in organic solvents (alkylthiols, phenylethanethiols) as ligands.

Scheme 1



PVP is poly(*N*-vinyl-2-pyrrolidone)

The Brust–Schiffrin method[38] involves reduction of the Au^{III} complex with organic thiols affording polymer chains of the composition $[Au^ISR]_x$. Reduction with bulky thiols (*e.g.*, benzenethiol) mainly leads to short oligomers ($x = 1-3$) with a double-helix structure in the crystalline state.[110] In spite of advances in the structural studies of the polymeric fragment $[Au^ISR]_x$, the mechanism of the reaction of $[AuCl_4]^-$ with thiol remains unclear. The addition of $NaBH_4$ to a solution of $[Au^ISR]_x$ oligomers causes further reduction of Au^I to Au^0 to give nanoclusters stabilized by thiols and oligomeric chains $[SR(AuSR)_x]$. Selective formation of clusters occurs after removal of excess RSH. The composition of the cluster depends on the thiol-to-salt concentration ratio, solvent, the structure of the thiol, the temperature and pH.[111] For instance, low temperatures favour the formation of small clusters. Reactions using THF or acetone result in the $Au_{25}(SR)_{18}$ cluster as major product, while processes in methanol or acetonitrile mainly lead to formation of larger clusters, *e.g.*, $Au_{144}(SR)_{60}$.[112] Reduction of an Au^{III} salt under the action of $NaBH_4$ in the presence of glutathione (GSH) affords a mixture of clusters including $Au_{10}(SG)_{10}$, $Au_{15}(SG)_{13}$, $Au_{18}(SG)_{14}$, $Au_{22}(SG)_{16}$, $Au_{25}(SG)_{18}$, $Au_{29}(SG)_{20}$, $Au_{33}(SG)_{22}$ and $Au_{39}(SG)_{24}$.[113] When a softer reducing agent ($NaBH_3CN$) is used, only the $Au_{18}(SG)_{14}$ cluster is formed selectively. The use of another soft reducing agent, carbon monoxide, leads to selective formation of two clusters, $Au_{25}(SR)_{18}$ (Ref. 114) and $Au_{15}(SR)_{20}$.[115]

Owing the strong Au–S bond, the $Au_n(SR)_m$ clusters can be formed from $Au_n(PR_3)_m$ or Au–PVP by ligand exchange (see Scheme 1). The first step also involves reduction of gold and formation of the cluster core stabilized by phosphine and halogen ligands. Subsequent introduction of thiol results in $Au_n(SR)_m$ formation. A study on the ligand exchange mechanism revealed a multistep process.[116] The

first step involves replacement of Cl by the SR group followed by removal of PPh_3 and formation of $Au_n(SR)_m$.

All these methods for the synthesis of $Au_n(SR)_m$ clusters are characterized by low yields. The reaction yield can be increased on going to the two-step method [117] which was used to obtain a $Au_{38}(SCH_2Bn)_{24}$ cluster.[118] The first step involved the synthesis of $Au_n(SG)_m$ ($38 \leqslant n \leqslant 100$). Ligand exchange, namely, replacement of $BnCH_2SH$ by SG groups of the cluster causes transformation of clusters of different composition to $Au_{38}(SCH_2Bn)_{24}$. Analogously, following the ligand exchange procedure, the $Au_{28}(SC_6H_4Bu^t_4)_{20}$ cluster was synthesized from $[Au_{25}(SCH_2Bn)_{18}]^-$ in 90% yield [46] and the $Au_{36}(SC_6H_4Bu^t_4)_{24}$ cluster was synthesized from $Au_{38}(SCH_2Bn)_{24}$ in 92% yield.[49] In the two-step method, the acidity of the medium also influences the composition of the cluster being formed, namely, $Au_{15}(SG)_{13}$ can be obtained at pH 2, while $Au_{18}(SG)_{14}$ at pH 2.7.[119]

To increase the efficiency of transfer of particles from the aqueous to organic phase, the 'protection–deprotection' method [120] is used. To a solution containing $[Au^ISR]_x$, a surfactant [*e.g.*, cetyltrimethyl ammonium bromide (CTAB)] is added. The surfactant stabilizes the particle through electrostatic interaction with ligands and forms a protective layer. Also, the surfactant shell imparts hydrophobic properties to the particle. Under the action of $NaBH_4$, Au^I is reduced to Au^0, and the particles thus formed go to the organic phase in the presence of tetramethylammonium decanoate. The final step involves removal of the surfactant protective layer as a result of formation of an ion pair comprising the decanoate anion and the hydrophobic surfactant cation. This approach was used to synthesize $[Au_{25}(SCH_2CH(NH_2)CO_2H)_{18}]^-$.[120] Clusters of the general formula $Au_n(SR)_m$ (R = CH_2Bn, $C_{12}H_{25}$, G) can be obtained in high yield using the method of kinetic control.[121]

Phosphine-protected gold clusters are traditionally synthesized by reduction of salts $[Au(PPh_3)Cl$, $(PhPy_2P)AuCl]$ or clusters $\{Au_2(dppm)(NO_3)_2$ [dppm is 1,1-bis(diphenylphosphino)methane], $Au_4(PP_3)Cl_4$, $[Au_6(dppp)_4](NO_3)_2\}$. For instance, a cluster with the icosahedral Au_{13} core was obtained in 26% yield (conditions: ethanol, 50 °C).[122]

$$Au_2(dppm)(NO_3)_2 + NaBH_4 \longrightarrow Au_{13}(dppm)_6(NO_3)_4$$

Six chelating ligands, dppm, protect the Au_{13} cluster from aggregation. The mechanism of increasing the number of Au atoms in the cluster core from 2 to 13 is unknown.[21] The $Au_{55}(PPh_3)_{12}Cl_6$ cluster was synthesized in 30% yield by dissolution of $Au(PPh_3)Cl$ in benzene followed by treatment with gaseous diborane B_2H_6 at 60 °C.[37]

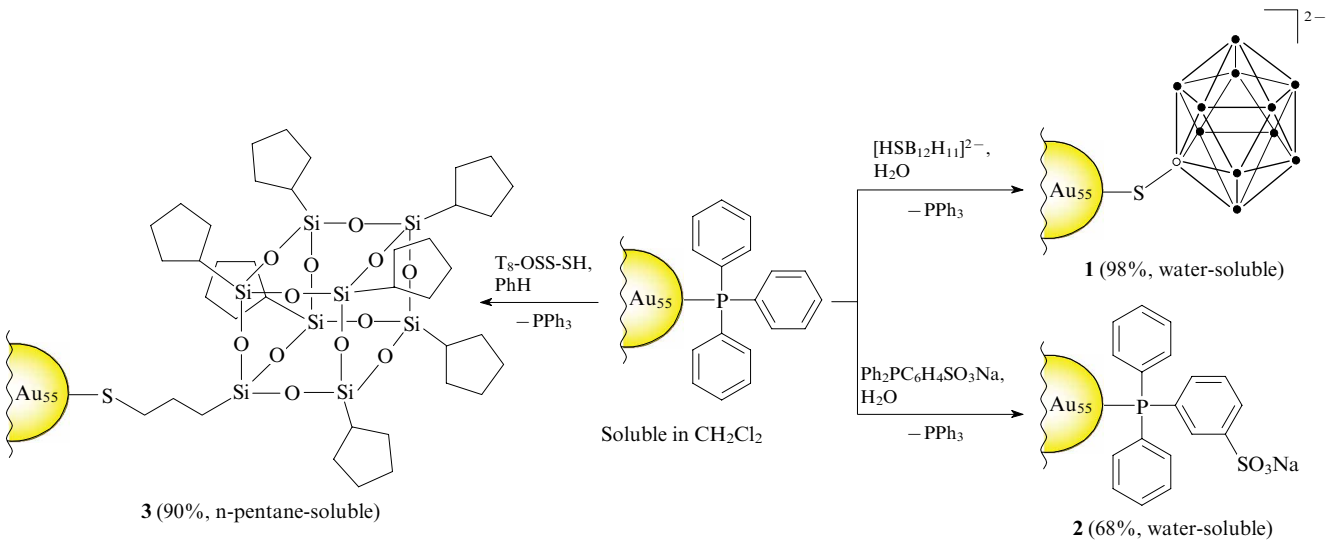
$$Au(PPh_3)Cl + B_2H_6 \longrightarrow Au_{55}(PPh_3)_{12}Cl_6 + Ph_3PBH_3$$

An important role of B_2H_6 consists in (i) reduction of Au^I ions to Au^0 and (ii) transformation of PPh_3 to a tightly bound adduct Ph_3PBH_3 (a Lewis acid–Lewis base complex). The $Au_{55}(PPh_3)_{12}Cl_6$ cluster can be dissolved only in CH_2Cl_2. In aqueous solution, some weakly bound PPh_3 ligands are eliminated and the atomic composition of the cluster thus changes due to aggregation. Using the labile behaviour of the PPh_3 ligands, one can carry out ligand exchange and thus obtain pentane- or water-soluble clusters **1**–**3** with the Au_{55} core (Scheme 2).[123–125] Establishment of the mechanism of the process leading from $Au(PPh_3)Cl$ to the Au_{55} cluster is precluded by the lack of reliable methods of investigation of intermediates. Presumably, the process involves dissociation of the starting gold salt, reduction with the formation of Au^0L particles, subsequent increase in nuclearity, ligand exchange, cluster growth and formation of a colloidal solution.[126]

The $[Au_7(dppp)_4]^{3+}$ cluster was obtained in 51% yield by adding silver ions to a solution of $[Au_6(dppp)_4]^{2+}$ in methanol.[53] The reaction mechanism is still to be clarified; it was assumed [53] that the role of silver cations consists in the formation of important intermediates. The addition of $Au(PPh_3)NO_3$ to a solution of $[Au_6(dppp)_4]^{2+}$ followed by reduction under the action of $NaBH_4$ results in the $[Au_8(dppp)_4]^{2+}$ cluster in 59% yield.[54]

Monodispersity of a cluster is a necessary condition for its crystallization and subsequent investigation of proper-

Scheme 2



T_8-OSS-SH = (cyclo-C_5H_9)$_7Si_8O_{12}(CH_2)_3SH$; • BH; ○ B

ties. Most methods for the synthesis of $[L_sAu_nX_m]^q$ clusters result in crude mixtures of clusters of different composition which should be separated by deposition,[127] gel electrophoresis or liquid chromatography. By varying the solvent polarity one can separate various compounds including $[Au_{11}(PPh_3)_8Cl_2]^+$, $[Au_{11}(BINAP)_4X_2]^+$ [BINAP is 2,2′-bis(diphenylphosphino)-1,1′-binaphthyl; X = Cl, Br],[128] $[Au_{25}(PPh_3)_{10}(SC_nH_{2n+1})_5Cl_2]^{2+}$ (n = 2, 8, 10, 12, 14, 16, 18),[63] and $[Au_{37}(PPh_3)_{10}(SCH_2Bn)_{10}Cl_2]^+$.[129]

The 'host–guest' approach, as applied to the synthesis of gold clusters, is practically implemented using α-, β- and γ-cyclodextrins (CD).[130, 131] The cavity of the cyclodextrin molecule has the shape of a truncated cone and only small clusters can accommodate within.

$$Au_n(SG)_m + CD \longrightarrow Au_{n-x}CD(SG)_{m-k} + Au_x(SG)_k$$

Besides, cyclodextrin forms a shell which precludes further growth of the cluster. This method was used to synthesize the Au_{15}@CD[130] and Au_{25}@CD clusters.[131] Organic molecules of complex structure, *e.g.*, dendrimers[132] containing RS groups (R = Bn, *etc.*) can stabilize the Au_{25},[133] Au_{55} (Ref. 134) and Au_{144} (Ref. 135) clusters through Au–S interaction.

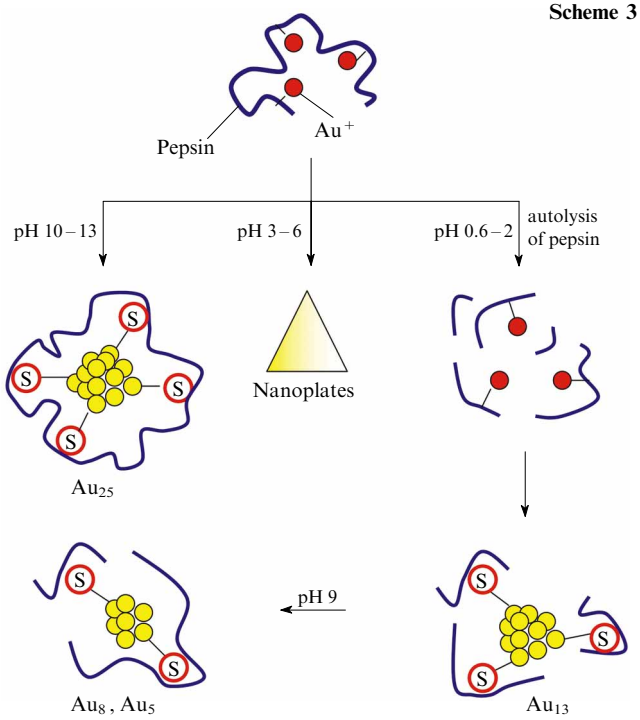
Proteins can also be used to protect gold clusters.[85] On the one hand, protein molecules contain groups which play the role of reducing agents under particular conditions. On the other hand, proteins provide conditions for the synthesis of clusters of particular size owing to spatial protection and electronic stabilization through Au–S interaction. The composition of a gold cluster formed in the presence of a protein is determined by the structure of the protein molecule and by the reaction conditions. The higher the molecular mass, the larger the size of the cluster to be stabilized. The Au_{55} cluster was synthesized in a solution of bovine serum albumin,[136] while smaller clusters (Au_{10}, Au_{11}, Au_{12}) were obtained using lysocyme (LYZ).[137] However, a MALDI-MS§ study[138] of a solution containing Au_n-LYZ clusters also revealed larger clusters, namely, Au_{25}^+, Au_{38}^+ and Au_{102}^+. Since lysocyme is a small protein and cannot stabilize large clusters, their large size may be a result of laser irradiation under conditions of the MALDI experiment.

The influence of reaction conditions on the compositions of clusters formed in proteins can be monitored taking the synthesis of gold clusters in pepsin as an example.[85] The process shown in Scheme 3 results in Au_{25} in the basic medium and in smaller clusters (Au_{13}, Au_8, Au_5) in the acidic medium due to autolysis of pepsin.

Thus, the formation of $[L_sAu_nX_m]^q$ clusters is due to strong interaction of gold atoms with SR groups, Hal atoms or other functional groups of protein molecules, which precludes cluster growth. Clusters comprising a few gold atoms can be formed on the surface of inorganic materials; in this case, the small clusters are stabilized through the interaction with the surface groups or defects of the support.[72, 139, 140] The reaction of $Au_n(SG)_m$ with trimethoxy(3-sulfanylpropyl)silane at room temperature followed by base hydrolysis at 65 °C gave an Au_{25} cluster immobilized on SiO_2.[35] The Au_{20} cluster was synthesized by

§ Matrix-activated laser desorption–ionization mass spectrometry; LDI is laser desorption–ionization.

Scheme 3



deposition onto carbon surface using magnetron sputtering.[34] According to transmission electron aberration-corrected microscopy data (Fig. 3), the cluster has a tetrahedral structure, as was predicted earlier by quantum chemical calculations.[141, 142] A dynamic structure of the Au_{20} cluster on carbon surface was reported.[34] The Au_{12} cluster also has a dynamic structure both in the gas phase and on a regular MgO(111) surface.[143] Probably, it is the dynamic properties of gold clusters that are responsible for the high catalytic activity of these species. Indeed, they can vary the structure on activation of the reactant molecule or on the formation of an intermediate. For instance, the reaction of acetylene with Au_{12} affords a bridging complex $Au_{12}C_2H_2$ due to the

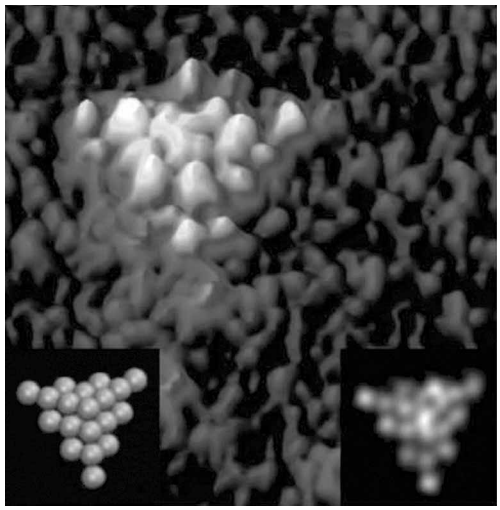


Figure 3. Individual frames from a time-lapse series of HAADF STEM images of Au_{20}/C (2.8 × 2.8 nm).[34]
The inset on the right: model image (simulation) of Au_{20} tetrahedral cluster with orientation shown in the inset on the left.

dynamic structure of the cluster.[144] Considerable activation of the hydrocarbon in the complex favours efficient hydrogenation of acetylene.[145]

Supported gold nanoparticles are widely used in heterogeneous catalysis. These catalysts are prepared by traditional chemical methods, *e.g.*, impregnation of support with Au^{III} or Au^{I} salts and subsequent reduction and calcination.[72] It was shown that the surface of the Au(2.9%)/FeO_x composite kept in a chromatograph for 16 h at 120 °C is covered with not only particles 1–7 nm in size, but also Au_{10} atomic clusters with a bilayer structure.[33] The catalytic activity of Au/FeO_x in CO oxidation is just due to the presence of Au_{10} clusters on the surface. Recently,[146, 147] we used the Au_{10} cluster with the bilayer structure as model in the quantum chemical studies of the adsorption and catalytic properties of gold clusters. The catalytic activity of atomic gold clusters Au_n (n = 2, 6–9, 12, 18, 20) supported on MgO in CO oxidation was studied.[148] The clusters were obtained with a supersonic nozzle and then separated by mass. The catalytic properties of the samples studied were shown to depend on the cluster size and on the support nature; the smallest cluster exhibiting catalytic properties in CO oxidation is Au_8. The catalytic activity of the zeolite-supported Au_{55} cluster in CO oxidation was studied by a number of physicochemical methods.[36] However, zeolites are not the best materials for stabilization of gold clusters for catalytic applications because metal clusters may be confined within the zeolite cavities, thus being inaccessible to reactant molecules.[149]

IV. Methods for determination of the structure and properties of clusters

The key characteristics of clusters include the general chemical formula, the structural type, thermal stability, laser radiation resistance, as well as the electronic, optical and magnetic properties. They can be determined using a number of physicochemical and quantum chemical methods. The atomic composition of $[L_sAu_nX_m]^q$ clusters is established by MALDI/LDI-MS and transmission electron microscopy (TEM). Structure elucidation is performed by X-ray diffraction and computational methods based on DFT using different functionals. A comparison of the calculated absorption spectrum in the visible region for the tentative structure with the experimentally measured spectrum allows the cluster structure to be assessed indirectly. The charge of the cluster is determined by X-ray photoelectron spectroscopy (XPS).[150] The thermal stability is studied by thermogravimetric analysis (TGA) and absorption IR spectroscopy. In the text below we present examples of application of the methods listed above in studies on the structure and properties of $[L_sAu_nX_m]^q$ clusters; the potential and limitations of these methods will also be discussed.

As mentioned above, monodispersity is an important property of clusters. On the one hand, it deserves further investigation; on the other hand, it may be utilized in some way. If a system under study contains clusters of different composition, it is impossible to relate a measured property to a particular composition. Mass spectrometry belongs to the most popular methods for the determination of the degree of dispersion and the general formula of clusters. Earlier, the cluster compositions were studied using two ionization methods, LDI and MALDI.[11] Since in both cases one deals with dissociation of chemical bonds (*e.g.*, Au–S and S–C) in the clusters, attempts to detect a peak of undamaged cluster failed. At present, electrospray ionization (ESI) mass spectrometry has been widely used to investigate the composition of atomic clusters; this method is softer and non-destructive.[151] FT-IR spectroscopy is also used to verify the monodispersity of clusters.[152]

The charge of a newly forming cluster is determined by UV-Vis absorption spectroscopy.[11, 153–155] For instance, the spectrum of $[Au_{25}(SR)_{18}]^-$ anionic cluster exhibits three well-defined peaks at 400, 450 and 670 nm and one diffuse peak at 800 nm (Fig. 4 *a*). For the neutral cluster $Au_{25}(SR)_{18}$, absorption in the region of 400 nm increases and absorption at 450 nm decreases. The spectrum of a cationic cluster exhibits diffuse peaks at 400 and 450 nm and an absorption line shifted from 800 nm to 660 nm. Not only the charge, but also the electronic properties of clusters can be predicted from their absorption spectra. It should be noted that the molecular type of absorption spectrum

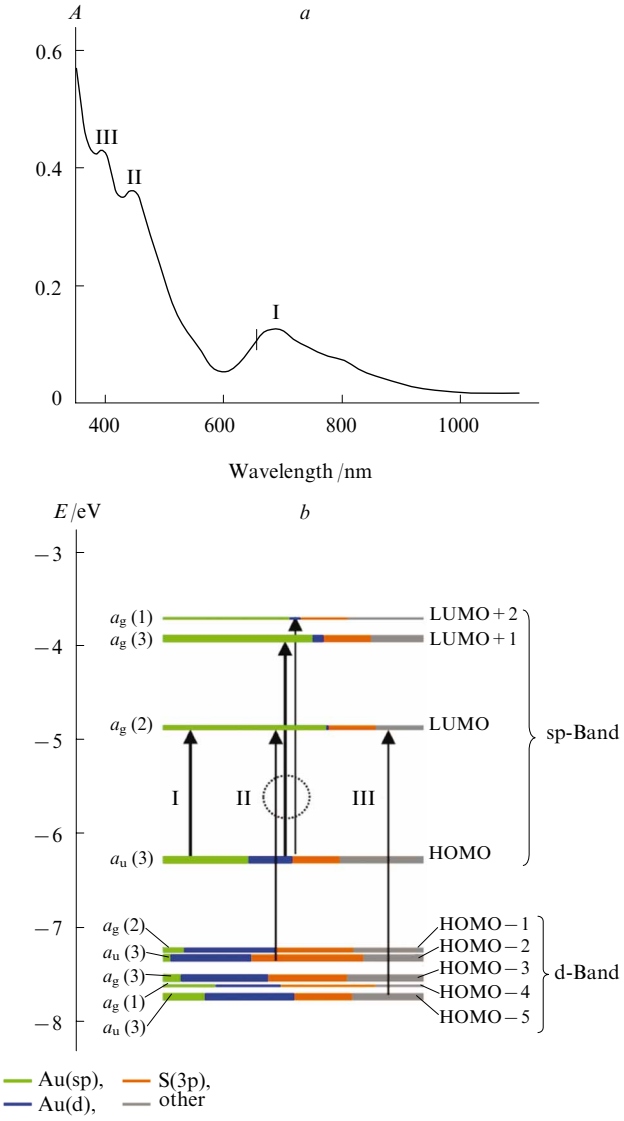


Figure 4. UV-Vis spectrum of $Au_{25}(SCH_2Bn)_{18}$ cluster (*a*)[153] and its interpretation based on the Kohn–Sham orbitals (*b*).[11]
A is the absorbance.

characteristic of atomic gold clusters is a consequence of one-electron transitions between energy levels. This behaviour significantly distinguishes atomic clusters from nanoparticles whose spectrum is determined by the intense transition upon co-operative excitation of conduction electrons.

The structures of ligand-protected clusters are determined by X-ray diffraction analysis. Earlier, this method was used to establish the crystal structures of small phosphine-containing clusters $Au_{11}(PPh_3)_7(SCN)_3$,[16] $Au_{13}(dppm)_6(NO_3)_4$,[56] and $[Au_{39}(PPh_3)_{14}Cl_6]Cl_2$.[17] The structures of thiolate-protected gold clusters were determined by this method more recently because of difficulties in crystallization from solutions. Two independent research groups simultaneously reported the crystal structures of $[Au_{25}(SCH_2Bn)_{18}]^-$ (see Refs 43 and 44) and then $Au_{102}(SC_6H_4CO_2H\text{-}4)_{44}$.[51] The crystal structures of the following mono- and bimetallic clusters are also available: $Au_n(SR)_m$,[30, 31, 39–42, 46–51] $Au_n(PR_3)_m$,[16, 17, 52–63] $Au_{38}(SeR)_{24}$,[25] $AgAu_nL_m$,[103, 104] and $CuAu_nL_m$.[105, 106] Traditionally, the structure of nanomaterials is investigated by TEM; however, this method seems to be inefficient in the cluster structure studies because the cluster size is too small for standard-resolution TEM and electronic radiation causes structural rearrangements in the clusters or their aggregation.

Considerable progress in understanding the structure of ligand-protected gold clusters was made using theoretical methods. Pioneering molecular dynamics studies were aimed to determine the structure of large $Au_n(SR)_m$ clusters with n = 140, 201, 459 and 586.[127, 156] This method was also used to predict changes in the structure of a gold cluster upon adsorption of a MeSH molecule[157] ['herringbone reconstruction' called by analogy with the structural changes on the Au(111) surface upon adsorption of thiols].[158]

At present, the most popular methods for structural studies of gold clusters are based on the DFT, which was used to predict the structure of the following clusters: $Au_{10}(SC_6H_4Bu^t\text{-}4)_{10}$,[159] $[Au_{12}(SMe)_9]^+$,[160] $Au_{15}(SR)_{13}$ (R = Me, G),[161, 162] $Au_{18}(SMe)_{14}$,[163] $Au_{40}(SCH_2Bn)_{24}$,[164] $[Au_{44}(SMe)_{28}]^{2-}$,[165] $[Au_{67}(SR)_{35}]^{2-}$ (R = CH_2Bn, C_6H_{13}),[166] and $Au_{130}(SC_{12}H_{25})_{50}$.[167] It should be noted that calculations of the structure of ligand-protected gold clusters are complicated by the need to take into account relativistic effects in order to correctly describe the Au–Au, Au–X and Au–L interactions and eventually to correctly predict the structures of the cluster core and shell.[84, 168] Calculations with no relativistic corrections applied give incorrect geometry of the gold clusters, as is the case of, *e.g.*, Au_8 (MP2/cc-pVTZ)[169] and Au_6 (CASSCF/CI).[170] The best way to take into account relativistic effects is to use relativistic Hamiltonians,[143, 171] but the computational cost

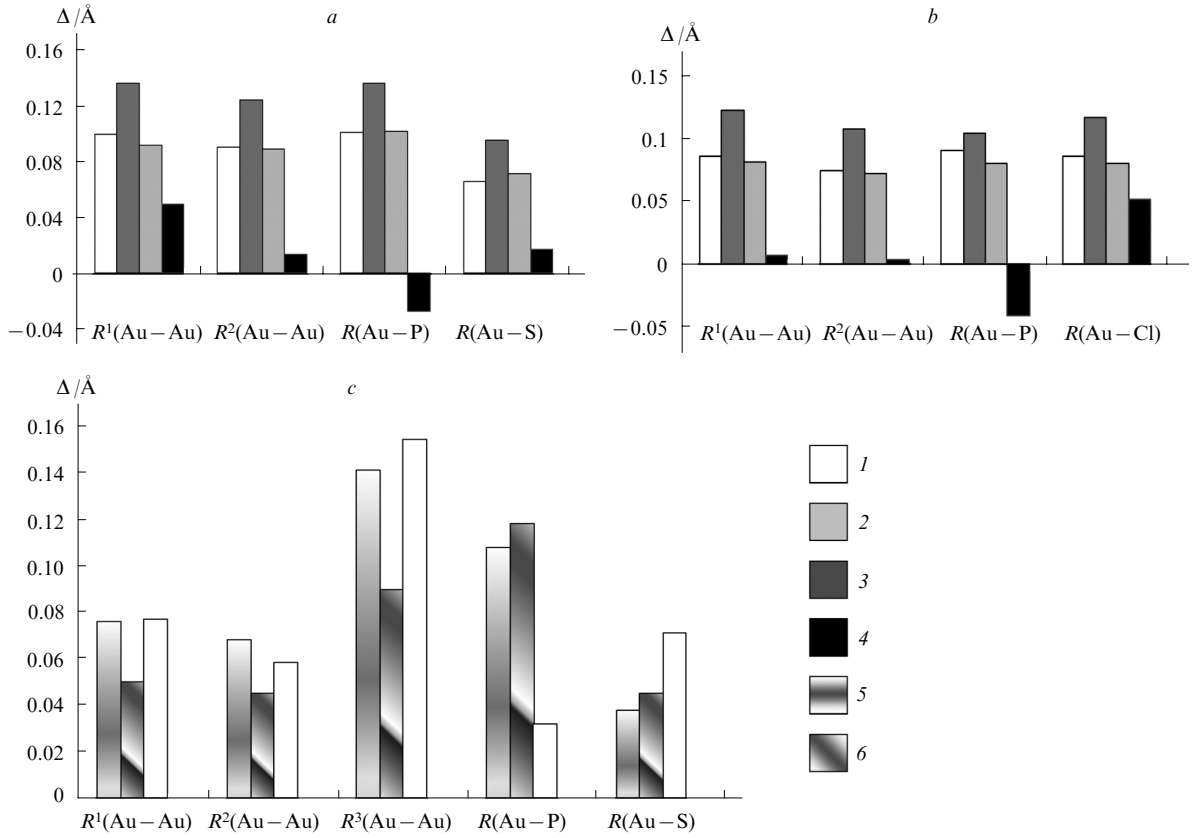


Figure 5. Differences between the interatomic distances in the clusters calculated by the DFT/LANL2dz method[174] and crystallographic data:[55, 175] $Au_{11}(PPh_3)_7(SPy\text{-}4)_3$ (*a*),[55] $Au_{11}(PPh_3)_7Cl_3$ (*b*), and $[Au_{24}(PPh_3)_{10}(SCH_2Bn)_5ClBr]^+$ (*c*).
R^1(Au–Au) is the average distance between the atoms on the core surface, R^2(Au–Au) is the average distance between the central atom and the atoms on the core surface, R^3(Au–Au) is the distance between two atoms belonging to different fragments of the cluster.
The functionals used: B-PBE (*1*), CAM-B3LYP (*2*), B3LYP (*3*), M06-HF (*4*), PBE (*5*) and TPSS (*6*).

in this case is high. The most popular methods of investigation of the structure of gold clusters include calculations using pseudopotentials to describe the core electrons[29] (in particular, LANL2dz, see Ref. 172). However, the cluster structure obtained from calculations using the LANL2dz pseudopotential may be incorrect in some cases.[173]

When determining the most stable structure of isomeric clusters, one should unavoidably consider different configurations of the cluster core and various types of ligand coordination. This complicates the problem and increases the time needed for geometry optimization because of a large number of isomers, especially if clusters contain more than twenty gold atoms. Traditionally, the stabilities of isomeric clusters are assessed using their relative energies and the HOMO–LUMO gap value (for a stable cluster, it should be $\geqslant 0.5$ eV). The calculated cluster energies depend on the exchange-correlation functional.[20] Therefore, it is of great importance to test the DFT methods for, *e.g.*, correct description of experimental parameters of clusters, such as the interatomic distances, the HOMO–LUMO gap, peak positions in the optical spectrum or in the X-ray powder diffraction pattern.[19]

Recently, different functionals were tested in the context of structure description of the clusters $Au_{11}(PPh_3)_7X_3$ (X = Cl, SPy-4) and $[Au_{24}(PPh_3)_{10}(SCH_2Bn)_5ClBr]^+$.[174] The interatomic distances calculated using the LANL2dz pseudopotential for the gold atoms and the 6-3111G(d,p) basis set for other atoms were compared with the X-ray data.[55,175] Figure 5 presents how the difference between the theoretical and experimental values (Δ/Å) depends on the functional chosen. All functionals overestimate the interatomic distances in the cluster compared to the X-ray data. This is not surprising because the optimized cluster structure obtained from DFT calculations corresponds to the gas phase. Among the tested functionals, the largest error in calculations of interatomic distances was found for B3LYP; geometry optimization within the framework of the DFT/B3LYP method led to a slightly distorted structure. The B-PBE, PBE and TPSS functionals provide a qualitatively correct reproduction of the cluster geometry with a mean error of less than 0.1 Å for the interatomic distances and 0.1 eV for the HOMO–LUMO gap. The Au–Au distances in Au_n obtained from DFT/PBE/cc–pVTZPP calculations differ from those calculated using a more exact and time-consuming CCSD(T)–F12 method by merely 0.03 Å.[176] The differences between the Au–P interatomic distances in $AuPH_3$, Au_2PH_3, $AuPH_3^+$ and $Au_2PH_3^+$ calculated at the DFT and CCSD(T) levels of theory are even smaller, namely, 0.01 Å.[177]

The persion-corrected PBE-D3, TPSS-D3 functionals are recommended for calculations of bond energies in the Au_n clusters ($n \leqslant 20$) with an accuracy of 4 kJ mol^{-1}.[176] The contribution of spin–orbit coupling to the Au–Au bond energy can be correctly included using the PBE-PBE-2c functional.[176] It seems appropriate to carry out theoretical studies of clusters containing PR_3 ligands using dispersion-corrected functionals, *e.g.*, PBE-D3.[178] A reasonable balance between the accuracy of calculations and the time needed for calculations of the adsorption energies of the test molecules on gold clusters can be achieved using the HSE06 and HISSb functionals.[179]

Although being run on powerful modern computers, energy calculations and geometry optimization of ligand-protected gold clusters remain time-consuming. To reduce the computing time, the number of atoms in the cluster is decreased, bulky substituents R in $Au_n(SR)_m$ are replaced by Me groups, while PPh_3 groups in $Au_n(PR_3)_m$ are replaced by PH_3 or PMe_3 ligands. Using the $Au_4(PR_3)_4$ clusters (R = H, Me, Ph) as examples, it was shown that replacement of PPh_3 by PH_3 has no effect on the cluster geometry, but taking into account the PPh_3 ligand in explicit form is necessary to describe the experimental excitation spectra.[180]

In addition to the DFT-based methods, the structure of gold clusters is studied by molecular dynamics methods. For instance, a version of the Monte Carlo method was proposed for structure calculations of the Au_{24} cluster with an accuracy comparable to that of CCDT in reasonable time.[181] The computing time can be shortened using the reactive force field method. However, the structure of the $-SR-(Au-SR)_x-$ 'staple' unit predicted by this method is significantly different from that obtained from DFT calculations.[182] A new potential parameterized using the DFT data made it possible to solve the problem and correctly describe the structure of the fragment in question.[183] Thus, molecular dynamics methods combined with DFT data (QM/MM) can be successively used in structure elucidation of the $Au_n(SR)_m$ clusters. In particular, the accuracy of the QM/MM calculations of interatomic distances in the $Au_{25}(SR)_{18}$ and $Au_{38}(SR)_{24}$ clusters is $\sim 3\%$.[184]

V. Clusters with strong metal–ligand interaction

V.1. The structure of thiolated clusters

Compounds $[Au_n(SR)_m]^q$ [R = C_nH_{2n+1} (n = 2, 6, 10, 12), Ph, CH_2Bn, $C_6H_4CO_2H$-4, G]. Clusters stabilized by sulfur-containing ligands (SR) provide good examples of the $[L_sAu_nX_m]^q$ systems where ligands form strong bonds with gold atoms. Many of them were structurally characterized by X-ray diffraction or their structures were predicted by DFT calculations. In the text below we will discuss specific features of the cluster structures in the order of increasing number of gold atoms in the context of the superatom theory, the structure of the cluster core, the nature of the Au–S bond and the mechanism of formation of the $-SR-Au-SR-$ 'staple' units. Particular attention will be given to analysis of the applicability of DFT calculations to structure elucidation and to prediction of properties of the $[Au_n(SR)_m]^q$ clusters.

$Au_{15}(SR)_{13}$ (R = G; n_e = 2). The synthesis of the cluster[185,186] was accompanied by elaboration of structural models using the DFT/PBE method.[161,162] One model includes a tetrahedral Au_4 core surrounded by two 'staple' units, $SR(AuSR)_5$ and $SR(AuSR)_6$.[162] In the other model the tetrahedral Au_4 core is surrounded by the cyclic $(Au^ISR)_5$ pentamer and two $SR(AuSR)_3$ trimers (Fig. 6,*a*).[161] Yet another possible cluster core composition is Au_6, as in $[Au_{15}(SMe)_{12}]^+$.[187] It seems reasonable to assume that the cluster contains long $SR(AuSR)_n$ units formed from Au^ISR during the synthesis.

$Au_{18}(SR)_{14}$ (R = G, CH_2Bn; n_e = 4). Cluster $Au_{18}(SG)_{14}$ was isolated upon separation of a crude mixture containing nine small clusters with different gold : ligand ratios (10 : 10, 15 : 13, 18 : 14, 22 : 16, 22 : 17, 25 : 18, 29 : 20, 33 : 22, 39 : 24).[185] The mixture of $Au_n(SCH_2Bn)_m$ clusters was enriched with $Au_{18}(SCH_2Bn)_{14}$ using SCH_2Bn as ligand.[163] According to DFT calculations, the cluster has a bitetrahedral core of the formula Au_8, while the shell comprises two

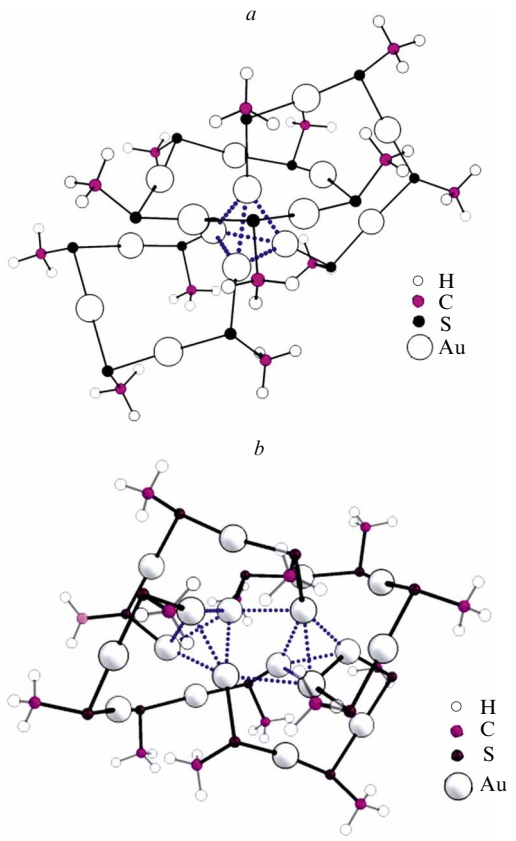


Figure 6. Structures of the $Au_{15}(SMe_3)_{13}$ (*a*) and $Au_{18}(SMe_3)_{14}$ (*b*) clusters obtained from DFT calculations (reproduced using the atomic coordinates taken from 'Support Information' to Refs 160 and 161).
Dotted lines connect the gold atoms of the cluster core.

dimeric $[SR(AuSR)_2]$ and two trimeric units $[SR(AuSR)_3]$ (see Fig. 6 *b*).[160] Reliability of the results of calculations is confirmed by reproduction of the visible absorption spectrum and the circular dichroism spectrum.[163] A time-of-flight mass spectrometry (MALDI-TOF-MS) study[163] predicted high stability of $Au_{18}(SR)_{14}$; therefore, one can expect that the cluster structure would be determined more accurately in the case of crystallization.

$Au_{19}(SR)_{13}$ (R = CH_2Bn; n_e = 6). Two structural models, $Au_{1+10}(SRAuSR)_2\{SR(AuSR)_2\}_3$ and $Au_{12}(SRAuSR)_5\{SR(AuSR)_2\}$, were proposed for this cluster.[121] According to EXAFS and XPS data, the first model is more probable.[188]

$Au_{20}(SC_6H_4Bu^t\text{-}4)_{16}$ (n_e = 4). The structure of the cluster was determined by X-ray diffraction (Fig. 7 *a*).[39] The Au_7 core formed by two vertex-sharing tetrahedra is surrounded by the $(AuSR)_8$ cyclic octamer, one $SR(AuSR)_3$ trimer and two SRAuSR units. Noteworthy is that none of the sulfur atoms is bonded to the gold atoms of the core. The core–shell interaction occurs through Au—Au bonds of length 3.02 Å characteristic of aurophilic interaction. The chiral properties of the cluster arise from different orientations of the ring and 'staple' units.

$[Au_{23}(SR)_{16}]^-$ (R = Cy; n_e = 8). The cluster structure was determined by X-ray diffraction (see Fig. 7 *b*).[40] The central gold atom is surrounded by 12 metal atoms. There are two extra gold atoms located above the core planes, so that the cluster core has the formula Au_{15} and the shape of a bipyramid. The cluster shell is formed by two $SR(AuSR)_3$ trimers, two monomeric SRAuSR units and four RS ligands.[40]

$Au_{24}(SAd)_{16}$ (n_e = 8). According to X-ray data, this cluster is structurally similar to $[Au_{23}(SCy)_{16}]^-$ (see Fig. 7 *c*).[41] The Au_{15} core is surrounded by two $SR(AuSR)_3$ trimers, one SRAuSR monomer and one $SR(AuSR)_2$ dimer; five RS ligands are coordinated to the gold atoms of the cluster core.

$Au_{24}(SR)_{20}$ (R = CH_2Bn, $CH_2C_6H_4B^t_4$; n_e = 4). Cluster $Au_{24}(SCH_2Bn)_{20}$ is characterized by a small gold : sulfur ratio of 1.2.[189] According to DFT calculations of possible isomers with the formula $Au_{24}(SR)_{20}$, the lowest-energy cluster has a prolate bi-tetrahedral Au_8 core and a shell comprised of pairs of $SR(AuSR)_3$ and $SR(AuSR)_5$ units (see Fig. 7 *d*).[190] Distant atoms of the core are connected by 'catenane' fragments $SR(AuSR)_5$ (by analogy with the polynuclear thiolate complexes Au^I (Ref. 191) and $Au_{15}(SR)_{13}$); this is atypical of clusters with the core–shell structure. An X-ray diffraction study of the structure of the cluster with R = $CH_2C_6H_4Bu^t_4$ confirmed the predicted composition and core structure, but the shell structure appeared to be different, being formed by four $SR(AuSR)_4$ units.[42]

$[Au_{25}(SR)_{18}]^-$ (R = CH_2Bn, Et; n_e = 8). According to X-ray diffraction data[43–45] and DFT calculations,[192] this cluster has a core–shell structure and quasi-D_{2h} symmetry (Fig. 8 *a*). The core represents the Au_{13} icosahedron, while the other twelve gold atoms are in the shell, being incorporated into six 'staple' dimeric units $SR(AuSR)_2$. It is noteworthy that the structure of $[Au_{25}(SMe)_{18}]^-$ was initially predicted theoretically by the DFT method. A few months later, the crystal structure of the cluster in compound $[Au_{25}(SCH_2Bn)_{18}]^-[TOA]^+$ was determined by two independent groups of experimentalists.[43,44] The composition and structure of the cluster core and shell appeared to be in excellent agreement with the theoretical predictions. The use of other ligands [R = $CH_2CH(NH_2)Ph$, $CH_2CHMePh$] may cause distortion of the cluster structure.[193]

The HOMO of the $[Au_{25}(SMe)_{18}]^-$ anion is triply degenerate, which corresponds to superatomic p-orbitals delocalized over the Au_{13} core; the LUMO is doubly degenerate and represents a set of split superatomic d-orbitals.[192]

The anionic cluster $[Au_{25}(SR)_{18}]^-$ was transformed to structurally similar clusters $Au_{25}(SR)_{18}$ and $[Au_{25}(SR)_{18}]^+$ (Ref. 194) using appropriate oxidizing agents. Both clusters are characterized by lower thermal stability.[195] The transformation was shown to be irreversible.[196] The anionic cluster HOMO responsible for the electron-donating properties includes a large contribution from the orbitals of the core gold atoms rather than the orbitals localized on the Au—S bonds. Therefore, oxidation of the $[Au_{25}(SR)_{18}]^-$ cluster leads to the loss of the negative charge localized on the Au_{13} core. This mechanism differs from the oxidation mechanism of thiol monolayers adsorbed on gold surface which begins with the oxidation of the adsorbed thiol.[197] We believe this difference to be due to different electronic structures of metallic gold having a conduction band and the molecular cluster having a discrete set of electronic energy levels.

The $[Au_{25}(SR)_{18}]^-$ cluster exhibits strong two-photon absorption, while its oxidized form, $[Au_{25}(SR)_{18}]^0$, exhibits

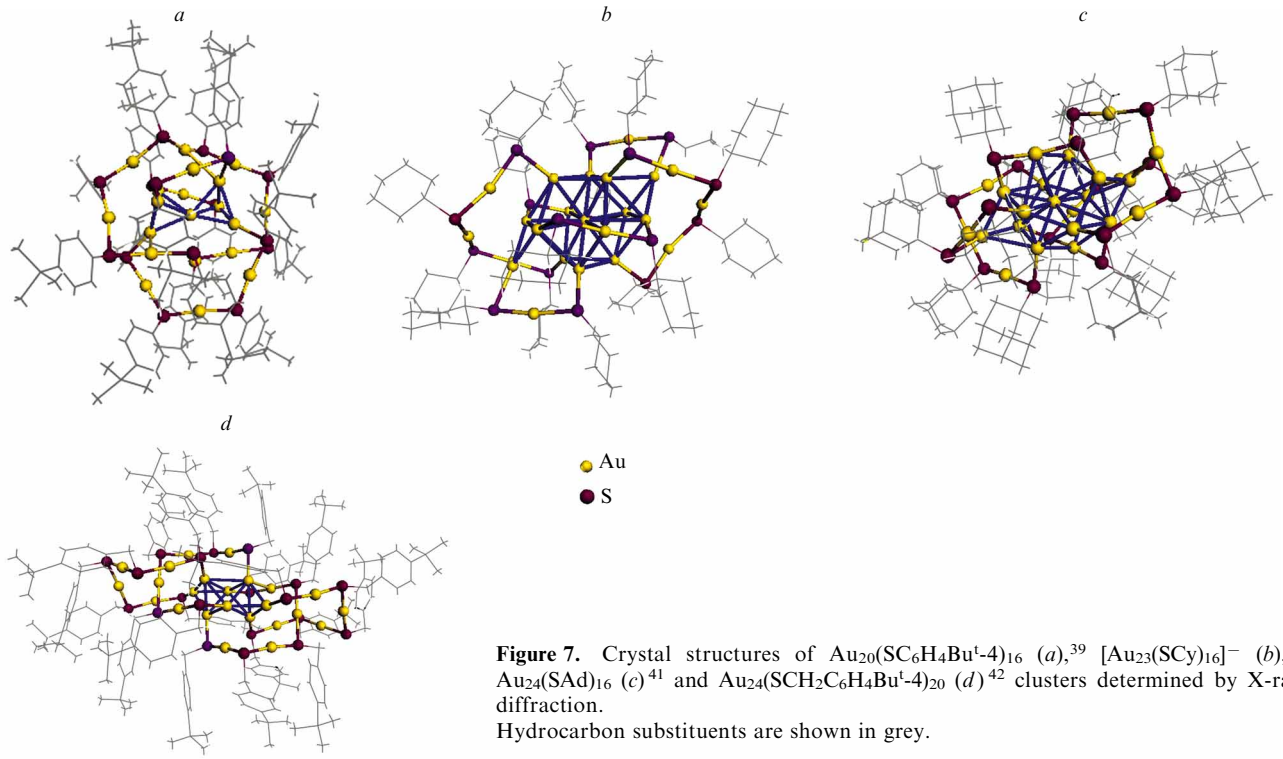


Figure 7. Crystal structures of $Au_{20}(SC_6H_4Bu^t\text{-}4)_{16}$ (*a*),[39] $[Au_{23}(SCy)_{16}]^-$ (*b*),[40] $Au_{24}(SAd)_{16}$ (*c*)[41] and $Au_{24}(SCH_2C_6H_4Bu^t\text{-}4)_{20}$ (*d*)[42] clusters determined by X-ray diffraction.
Hydrocarbon substituents are shown in grey.

paramagnetism arising from 'itinerant' electrons.[11] According to femtosecond dynamics data, internal conversion between the excited electronic states of the Au_{13}^- core takes only 200 fs and the core-to-shell relaxation occurs within merely 1.2 ps.

$Au_{28}(SR)_{20}$ ($R = C_6H_4Bu^t\text{-}4$; $n_e = 8$). A compound of the general formula $Au_{20}[Au_2(SR)_3]_4(SR)_8$ crystallizes in the space group $P\bar{1}$.[46] The kernel-type Au_{20} core is formed by two interpenetrating slightly distorted Au_{13} cuboctahedra sharing six common atoms (see Fig. 8 *b*). It can be treated as fragment of the fcc lattice of metallic gold. Four $SR(AuSR)_2$ dimers are coordinated to the cluster core, while the other eight RS groups bridge on the core edges.

$Au_{30}S(SR)_{18}$ ($R = Bu^t$; $n_e = 10$). According to X-ray data and DFT calculations, the kernel-type Au_{22} core is surrounded by two $SR(AuSR)_3$ trimers and two SR(AuSR) units, the other six RS groups being coordinated to the surface atoms of the core (see Fig. 8 *c*).[47,48] The central fragment of the Au_{20} core comprises two nested distorted Au_{13} cuboctahedra, as in the $Au_{28}(SC_6H_4Bu^t\text{-}4)_{20}$ cluster.

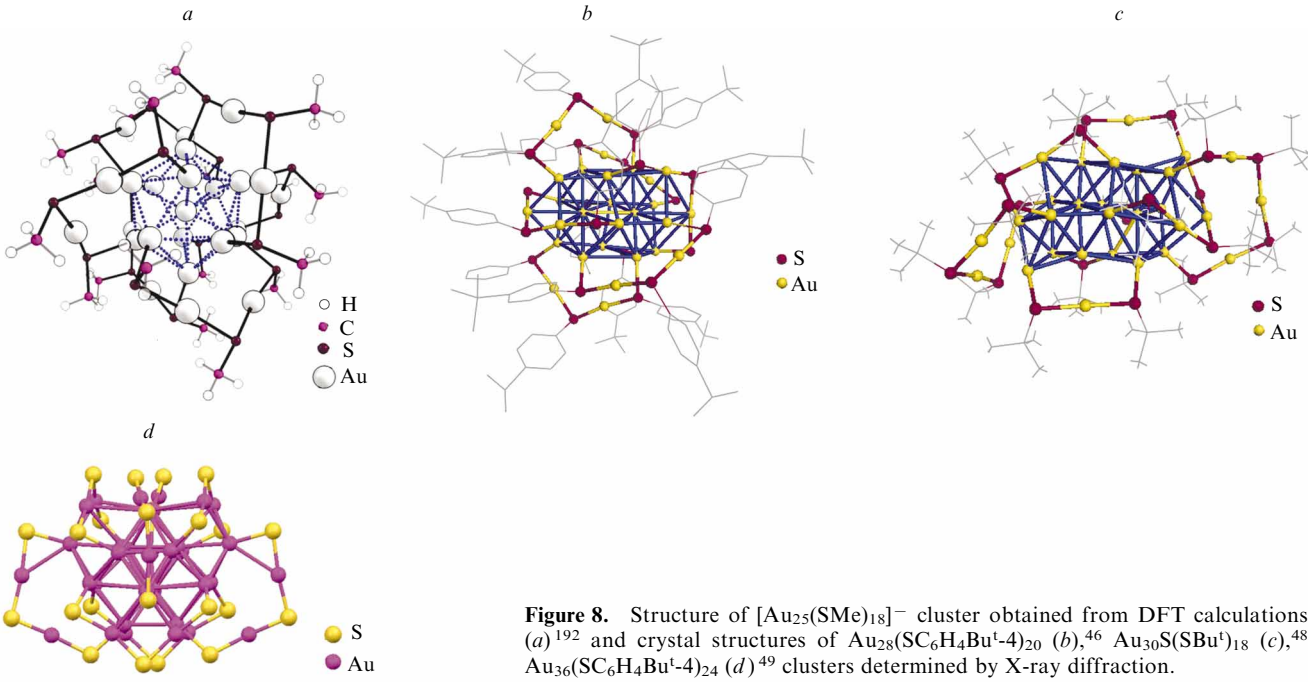


Figure 8. Structure of $[Au_{25}(SMe)_{18}]^-$ cluster obtained from DFT calculations (*a*)[192] and crystal structures of $Au_{28}(SC_6H_4Bu^t\text{-}4)_{20}$ (*b*),[46] $Au_{30}S(SBu^t)_{18}$ (*c*),[48] $Au_{36}(SC_6H_4Bu^t\text{-}4)_{24}$ (*d*)[49] clusters determined by X-ray diffraction.

This is the only cluster with μ-coordination of the S^{2-} anion. It follows that the core of the $Au_n(SR)_m$ clusters can be stabilized by not only $SR(AuSR)_x$ 'staple' units, but also involving the μ-S^{2-} group.

$Au_{36}(SR)_{24}$ (R = $C_6H_4Bu^t$-4; n_e = 12). The Au_{28} core represents a truncated fcc tetrahedron stabilized by four $SR(AuSR)_2$ dimers, the remaining twelve RS groups being coordinated to the gold atoms on the core surface (Fig. 8 *d*).[49] The HOMO–LUMO gap obained from DFT calculations is 1.7 eV, thus indicating high electronic stability of the cluster.

$Au_{38}(SR)_{24}$ [R = CH_2Bn, C_nH_{2n+1} (n = 6, 10, 12); n_e = 14]. As mentioned above, isolation of an individual cluster from a crude mixture and determination of its composition is a complicated task which has no unambiguous solution. An example is provided by checkered history of the synthesis of the $Au_{38}(SR)_{24}$ cluster. In 2004, Murray and co-workers [198] reported the synthesis of a new cluster of the general formula $Au_{38}(SCH_2Bn)_{24}$. Later on, it was found that the cluster composition is $[Au_{25}(SCH_2Bn)_{18}]^-$.[113] Consequently, a question arose regarding the existence of $Au_{38}(SR)_{24}$ clusters. These systems were synthesized as $Au_{38}(SC_nH_{2n+1})_{24}$ (n = 6, 10, 12) [67] and $Au_{38}(SCH_2Bn)_{24}$.[118, 199] Mass spectrometric and UV–Vis absorption spectroscopy studies confirmed individual character of these compounds.

Experimental investigations of the $Au_{38}(SR)_{24}$ clusters were accompanied by structure elucidation within the framework of DFT.[20, 65, 67, 68, 200] The main goal was to determine the composition of the cluster core and shell. According to the first model by Häkkinen, gold atoms of the cluster form an Au_{38} truncated octahedron with the outer layer comprised of six square Au_4 units and the shell formed by twenty-four RS groups.[20] It was found that the symmetric model experiences strong structural relaxation.[200] The other structure proposed [68] for $Au_{38}(SR)_{24}$ was based on the 'divide and protect' concept,[65] which postulates that gold atoms may be constituents of the cluster shell. In the new structural model, the cluster was described by the revised formula $Au_{14}[(AuSR)_4]_6$ and comprised the Au_{14} core with O_h symmetry and six plain ring tetramers $(AuSR)_4$. A drawback of the formula $Au_{14}[(AuSR)_4]_6$ consists in low energy of the bond between the $(AuSR)_4$ unit and the Au_{14} core, which suggests the existence of yet another structure with stronger interaction between the core and shell atoms.

The next model proposed for $Au_{38}(SR)_{24}$ was based on the gold : sulfur atomic ratio. In this case, the Au_{24} core is surrounded by a shell comprising monomeric and dimeric units SR(AuSR) and $SR(AuSR)_2$, respectively.[201] Although the structure described by the formula $Au_{24}[Au(SR)_2]_6[Au_2(SR)_3)]_4$ was characterized by the lowest total energy among the models proposed earlier, it also appeared to be incorrect. The actual structure of the $Au_{38}(SR)_{24}$ cluster was theoretically predicted on the basis of structure similarity rules.[67] A total of five possible formulas with different core composition and 'staple' unit lengths were proposed for the cluster structure, namely, $Au_{2+24}[Au(SR)_2]_{12}$, $Au_{3+22}[Au(SR)_2]_9[Au_2(SR)_3]_2$, $Au_{4+20}[Au(SR)_2]_6[Au_2(SR)_3]_4$, $Au_{5+18}[Au(SR)_2]_3[Au_2(SR)_3]_6$ and $Au_{6+16}[Au_2(SR)_3]_8$. Based on the results of total energy calculations, the $Au_{5+18}[Au(SR)_2]_3[Au_2(SR)_3]_6$ cluster with

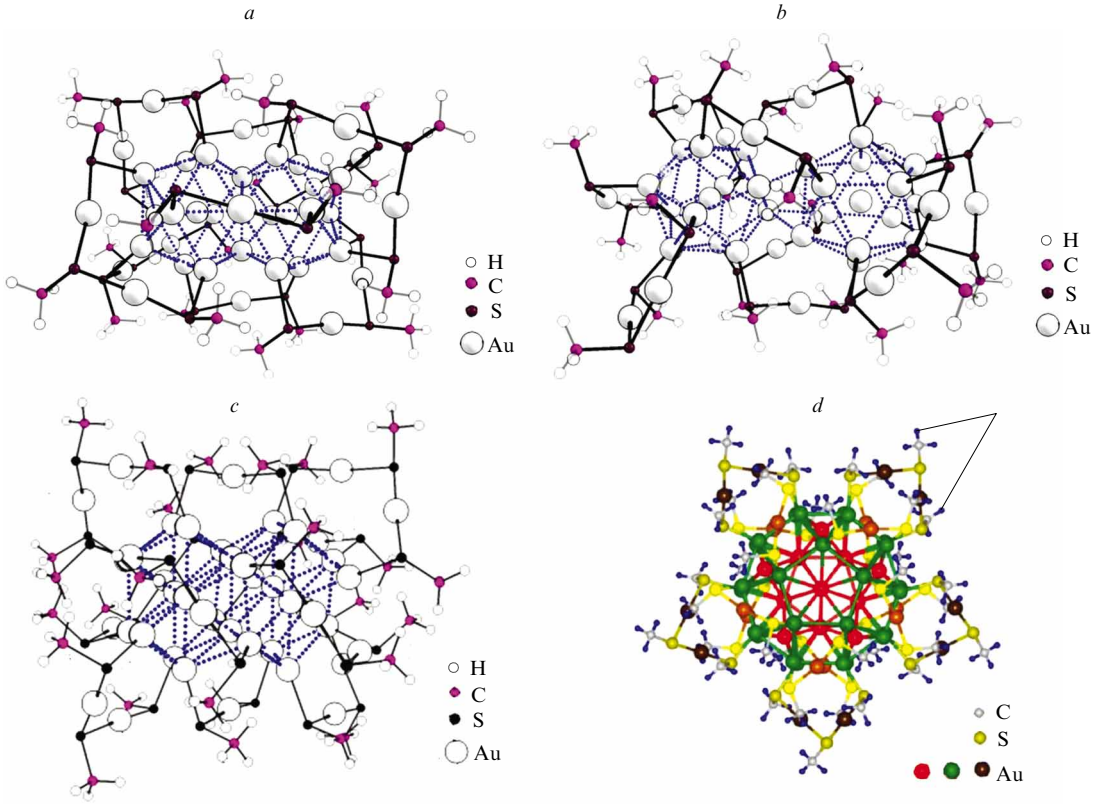


Figure 9. Structures of $Au_{38}(SMe)_{24}$ (*a*),[67] $Au_{40}(SMe)_{24}$ (*b*),[204] $[Au_{44}(SMe)_{28}]^{2-}$ (*c*) [206] and $[Au_{67}(SMe)_{35}]^{2-}$ (*d*) [166] clusters obtained from DFT calculations.

R = Me was chosen to be the most plausible model for the structure of the $Au_{38}(SR)_{24}$ system.[67] Here, one deals with a prolate Au_{23} cluster core formed by two Au_{13} icosahedra fused together *via* sharing a common Au_3 face (Fig. 9 *a*). Six $Au_2(SMe)_3$ units are coordinated to the icosahedra, while three $Au(SMe)_2$ units are bonded to the central atoms of the core. Large HOMO–LUMO gap value (0.9 eV) obtained for this structure points to high stability of the model.

An X-ray diffraction study[50] of the $Au_{38}(SCH_2Bn)_{24}$ cluster indeed revealed fused Au_{23} icosahedra stabilized by six dimeric and three monomeric 'staple' units in excellent agreement with the theoretically predicted structure.[67] The chirality of the $Au_{38}(SCH_2Bn)_{24}$ cluster arises from different arrangement of the 'double propeller' staple units and corresponding formation of two enantiomers. The energy barrier to interconversion of the enantiomers is low, so the cluster loses optical activity at at 40 °C.[202] This makes the cluster of limited use in asymmetric catalysis and as component of chiral sensors at temperatures above 40 °C. The problem can be solved by introducing one or two 1,1′-binaphthyl-2,2′-dithiol substituents into the cluster.[203] In this case, the energy barrier to interconversion of enantiomers increases and the optical properties of the cluster are retained in a wide temperature range.

$Au_{40}(SR)_{24}$ (R = CH_2Bn; n_e = 16). Cluster $Au_{40}(SCH_2Bn)_{24}$ was isolated recently.[164, 199] Its theoretically predicted structure has not been confirmed by X-ray diffraction as yet. The stabilities of the available structural models were studied by DFT.[204] The lowest-energy structure obtained from DFT calculations is shown in Fig. 9 *b*. The cluster core, Au_{26}, is formed by two Au_{13} icosahedra having an edge–edge contact, rotated by 90° to each other. The cluster shell comprises six SR(AuSR) monomers and four $SR(AuSR)_2$ dimers. Good reproduction of the experimental optical spectrum of the cluster[164] obtained using this model holds out a hope of correct structure determination. It is noteworthy that, similarly to $Au_{38}(SR)_{24}$, the $Au_{40}(SR)_{24}$ cluster does not belong to the 'magic' clusters, being comprised of two subunits, each obeying the electron count rule for stable systems.

$[Au_{44}(SR)_{28}]^{2-}$ (R = Ph; n_e = 18). The $[Au_{44}(SPh)_{28}]^{2-}$ cluster was synthesized and isolated,[205] but its structure was not determined by X-ray diffraction. Based on the structure principles, two model stuctures were proposed for $[Au_{44}(SMe)_{28}]^{2-}$.[165] In the first model, the cluster composition is $Au_{28}[SRAuSR]_8[SR(AuSR)_2]_4$, the Au_{28} core is surrounded by eight monomeric and four dimeric 'staple' units; the second model assumes the existence of a polymeric shell $SR(AuSR)_x$ and the core composition Au_{16}. According to DFT calculations of the energies of two isomeric clusters, the former model is 2 eV more stable than the latter. The theoretical diffraction pattern of the dimeric-monomeric model better agrees with experimental data.[205] However, an analysis of the electronic structure of the $Au_{28}[SRAuSR]_8[SR(AuSR)_2]_4$ cluster revealed an open-shell structure; therefore, the structure may appear to be unstable. The calculated optical spectra of both model structures are in poor agreement with the measured spectrum.[205] We believe these facts suggest that a more correct model for the $[Au_{44}(SR)_{28}]^-$ cluster can be proposed. Yet another predicted structure[206] is similar to those of $Au_{28}(SC_6H_4Bu^t_4)_{20}$ (Ref. 46) and $Au_{36}(SC_6H_4Bu^t_4)_{24}$.[49] The binuclear core of the Au_{26} cluster is stabilized by eight $SR(AuSR)_2$ and two SR(AuSR) groups (see Fig. 9 *c*). The energy of the $Au_{26}[SRAuSR]_2[SR(AuSR)_2]_8$ cluster obtained from PBE/TZP calculations is 1.02 eV lower than that of the $Au_{28}[SRAuSR]_8[SR(AuSR)_2]_4$ structure.[165]

$[Au_{67}(SR)_{35}]^{2-}$ (R = CH_2Bn, C_6H_{13}; n_e = 34). Very recently, the cluster containing 67 gold atoms was synthesized and its composition was determined.[166] As was shown theoretically, the inner part of the Au_{30} core comprises two pentagonal 'caps' surrounded by the outer layer containing seventeen gold atoms that form a distorted pentagonal prism (see Fig. 9 *d*). The cluster core is stabilized by ten monomeric and five dimeric 'staple' units. The cluster bears a charge of 2− which corresponds to two valence electrons. This is sufficient to form a stable state within the framework of the superatom model. The calculated HOMO–LUMO gap is 0.75 eV, thus indicating high stability of the cluster. Nevertheless, the optical spectrum and the differential pulse voltammogram of the $[Au_{67}(SR)_{35}]^{2-}$ cluster correspond to simultaneous presence of molecular clusters and particles a few micrometres in size in the sample. Therefore, one can assume that $[Au_{67}(SR)_{35}]^{2-}$ occupies an intermediate position between molecular clusters and clusters with metallic properties.

$Au_{102}(SR)_{44}$ (R = $C_6H_4CO_2H$-4; n_e = 58). The determination of the crystal structure of $Au_{102}(SC_6H_4CO_2H\text{-}4)_{44}$ (Ref. 51) contributed largely to the development of a unified theory of the structure of clusters stabilized by sulfur-containing ligands. The crystal lattice of $Au_{102}(SC_6H_4CO_2H\text{-}4)_{44}$ is formed by pairs of enantiomeric clusters. The arrangement of gold atoms in the each cluster core corresponds to an Au_{39} dodecahedron with a radius of 5.3 Å, which is surrounded by two twenty-atom 'caps' of radius 6.1–6.4 Å (Fig. 10 *a*). The cluster structure can be described by the formula $Au_{79}[SR(AuSR)]_{19}[SR(AuSR)_2]_2$, which corresponds to the shell comprising nineteen [SR(AuSR)] monomeric units and two $[SR(AuSR)_2]$ dimeric units. The chirality of the cluster originates from the peculiar arrangement of the 'staple' ligands.

Stability of the $Au_{102}(SC_6H_4CO_2H\text{-}4)_{44}$ cluster was explained using the superatom theory.[66] Later on, DFT calculations of the geometry and electronic properties of the $Au_{102}(SC_6H_4CO_2H\text{-}4)_{44}$ cluster[207–210] revealed three reasons for its stability, *viz.*, large HOMO–LUMO gap (0.5 eV),[207, 208] optimum distribution of the 'staple' units on the core and high thermodynamic stability against disintegration into smaller clusters.[209] An analysis of the radial electron density distribution in the $Au_{102}(SC_6H_4\text{-}CO_2H\text{-}4)^q_{44}$ cluster (q = 0, ±1)[20] showed that the Au_{79} core is almost electrically neutral and can be treated as individual 'magic' cluster with closed electron shell. As to the charged clusters, main changes in the radial electron density distribution occur in the $Au_{23}(SC_6H_4CO_2H\text{-}4)_{44}$ shell and only 10% of changes fall on the region between the cluster core and shell. Similarly to the electronic structure of ligand-free small atomic clusters Au_n,[210] that of the Au_{79} core is characterized by a delocalized electron shell. The $Au_{102}(SC_6H_4CO_2H\text{-}4)_{40}(SC_6H_4Br\text{-}4)_4$ cluster obtained by ligand exchange is structurally similar to the $Au_{102}(SC_6H_4CO_2H\text{-}4)_{44}$ cluster.[211] Ligand exchange is assumed to proceed by the associative mechanism because the SC_6H_4Br-4 ligands are coordinated to neighbouring gold atoms.

$Au_{130}(SR)_{50}$ (R = $C_{12}H_{25}$; n_e = 80). The structure of this recently synthesized cluster[212, 213] was predicted in the PBE/DZ density functional calculations for R = H.[167] The

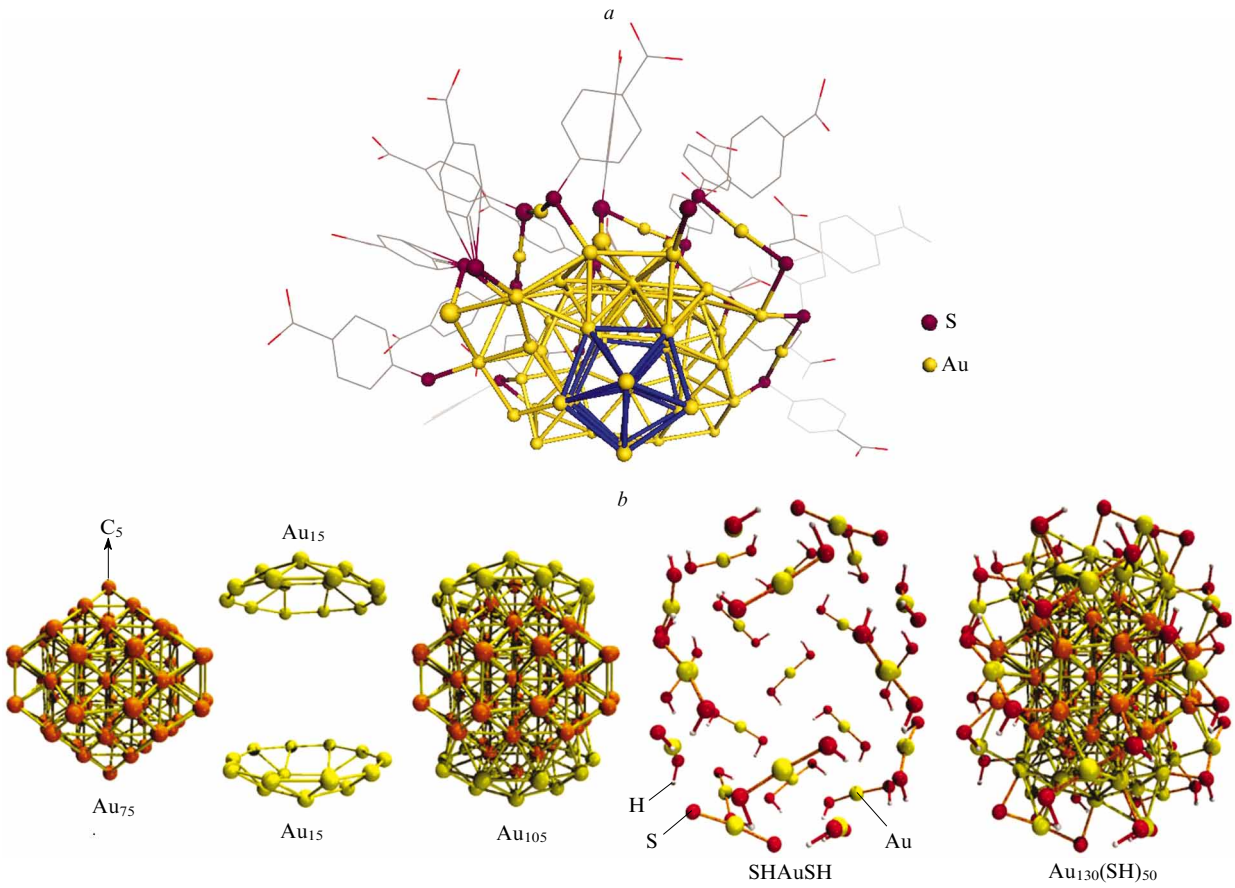


Figure 10. Structures of the upper fragment of the $Au_{102}(SC_6H_4CO_2H\text{-}4)_{44}$ cluster (based on X-ray data) (*a*)[51] and $Au_{130}(SH)_{50}$ cluster (obtained from DFT calculations) (*b*).[167]

cluster core represents an Au_{75} Marks decahedron capped by two Au_{15} hemispheres and stabilized by twenty-five SHAuSH units (see Fig. 10 *b*). Structurally, the cluster differs from other known $Au_n(SR)_m$ clusters in that gold atoms on the core surface form no bonds with RS groups.

$Au_{144}(SR)_{60}$ [$R = C_nH_{2n+1}$ ($n = 6$, 10, 12), CH_2Bn; $n_e = 84$]. The cluster composition, initially determined to be $Au_{144}(SR)_{59}$ ($R = C_nH_{2n+1}$),[67] was then refined and changed to $Au_{144}(SR)_{60}$ ($R = CH_2Bn$).[214] A recently published[215] method for the synthesis of monodisperse $Au_{144}(SR)_{60}$ cluster holds out a hope of crystallization and structure determination in the near future. Tentatively, the Au_{114} cluster core is stabilized by thirty monomeric 'staple' units.[216] It was also reported[217] that the cluster is in the pseudocrystalline state, namely, four cluster cores are arranged periodically, while the stabilizing ligands form an amorphous structure. Note that DFT quantum chemical studies of the properties and structure of this large cluster using known functionals are labour-consuming.[218] The $Au_{144}(SR)_{60}$ cluster is a popular model for simulating the interaction between functionalized thiols and gold particles using molecular dynamics.[219]

V.2. The nature of Au–SR interaction and the mechanism of formation of $[Au_n(SR)_m]^q$ clusters

The stability and variety of $Au_n(SR)_m$ clusters are due to formation of strong bonds between gold and sulfur atoms. High chalcophilicity of gold underlies the existence and properties of the ligand-protected clusters considered above, homoleptic and cyclic thiolate complexes of gold,[220,221] and influences the structure of self-assembled monolayers formed upon adsorption of sulfur-containing organic molecules on gold surface (Fig. 11). Self-assembled monolayers are of great practical value and their structure, electronic properties and mechanism of formation on the Au(111) face have been intensively studied.[28,222] Adsorption of thiol molecules, HSR, on the Au(111) surface is accompanied by dissociation of the H–S bond and formation of thiolates RS^-.[223] The coordination fashion of the RS groups to the gold surface remained unclear for long. Pioneering studies by DFT[224] and scanning tunneling microscopy[225] suggested three equivalent Au–SR covalent bonds for a thiolate group adsorbed on Au(111). Later on, it was found that the strongest bonding to the Au(111) face occurs in the case of bidentate bridging coordination, Au–S(R)–Au.[226–229] The Au(111) surface is modified through the interaction with RSH; this is the so-called 'herringbone reconstruction' accompanied by migration of gold atoms from the surface layer to the –RS–Au–SR– 'staple' unit (see Fig. 11).[230–236] These 'staple' bonds are also present in the cyclic complexes $(Au^ISR)_x$ (Ref. 237) and clusters $Au_n(SR)_m$. Thus, in spite of differences in the properties of the surface and the cluster, self-assembled monolayers and $Au_n(SR)_m$ exhibit the formation of similar 'staple' units.

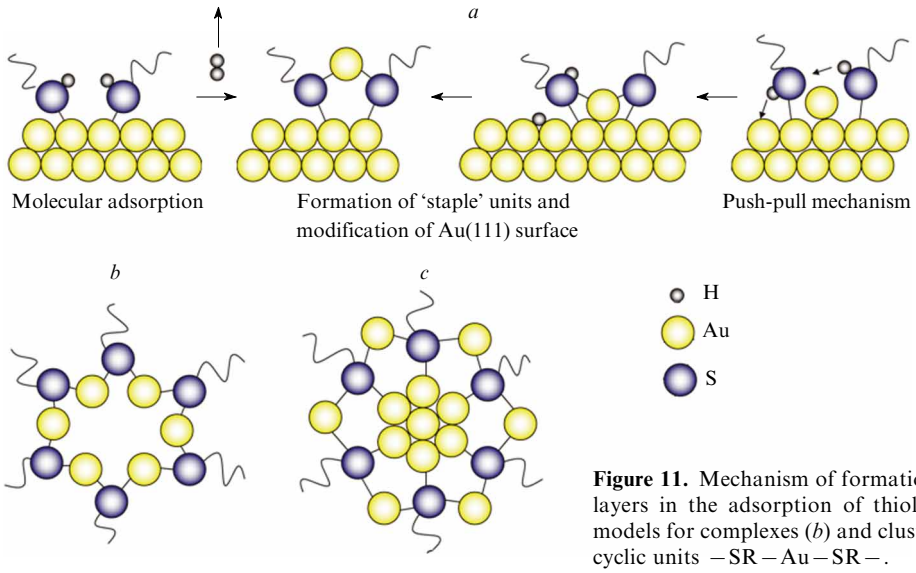


Figure 11. Mechanism of formation of self-assembled monolayers in the adsorption of thiols on gold surface (*a*) and models for complexes (*b*) and clusters (*c*) containing staple or cyclic units $-SR-Au-SR-$.

The formation of the $-RS-Au-SR-$ unit is preceded by the reaction of HSR with metal atoms of the cluster or surface. At low pressures, thiol is molecularly adsorbed on Au(111) with retention of the S–H bond.[229] If gold atoms have a small coordination number, one deals with dissociation of the S–H bond and formation of surface thiolates and molecular hydrogen. To clear the mechanism of formation of $Au_n(SR)_m$ clusters, which specifies the composition of the cluster being formed, one should know how hydrogen is eliminated from the thiol molecule. Our quantum chemical simulation of the process on the Au_{20} cluster

$$MeSH + Au_{20} \longrightarrow MeSH-Au_{20} \longrightarrow MeS-Au_{20}-H$$

showed that oxidative addition of thiol with dissociation of the S–H bond requires high activation energy.[29] The energy barrier to the formation of the $-SR-Au-SR-$ 'staple' bonds can be reduced in the case of co-adsorption of two MeSH molecules on the same site (vertex of the cluster).

$$2\,MeSH + Au_{20} \longrightarrow MeSH-Au_{20}-HSMe \longrightarrow$$
$$\longrightarrow Au(MeS)_2Au_{19} + H_2$$

A reaction following this new pathway proceeds by the push-pull mechanism and involves transfer of H^+ from one adsorbed MeSH molecule to the second MeSH molecule adsorbed on the same active site in the cluster. As a result, the gold atom no longer belongs to the cluster and a primary $HSR-Au-SR-Au$ unit, precursor of the 'staple' bond, is formed (see Fig. 11 *a*). This mechanism was confirmed theoretically taking clusters Au_n^q ($n = 2-8$, 12, 13, 20; $q = 0, \pm 1$) as examples.[238] This suggests that the shell of the $Au_n(SR)_m$ cluster is formed by a similar mechanism through migration of gold atoms from the surface of the Au_n cluster to the $-SR-Au-SR-$ units in the shell. However, the involvement of oxygen in the initial oxidation of thiol and in subsequent formation of the shell cannot be ruled out.

Besides, the $-SR-Au-SR-$ 'staple' units can form during the reaction between the starting complex $[AuCl_4]^-$ and thiol RSH prior to the formation of the cluster core (see Scheme 1). Homoleptic thiolate complexes $[Au^ISR]_x$ associate through formation of the metallic bond between the emerging Au^0 sites or small clusters constituting the core. As the cluster size increases, the core composition changes from Au_4 (a tetrahedron) to Au_{13} (an icosahedron) and then to Au_{39} (a dodecahedron). The presence of long 'staples', $SR(AuSR)_5$, in small clusters can be explained using the 'structure rule', according to which the smaller the gold : ligand ratio the longer the $SR(AuSR)_x$ units in the cluster. Larger $Au_n(SR)_m$ clusters can be stabilized by not only 'staple' bonds, but also RS and S^{2-} groups.

V.3. Selenolate-protected clusters

As mentioned above, the $Au_n(SR)_m$ clusters are difficult to crystallize because they are unstable in water. For instance, the characteristic peaks in the optical absorption spectrum of a solution containing $[Au_{25}(SC_8H_{17})_{18}]^-$ disappear after 48 h.[22] Degradation of the cluster in solution is a result of solvolysis upon dissociation of the Au(core)–SR bonds. Also, the $Au_n(SR)_m$ clusters are characterized by low thermal stability and laser radiation resistance. For instance, the $[Au_{25}(SC_8H_{17})_{18}]^-$ anion loses the alkyl group at 165 °C, while laser radiation causes detachment of $Au_4(SC_8H_{17})_4$ cyclic unit from the cluster shell.[22]

$$[Au_{25}(SC_8H_{17})_{18}]^- \longrightarrow [Au_{21}(SC_8H_{17})_{14}]^- + Au_4(SR)_4$$

If the ligand strongly interacts with the gold atoms on the core, ligand-protected clusters should be sufficiently stable. Stabilization of gold clusters using selenolate ligands seems to be promising because the Au–Se bond is characterized by a higher degree of covalency, being stronger than the Au–S bond.

Recently, clusters described by the general formula $[Au_{25}(SeR)_{18}]^-$ (R = $C_{12}H_{25}$, Ph) were synthesized and studied.[23,24] The clusters are structurally similar to $[Au_{25}(SR)_{18}]^-$. The $[Au_{25}(SeR)_{18}]^-$ cluster appeared to be more stable than the thiolate analogue, namely, the optical absorption spectrum of the solution containing $[Au_{25}(SeR)_{18}]^-$ showed no visible changes within 48 h.[22] But since the energy of the $Se-CH_2$ bond is lower than that of the $S-CH_2$ bond, elimination of the alkyl fragment from

$[Au_{25}(SeC_8H_{17})_{18}]^-$ occurs faster and the cluster disintegration temperature is reduced to 136 °C. Ligands with longer carbon backbone improve the thermal stability of $[Au_{25}(SeR)_{18}]^-$. For instance, the disintegration temperature of the $[Au_{25}(SeC_{12}H_{25})_{18}]^-$ cluster is 186 °C, being comparable with that of $[Au_{25}(SC_{12}H_{25})_{18}]^-$.[22] Presumably, this is a consequence of strengthening of van der Waals intramolecular interactions between ligands. The yield of $[Au_{21}(SeC_8H_{17})_{14}]^-$ units upon laser irradiation of the $[Au_{25}(SeC_8H_{17})_{18}]^-$ cluster is much lower compated to that of $[Au_{21}(SC_8H_{17})_{14}]^-$ after irradiation of the sulfur-containing analogue. Thus, replacement of S by Se improves the stability of the cluster against Au–Se bond dissociation, but makes it less stable against chalcogen–carbon bond dissociation.

Recently, the $Au_{38}(SeR)_{24}$ cluster with $R = C_{12}H_{25}$ was synthesized and its structure was determined by X-ray diffraction.[25] The cluster is structurally similar to the sulfur-containing analogue, $Au_{38}(SC_{12}H_{25})_{24}$; it is characterized by a smaller shift of electron density from the core atoms to the shell ones compared to $Au_{38}(SC_{12}H_{25})_{24}$. The potential of RSe ligands for the stabilization of clusters was confirmed by recent synthesis of a silver cluster $[Ag_{12}Ag_{20}[Ag_2(SePh)_5]_6]$.[239] Taking $[Au_{25}(TePh)_n(SC_8H_{17})_{18-n}]^-$ anions ($n = 1-18$) as examples, it was shown that a tellurium-containing ligand (TePh) makes the clusters less stable.[240]

V.4. Stabilization of $Au_n(C_2Ph)_m$ clusters through Au–C covalent bonds

Clusters can also be stabilized using organic ligands which form Au–C covalent bonds. Recently, gold clusters containing C≡CPh groups in the shell were synthesized.[26, 27] Clusters $Au_n(C_2Ph)_m$ were obtained from PVP-protected gold nanoparticles by ligand exchange with HC≡CPh in toluene.[26] According to mass spectrometry data, the reaction results in a mixture containing a total of ten $Au_n(C_2Ph)_m$ clusters with the following gold to ligand atom ratio (n, m): (43, 22), (46, 24), (52, 26), (54, 26), (59, 27), (71, 32), (90, 36), (94, 38), (101, 38) and (110, 40). To determine possible structures of these compounds, it is interesting to compare their compositions with those of the $Au_n(SCH_2Bn)_m$ clusters (Fig. 12). In both cases, the number of ligands in the shell increases with the number of gold atoms in the cluster. However, the $m:n$ ratio for the $Au_n(C_2Ph)_m$ clusters is smaller; therefore, the surface of the core of the Au_n cluster can coordinate a smaller number of C≡CPh groups compared with the SCH_2Bn groups.

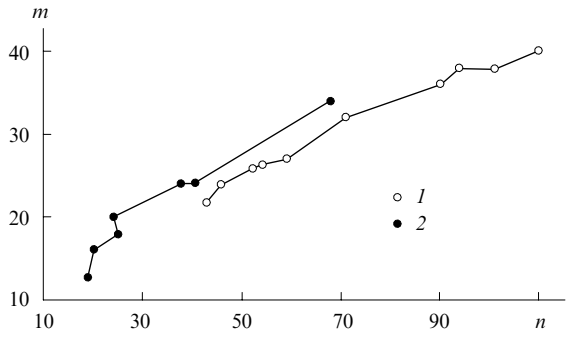


Figure 12. A comparison of the cluster compositions: $Au_n(C_2Ph)_m$ (*1*) and $Au_n(SCH_2Bn)_m$ (*2*).

By varying the synthesis conditions one can obtain a monodisperse fraction of $Au_n(C_2Ph)_m$ in high yield. For instance, the synthesis of the $Au_{54}(C_2Ph)_{26}$ cluster requires the use of Au_n hydrosol in PVP with a narrow nanoparticle size distribution (average particle size of 1.2 nm).[27] The $Au_{54}(C_2Ph)_{26}$ cluster was synthesized by adding the hydrosol to PhC_2H dissolved in chloroform; the yield was 90%. The use of toluene instead of $CHCl_3$ leads to a mixture of clusters and the yield decreases to 60%. The effect of solvent on the selectivity of the process can be explained by the fact that the simultaneously formed metastable clusters $Au_{43}(C_2Ph)_{22}$ and $Au_{46}(C_2Ph)_{24}$ are better soluble in chloroform than in toluene. This leads to an increase in their concentrations and favours more efficient transformation to the stable cluster $Au_{54}(C_2Ph)_{26}$ *via* bimolecular reactions.

A mass spectrometric study of the 'magic' cluster $Au_{54}(C_2Ph)_{26}$ confirmed its individual character.[27] All gold atoms belong to the 1.3 nm core. The average coordination number of gold atoms equal to 7.9 corresponds to cuboctahedral symmetry of the cluster core. An analysis of vibrational frequencies showed that the Au–C covalent bond is formed as a result of donor–acceptor transfer of electron density from the valence orbitals of gold atom to the antibonding π-orbitals of the alkynyl fragment. According to XPS data, transfer of electrons from atomic orbitals of gold to π-orbitals of the C_2Ph ligands leads to weakening of the C≡C bond.[27]

The $Au_n(C_2Ph)_m$ clusters are novel, poorly studied compounds with unknown structure. The covalent character of the Au–C bond in these systems was recently confirmed by physicochemical methods and DFT calculations.[241] It should be noted that their 'magic' composition cannot be explained within the framework of the superatom model. One can assume that the stability of $Au_n(C_2Ph)_m$ clusters of particular composition is due to high symmetry of the cluster core or is determined by the thermodynamic or kinetic stability of the particular cluster $Au_n(C_2Ph)_m$ in each step of decomposition.

VI. Gold clusters stabilized by phosphine ligands

Small atomic clusters $Au_{11}(PPh_3)_7X_3$ (X = CNR, SCN, SPy-4), $[Au_{13}(PMe_2Ph)_{10}Cl_2]^{3+}$, $[Au_{39}(PPh_3)_{14}Cl_6]^-$. Traditionally, the structure and properties of phosphine-stabilized clusters have been analyzed separately from those of thiolate-protected clusters. Classification and generalization of a considerable body of experimental data were precluded by the lack of universal theoretical concepts. Elaboration of the superatom theory made it possible to consider the structure and properties of the $Au_n(SR)_m$ and $Au_n(PR_3)_m$ clusters from a unified, electronic-structure point of view.

The $[Au_n(PR_3)_mX_y]$ clusters (X = CNR, SR, Cl) belong to the few ones with known structures. As in the case of thiolate clusters, the symmetric core, $Au_n(PR_3)_mX_y$, contains gold atoms only. But unlike thiolate ligands, the PR_3 ligands have little effect on the electronic structure of the cluster. The energy of the Au–PR_3 bond is too low to form stabilizing 'staple' units of the ligand shell. The $Au_n(PR_3)_mX_y$ clusters are stabilized in different fashion. The interaction of PR_3 ligands with gold atoms favours an increase in the hybridization of atomic orbitals of the metal

and enhancement of aurophilic interaction within the core, thus making the cluster core more stable.[242] The influence of the nature of ligands on the electronic structure of small gold clusters was studied within the framerwork of the DFT taking the bonding of donor ligands (PH_3, PMe_3, NH_3, NMe_3) with small clusters (Au_2, Au_4) as examples.[243] According to calculations, the bond energy and electronic effects increase in the order $NMe_3 \approx NH_3 < PH_3 < PMe_3$. In the text below we will consider specific features of the structure of phosphine-stabilized gold clusters.

$[Au_6(dppp)_4]^{2+}$ ($n_e = 4$). This is one of the first phosphine-stabilized gold clusters whose structure was determined by X-ray diffraction.[52] Four gold atoms form a tetrahedron, while the remaining two Au atoms are coordinated to two opposite edges (Fig. 13 *a*). Each terminal metal atom forms two Au–Au bonds and two bonds with ligands. This compound was used to obtain structurally similar clusters $[Au_7(dppp)_4]^{3+}$ and $[Au_8(dppp)_4Cl_2]^{2+}$.

$[Au_7(dppp)_4]^{3+}$ ($n_e = 4$). According to X-ray data, the cluster comprises the Au_6 bi-tetrahedron and one *exo* gold atom coordinated to the edge (see Fig. 13 *b*).[53] The vertices of the tetrahedron are linked by two dppp ligands through the *exo* gold atom, while the other two ligands are coordinated to the Au_6 edges. The stability of the cluster is due to the presence of four valence electrons; this n_e value corresponds to stable clusters with a prolate structure.

$[Au_8(dppp)_4Cl_2]^{2+}$ ($n_e = 4$). Six gold atoms form a bi-tetrahedron, while the two remaining (*exo*) gold atoms are coordinated to two opposite edges of the bi-tetrahedron (see Fig. 13 *c*).[54] Each *exo* gold atom is bridged to a vertex of the tetrahedron through the dppp ligand and coordinates, the Cl ligand. By analogy with the $[Au_7(dppp)_4]^{3+}$ cation, the two remaining dppp ligands connect the edges of the tetrahedron. Replacement of Cl ligands by C≡CR groups led to the $[Au_8(dppp)_4(C{\equiv}CR)_2]^{2+}$ clusters (R = Ph, Bu^n, 2-Py, 3-Py, 4-Py) exhibiting photoluminescent properties.[244]

$Au_{11}(PR_3)_7X_3$ (R = Ph; X = CNR, SCN, SPy-4, Cl; $n_e = 8$). The synthesis and crystallization of $Au_{11}(PPh_3)_7X_3$ clusters were followed by the determination of their crystal structure. It was found that the clusters have an icosahedral core; the PR_3 and X ligands are coordinated to twelve metal atoms of the core surface (see Fig. 13 *d*).[16, 35, 175, 245] The calculated HOMO–LUMO gap (1.5 eV for X = SR and 2.1 eV for X = Cl) suggests high electronic stability of these compounds. The total number of valence electrons is eight; changes in the symmetry type of electronic states in the HOMO–LUMO region correspond to the closed electron shell $1S^21P^6$. Structurally different groups X in the cluster

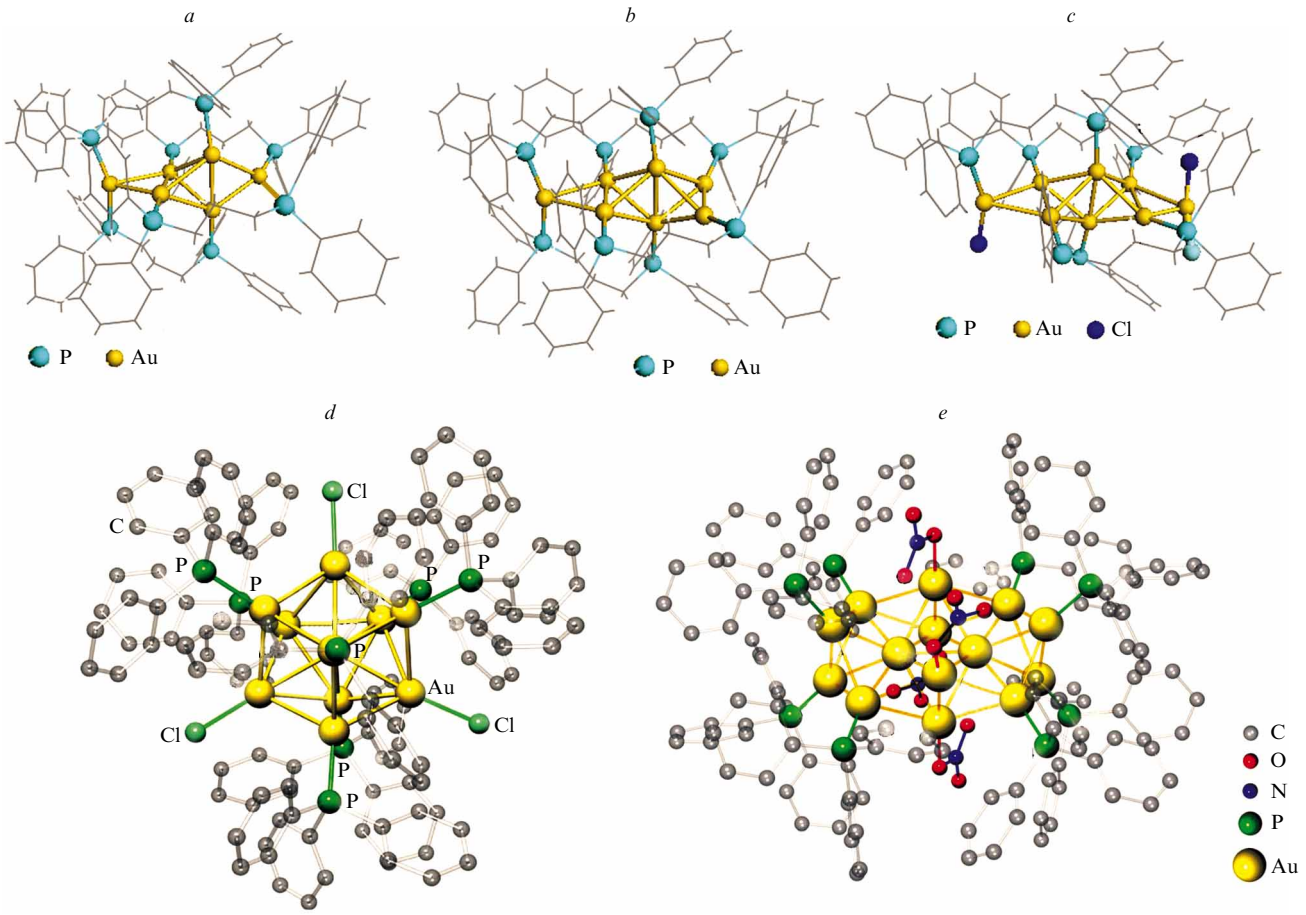


Figure 13. Crystal structures of clusters $[Au_6(dppp)_4]^{2+}$ (*a*),[52] $[Au_7(dppp)_4]^{3+}$ (*b*),[53] $[Au_8(dppp)_4Cl_2]^{2+}$ (*c*),[54] $Au_{11}(PPh_3)_7Cl_3$ (*d*)[175] and $Au_{14}(PPh_3)_8(NO_3)_4$ (*e*)[57] according to X-ray data.

have similar functions, *viz*., they create steric protection and stabilize the cluster core.

$[Au_{13}(PMe_2Ph)_{10}Cl_2]^{3+}$ and $[Au_{13}(dppe)_5Cl_2]^{3+}$ (dppe is 1,2-bis(diphenylphosphino)ethane; $n_e = 8$). The $[Au_{13}(PMe_2Ph)_{10}Cl_2]^{3+}$ cluster was synthesized and structurally characterized by X-ray diffraction.[56] Later on, the icosahedral structure of the cluster core was confirmed by cam-B3LYP/LANL2dz calculations.[242,246] The HOMO–LUMO gap calculated for the model cluster $[Au_{13}(PH_3)_{10}Cl_2]^{3+}$ is rather large (1.8 eV), as in the clusters with the Au_{11} core. Recently, the $[Au_{13}(dppe)_5Cl_2]^{3+}$ cluster was synthesized from a mixture of small gold clusters Au_n ($9 \leqslant n \leqslant 15$) in the presence of HCl.[247]

$$Au_2(dppe)Cl_2 \xrightarrow{NaBH_4,\ CH_2Cl_2} Au_n(dppe)_xCl_2 \xrightarrow{HCl,\ EtOH} [Au_{13}(dppe)_5Cl_2]Cl_3$$

$[Au_{14}(PPh_3)_8(NO_3)_4]$ ($n_e = 10$). According to X-ray data, this cluster has two central atoms and is characterized by short Au–Au distances (2.5817–2.9839 Å) (see Fig. 13 *e*).[57] This is the one and only example of the cluster with the ONO_2 ligand in the shell. The molecular and electronic structure calculations of the cluster revealed a closed electron shell.

$[Au_{20}\{PPh(Py\text{-}2)_2\}_{10}Cl_4]^{2+}$ ($n_e = 14$). The cluster core comprises two incomplete Au_{11} icosahedra fused *via* sharing two vertices (Fig. 14 *a*).[58] The overall stability of the cluster arises from considerable stabilization of the core by the bidentate $PPh(Py\text{-}2)_2$ ligands. The HOMO–LUMO gap is large than those of the $Au_{25}(SCH_2Bn)_{16}$ and Au_{20} clusters, namely, 2.24 eV *vs*. 2.15 and 1.77 eV, respectively. Since the number of valence electrons in the cluster does not obey the electron count rule for the closed shell, the stability of the system was not explained for long. It was proposed[248] to treat the cluster as two subunits, each having a closed shell containing seven own valence electrons and one electron from the neighbouring subunit.

$[Au_{20}(PP_3)_4]^{4+}$ (PP_3 is tris[2-(diphenylphosphino)ethyl]-phosphine; $n_e = 16$). According to X-ray data, the Au_{13} core is 'capped' by seven gold atoms (see Fig. 14 *b*).[59,60] The unusual cluster structure is due to high coordinative ability of the PP_3 ligands, namely, one PP_3 ligand is coordinated to four metal atoms from the 'cap', while the three remaining PP_3 ligands coordinate one Au atom from the 'cap' and three Au atoms from the core. The chirality of the cluster originates from peculiar structure of the core rather than the arrangement of ligands.[249] It is noteworthy that three gold atoms in the cluster are not coordinated by the PP_3 ligands; this offers prospects for application of this compound in catalysis.

$[Au_{20}(PPh_3)_8]^{2+}$ ($n_e = 18$). The Au_{20} cluster coordinated by eight PPh_3 ligands was obtained in a solution in pyridine.[250] Tentatively, the cluster has a tetrahedral structure like a cluster in the gas phase[141] and the Au_{20} particle immobilized on carbon surface.[34] When heated, $[Au_{20}(PPh_3)_8]^{2+}$ readily loses four ligands bonded to the gold atoms on a cluster facet and undergoes transformation to a stable cation $[Au_{20}(PPh_3)_4]^{2+}$ (in Fig. 14 *c* this transition is shown for the model cluster $[Au_{20}(PH_3)_8]^{2+}$). The four remaining PPh_3 ligands are coordinated to the top atoms. A large HOMO–LUMO gap of 1.44 eV obtained from DFT calculations of the neutral cluster $Au_{20}(PPh_3)_8$ suggests high stability of the system. However, calculations predict low first and second ionization potential for the neutral cluster, so the species can be readily oxidized to $[Au_{20}(PPh_3)_8]^{2+}$.

$[Au_{22}(dppo)_6]$ [dppo is 1,8-bis(diphenylphosphino)octane; $n_e = 22$]. The cluster was synthesized, crystallized and characterized by X-ray diffraction. It comprises two Au_{11} units linked by four PR_3 ligands (Fig. 15 *a*).[61] The other two PR_3 ligands are coordinated to the oppositely lying vertices of the Au_{22} core. Eight gold atoms in the cluster are accessible to reactants, being potential active sites in catalytic reactions. The HOMO–LUMO gap (1.9 eV) suggests a stable cluster.

$[Au_{24}(PPh_3)_{10}(SCH_2Bn)_5ClBr]^+$ ($n_e = 16$). According to X-ray data, the cluster represents two incomplete Au_{12} icosahedra linked by edge SR ligands (see Fig. 15 *b*).[62] The halide ligands, Cl and Br, are coordinated to the two apex gold atoms, while the PPh_3 ligands are coordinated to other ten metal atoms on the core surface. The cluster has a prolate geometry and a stable electronic structure ($n_e = 16$); the HOMO–LUMO gap is 1.35 eV.[62]

$[Au_{25}(PPh_3)_{10}(SC_nH_{2n+1})_5Cl_2]^{2+}$ ($n = 2-18$; $n_e = 16$). The cluster was synthesized by the reaction of $[Au_{11}(PPh_3)_8Cl_2]^+$ with n-alkanethiols $C_nH_{2n+1}SH$ ($n = 2$, 8, 10, 12, 14, 16, 18).[63] According to X-ray data, the cluster structure is formed by two Au_{13} icosahedra sharing a common vertex (see Fig. 15 *c*). Two Au_5 pentagons separated by the central gold atom are linked by the thiolate ligands. Gold atoms from peripheral pentagons coordinate

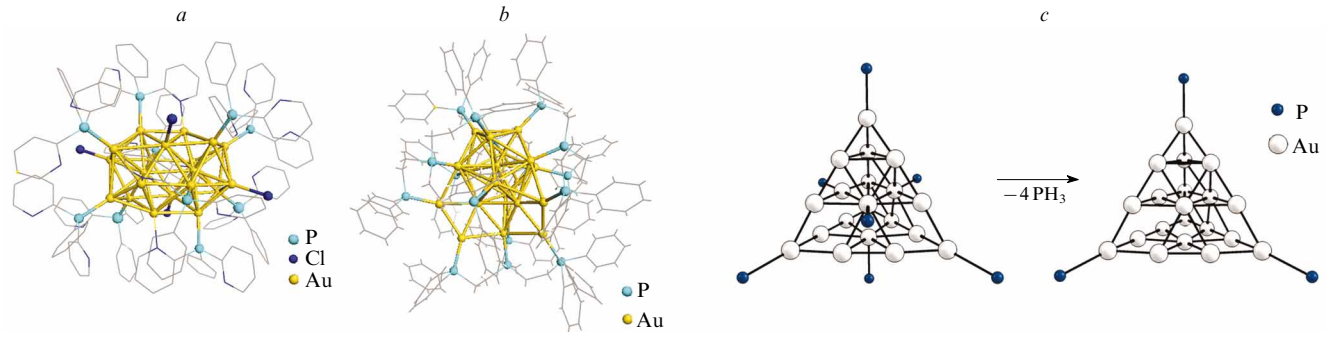


Figure 14. Crystal structures of clusters $[Au_{20}\{PPh(Py\text{-}2)_2\}_{10}Cl_4]^{2+}$ (*a*)[58] and $[Au_{20}(PP_3)_4]^{4+}$ (*b*)[59,60] determined by X-ray diffraction and structures of clusters $[Au_{20}(PH_3)_8]^{2+}$ and $[Au_{20}(PH_3)_4]^{2+}$ obtained from DFT calculations (*c*).[250]

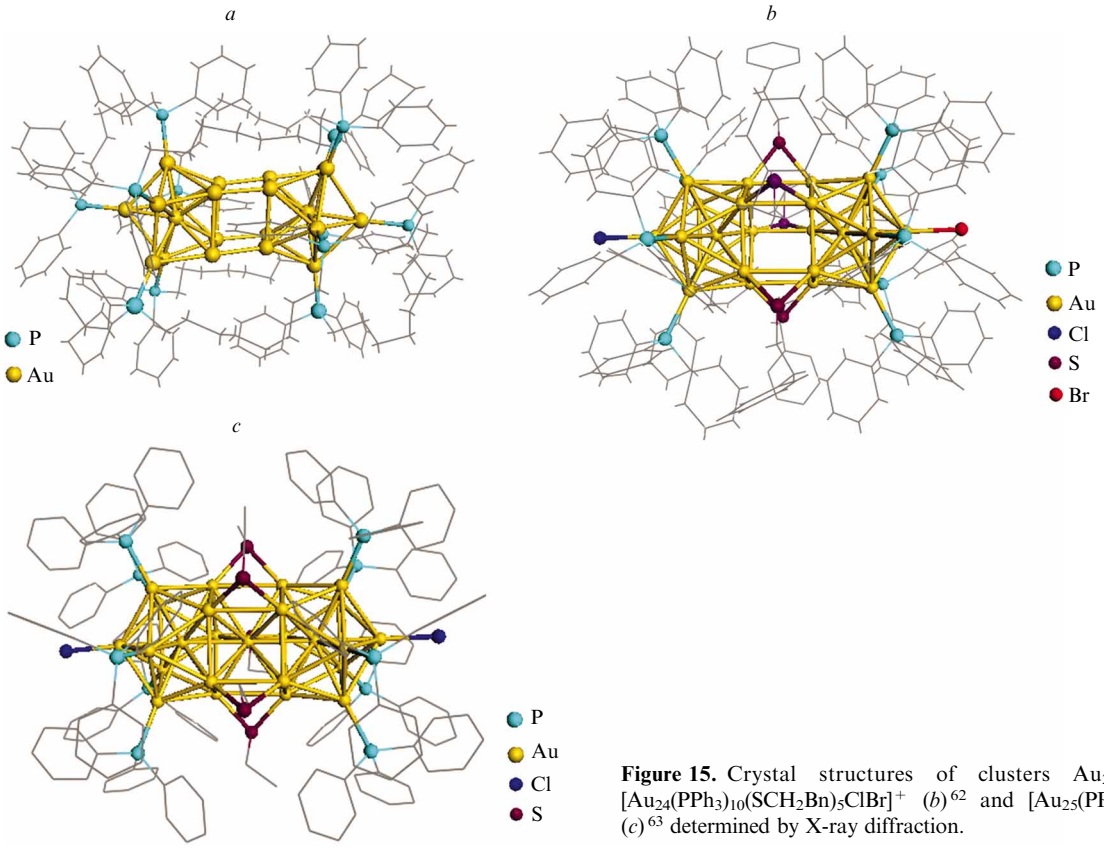


Figure 15. Crystal structures of clusters $Au_{22}(dppo)_6$ (*a*),[61] $[Au_{24}(PPh_3)_{10}(SCH_2Bn)_5ClBr]^+$ (*b*)[62] and $[Au_{25}(PPh_3)_{10}(SEt)_5Cl_2]^{2+}$ (*c*)[63] determined by X-ray diffraction.

ten triphenylphosphine ligands. The theoretically predicted optical properties of the cluster are due to specific features of the interaction of valence electrons in the two icosahedra, while the cluster stability is ensured by the closed electron shells ($n_e = 8$) in the two icosahedra.[251] Replacement of the central gold atoms in the icosahedra by Hg and Pt atoms gives the $[HgPtAu_{23}(PR_3)_{10}(SMe)_5Cl_2]^{2+}$ cluster characterized by a large dipole moment.[252]

$[Au_{39}(PPh_3)_{14}Cl_6]^-$ ($n_e = 34$). For long, this was the largest gold cluster with the unambiguously determined structure.[17] Two Au_{19} units represent a fragment of the hcp structure; they are rotated by 30° relative to each other and form an antiprismatic cavity with the Au atom at the centre. The calculated HOMO–LUMO gap equals 0.8 eV and thus points to high stability of the cluster. A symmetry analysis of the frontier orbitals revealed that all states with mainly F-character are filled, thus indicaiting the formation of a closed electron shell ($1S^21P^61D^{10}2S^21F^{14}$) for the thirty-four electrons delocalized over the cluster core, which corresponds to full acceptance of six electrons by the Cl atoms.

Major component of commercially available reagent Nanogold®: cluster $Au_{55}(PPh_3)_{12}Cl_6$. The so-called 'Schmid cluster'[37] with the tentative formula $Au_{55}(PPh_3)_{12}Cl_6$ is the major component of the commercially available product Nanagold®, which contains gold nanoparticles with an average size of 1.4 nm. Although the reagent is widely used, the structure, exact formula and molecular mass of its major component are unknown.[21] This is probably due to the fact that the product synthesized according to Schmid contains clusters of different composition and size, namely, $[Au_{39}(PPh_3)_{14}Cl_6]^-$, $Au_{101}(PPh_3)_{21}Cl_5$, $Au_{99}(PPh_3)_{24}Cl_{12}$, *etc.*[253–261] In particular, the mass spectra of Nanogold® exhibit three peaks corresponding to clusters with masses of 8, 13 and 18 kDa.[256] The peaks cannot be assigned to $[Au_{39}(PPh_3)_{14}Cl_6]^-$ (12 kDa) or $Au_{55}(PPh_3)_{12}Cl_6$ (14 kDa). Based on the superatom concept, it was assumed that the reagent contains $Au_{46}(PPh_3)_{12}Cl_6$, $Au_{67}(PPh_3)_{14}Cl_8$ and $[Au_{69}(PPh_3)_{20}Cl_{12}]^-$ (Fig. 16 *b*).[261]

However, a recent study[257] of the composition of Nanogold® confirmed the formula $Au_{55}(PPh_3)_{12}Cl_6$ proposed by Schmid. The structure and properties of the $Au_{55}(PPh_3)_{12}Cl_6$ cluster were studied by quantum chemical methods.[258–261] Different polyhedra were used to describe metallic core geometry, namely, a cuboctahedron, an icosa-

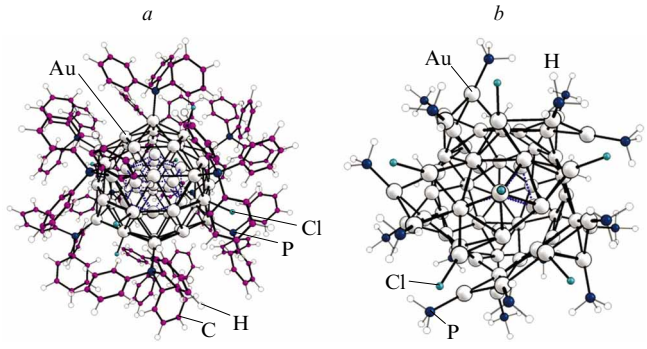


Figure 16. Tentative structures of commercially available Nanogold®: clusters $Au_{55}(PPh_3)_{12}Cl_6$ (*a*)[258] and $[Au_{69}(PH_3)_{20}Cl_{12}]^-$ (*b*).[261]

hedron and a decahedron. According to calculations, the icosahedral structure (see Fig. 16 *a*) is 2.23 eV more stable that the cuboctahedral one.[258] The stability of $Au_{55}(PPh_3)_{12}Cl_6$ has no explanation within the framework of the superatom theory. Probably, the stability of this cluster is determined by high symmetry. The 55-atom icosahedral fragments are known to form cluster cores, so large stable particles often contain the icosahedral fragments.[216] A high symmetry of the cluster polyhedron (icosahedron, decahedron, truncated octahedron) will favour its stability. Thus, the presence of highly symmetric fragments plays the decisive role in the formation of large clusters.

VII. Bimetallic clusters $M_xAu_nL_m$ (M = Pd, Pt, Cu, Ag)

Using the superatom theory, one can predict the stability of ligand-protected gold clusters when Au atoms are replaced by atoms of other metals. As mentioned above, $[Au_{25}(SR)_{18}]^-$ has a total of eight valence electrons. When a gold atom is replaced by the atom of a metal (M) having x valence electrons, the stable eight-electron configuration of the $[MAu_{24}(SR)_{18}]^q$ cluster will persist under the following conditions [see Eqn (1)]:

$$x + 24 - 18 - q = 8$$

$$x = q + 2$$

Usually, the total charge of the cluster (q) equals ± 2, ± 1, or 0. Therefore, a corresponding formula can be proposed for all metals in the periodic system using the possible oxidation states in the cluster. For instance, singly doped clusters containing Ni, Pd or Pt atoms with d^{10} electronic configuration ($x = 0$) are described by the formula $[MAu_{24}(SR)_{18}]^{2-}$, while clusters containing Group I metal atoms ($x = +1$) are described by the formula $[MAu_{24}(SR)_{18}]^-$.

There is a number of nonequivalent positions for the M atom in metal-doped clusters MAu_nL_m, *viz*., at the centre of the cluster, on the surface of the core or in the shell (Fig. 17). In most bimetallic systems, the heteroatom occupies a symmetric position at the centre.

The compositions of the MAu_nL_m clusters predicted using the concept of closed-shell electronic configuration can be tested by carrying out geometry optimization and total energy calculations; most often, DFT methods are used. A study of the $[MAu_{24}(SR)_{18}]^q$ clusters with the M atom at the centre made it possible to specify the possible metals M.[262] There is a total of 16 chemical elements suitabe for doping with retention of the closed electron shell and icosahedral structure of the cluster core. The existence of the following clusters was predicted: $[MAu_{24}(SR)_{18}]^{2-}$ (M = Pd, Pt, Ni), $[MAu_{24}(SR)_{18}]^-$ (M = Ag, Cu) and $[MAu_{24}(SR)_{18}]^{2+}$ (M = Ge, Sn). Clusters doped with Ni, Pt and Pd have the largest HOMO–LUMO gap, thus being the most stable.

Intensive experimental and theoretical research into doped gold clusters began with the synthesis of $PdAu_{24}(SR)_{18}$ (R = CH_2Bn, C≡CPh, $C_{12}H_{25}$).[94, 96, 263, 264]

Density functional calculations of $[PdAu_{24}(SMe)_{18}]^q$ ($q = \pm 2, \pm 1, 0$) revealed the most stable structure for a neutral cluster with the core–shell structure and the Pd atom at the centre of the core.[94]

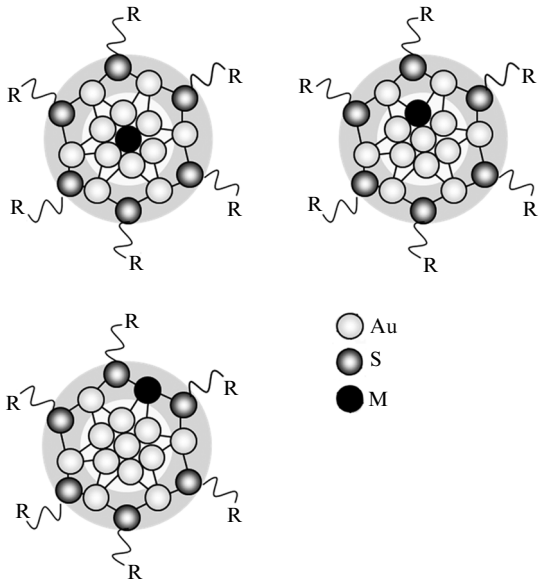


Figure 17. Different location of metal atom (M) in $[MAu_n(SR)_m]^q$ clusters.

Later on, the central position of the Pd atom in $PdAu_{24}(SC_{12}H_{25})_{18}$ was confirmed by Mössbauer spectroscopy and XPS.[265] The core–shell structure is also characteristic of other palladium-doped gold clusters, *e.g*., $[PdAu_{12}(PPh_3)_8Cl_4]^-$ (Ref. 12) and $PdAu_{37}(SCH_2Bn)_{24}$.[96] The stability of the $[PdAu_{24}(SR)_{18}]$ cluster is due to an increase in the $Pd-Au_{12}$ (core surface) and core–shell interaction energies compared with those obtained for the $Au_{25}(SR)_{18}$ cluster.[262] The thermodynamic stability of $PdAu_{24}(SMe)_{18}$ was predicted theoretically[266] and confirmed experimentally for $PdAu_{24}(SC_{12}H_{25})_{18}$.[94]

All $PdAu_{24}(SR)_{18}$ clusters that were isolated and investigated bear a zero charge, although the superatom theory predicts an anionic character of these systems ($q = -2$). Presumably, the formation of the $[PdAu_{24}(SR)_{18}]^{2-}$ cluster is accompanied by ready oxidation by atmospheric oxygen. For instance, an analysis of products formed during the synthesis of $PdAu_{24}(SR)_{18}$ revealed a small amount of $[PdAu_{24}(SR)_{18}]^-$.[96] Doped clusters containing different 'magic' numbers of gold atoms can exist. Recently, the $PdAu_{37}(SR)_{24}$ cluster was synthesized and studied.[96] The catalytic properties of the $PdAu_{37}(SR)_{24}$ and $PdAu_{24}(SR)_{18}$ clusters were studied taking selective hydrogenation of α,β-unsaturated ketones to corresponding alcohols as an example; the catalysts appeared to to be highly active in the reaction and provided a high conversion.[96] Synergistic effects in catalysis were also reported for nanoalloys based on gold.[267]

Platinum also forms singly doped clusters.[268] To date, the $PtAu_{24}(SCH_2Bn)_{18}$ cluster was synthesized.[269] Its structure and electronic properties were studied by XPS, EXAFS and theoretically using DFT calculations.[270] The Pt atom occupies position at the core centre, similarly to $PdAu_{24}(SR)_{18}$. A DFT study of unusual trimetallic cluster $PtAu_6Ag_6(AgI_3)_2(PR_3)_6$ (Ref. 98) was reported.[266] A bimetallic cluster $Pt_{13}[Au_2(PPh_3)_2]_2(CO)_{10}(PPh_3)_4$ with a Pt_{13} icosahedral core was synthesized and structurally characterized by X-ray diffraction.[271]

Unlike platinum and palladium, which form singly doped systems MAu_nL_m, silver and copper can form bimetallic variable-composition clusters. In particular, the $Ag_xAu_{25-x}(SC_{12}H_{25})_{18}$ ($x = 1-11$),[272] $Ag_xAu_{25-x}(SCH_2Bn)_{18}$ ($x = 1-8$),[273] $Ag_xAu_{25-x}(SCH_2Bn)_{18}$ ($x = 6.7$),[103] $Ag_xAu_{38-x}(SR)_{24}$ ($x = 1$, 3, 5, 6),[100] and $Ag_xAu_{144-x}(SCH_2Bn)_{60}$ ($x = 30$, 34, 52, 53, 60)[99] clusters were synthesized. They are multiply doped analogues to the $Au_{25}(SR)_{18}$, $Au_{38}(SR)_{24}$ and $Au_{144}(SR)_{60}$ clusters considered above. The content of silver in the clusters depends on the concentration ratio of metal salts in the starting solution and on the method of synthesis. For instance, the maximum number of silver atoms (x_{max}) is 60 for $Ag_xAu_{144-x}(SCH_2Bn)_{60}$ clusters[99] and only 8 for $Ag_xAu_{25-x}(SCH_2Bn)_{18}$.[273] Reactions of gold nanoparticles with $AgSCH_2Bn$ result in the $[Ag_xAu_{25-x}(PPh_3)_{10}(SCH_2Bn)_5Cl_2]^{2+}$ clusters containing at most twelve silver atoms.[274] The thirteenth silver atom can be introduced into the cluster by the reaction of Au_{11} with $AgSCH_2Bn$.

Bimetallic clusters $Ag_xAu_{n-x}(SR)_m$ have the core–shell structure, as $Au_n(SR)_m$. According to X-ray data for $Ag_xAu_{25-x}(SCH_2Bn)_{18}$ ($x = 6.7$),[103] gold atoms occupy the inner part of the core and participate in the formation of 'staple' bonds, while silver atoms form the surface of the cluster core. The $[Ag_xAu_{25-x}(PPh_3)_{10}(SCH_2Bn)_5Cl_2]^{2+}$ ($x \leqslant 13$) clusters have a bi-icosahedral structure by analogy with $[Au_{25}(PPh_3)_{10}(SCH_2Bn)_5Cl_2]^{2+}$ (see Fig. 15 *c*).[274] At $x \leqslant 12$, silver atoms occupy vertices and central edges of the polyhedron and the thirteenth silver is located at the core centre. Structure calculations for the $[Ag_xAu_{25-x}(SH)_{18}]^-$ ($x = 1$, 2, 4, 6, 8, 10, 12) clusters[275] and mass spectrometry studies of $Ag_xAu_{25-x}(SCH_2Bn)_{18}$ species[273] also showed that doping with silver is most probable at the core surface. In this case, silver atoms induce significant changes in the electron density distribution in the cluster, as was theoretically predicted for $Ag_{60}Au_{84}(SR)_{60}$ by the LDA/PAW method,[276] and an increase in the HOMO–LUMO gap.[277]

Also, it cannot be ruled out that silver atoms in the $AgAu_n(SR)_m$ clusters are constituents of the RS–Ag–RS 'staple' units. Recently, the crystal structures of $[Ag_{32}Au_{12}(SR)_{30}]^{4-}$ (R = C_6H_4F-4, $C_6H_3F_2$-3,4 and $C_6H_4CF_3$-4) were determined (Fig. 18 *a*).[104] The inner part of the cluster core represents the Au_{12} icosahedron. It is surrounded by the Ag_{20} dodecahedron and six $SR[Ag(SR)_2]_2$ 'staple' units forming the cluster shell. A theoretical analysis of the cluster predicts a closed 18-electron shell. Recently, the $[Ag_7Au_6(SR)_{10}]^+$ cluster with R = $CH(CO_2H)CH_2CO_2H$ was synthesized.[278] Its structure was studied theoretically taking the cluster with R = Me as an example.[279] The cluster is structurally similar to $[Au_{13}(SR)_{10}]^+$, *viz.*, the Ag_6 octahedral core is stabilized by two $SR(AuSR)_2$ units and one SR–Au(SR)–Ag(SR)–Au–SR unit containing both gold and silver atoms (see Fig. 18 *c*).

Clusters $Cu_xAu_{25-x}(SCH_2Bn)_{18}$ ($x = 1-5$) were synthesized by co-reduction of gold and copper salts under the action of $NaBH_4$ in the presence of $BnCH_2SH$.[102] In these systems, one copper atom occupies position at the core centre. Different types of structural organization of $CuAu_nL_m$ clusters are available. For instance, the copper atom can be located at the core surface, as in

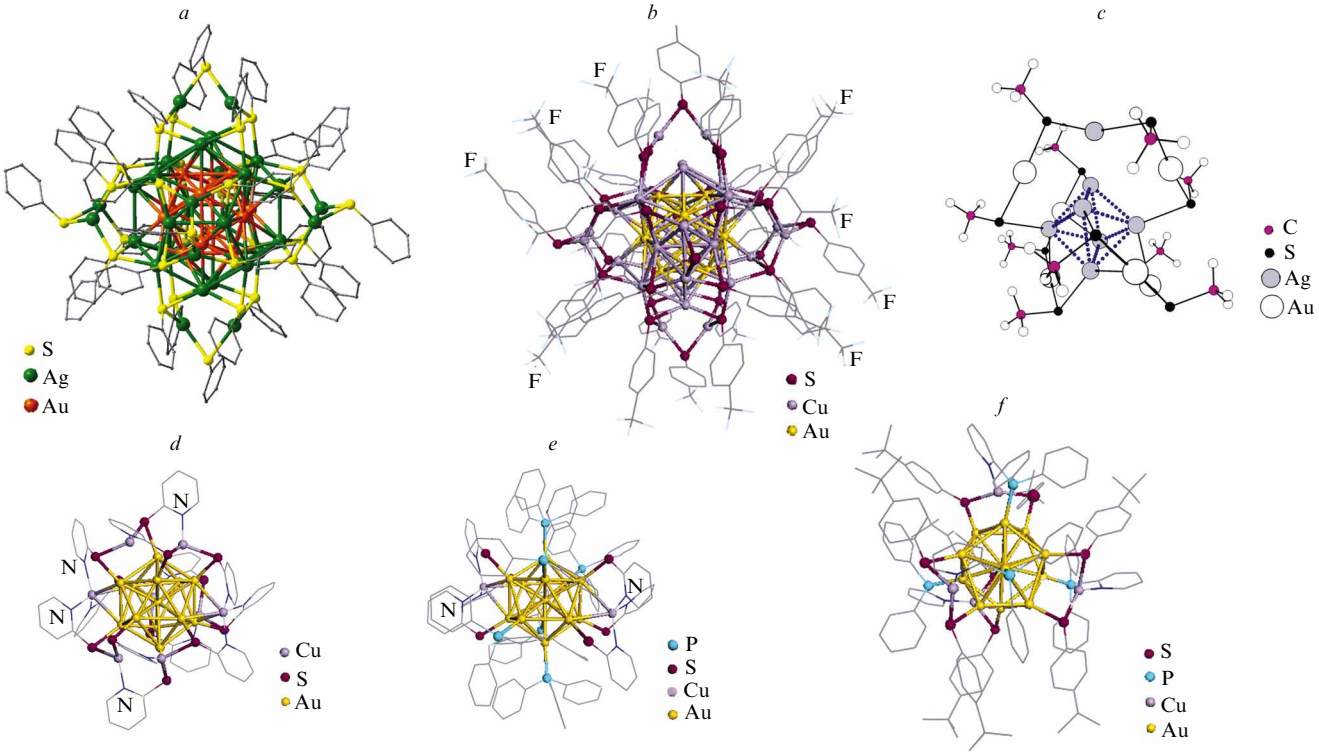


Figure 18. Crystal structures of clusters $[Ag_{32}Au_{12}(SPh)_{30}]^{4-}$ (*a*),[104] $[Cu_{32}Au_{12}(SC_6H_4CF_3\text{-}4)_{30}]^{4-}$ (*b*),[106] $[Cu_8Au_{13}(SPy\text{-}2)_{12}]^+$ (*d*), $[Cu_2Au_{13}(PPh_3)_6(SPy\text{-}2)_6]^+$ (*e*), $[Cu_4Au_{13}\{PPh_2(Py\text{-}2)\}_4(SC_6H_4Bu^t\text{-}4)_8]^+$ (*f*)[105] determined by X-ray diffraction and structure of cluster $[Ag_7Au_6(SMe)_{10}]^+$ (*c*)[279] obtained from DFT calculations.

$Cu_xAu_{25-x}(SCH_2Bn)_{18}$ ($x = 0-4$).[273] Clusters $Cu_xAu_{25-x}(SCH_2Bn)_{18}$ are unstable and undergo a spontaneous transformation to $Au_{25}(SCH_2Bn)_{18}$.[273] Recently, clusters $[Cu_8Au_{13}(SPy\text{-}2)_{12}]^+$, $[Cu_2Au_{13}(PPh_3)_6(SPy\text{-}2)_6]^+$ and $[Cu_4Au_{13}\{PPh_2(Py\text{-}2)\}_4(SC_6H_4Bu^t\text{-}4)]^+$ (see Fig. 18 *d–f*) were synthesized by the reaction of $Au(PPh_3)Cl$ with $Cu(OAc)_2$ and thiol under the action of $NaBH_4$ in a dichloromethane/methanol mixture at 0 °C; the yields were 25%, 20% and 40%, respectively.[105] According to X-ray data, the clusters have the Au_{13} icosahedral core; copper atoms are part of the 'staple' units or coordinate ligands (see Fig. 18 *d–f*). The clusters are thermally stable, the ligands are removed in the temperature interval between 200 and 325 °C. Removal of ligands from the surface allows active metallic sites $[Cu_nAu_{13}L_m]^+$ to be involved in catalytic reactions. After heat treatment at 325 °C these clusters exhibit higher activity and selectivity in aerobic oxidation of benzaldhyde compared to the $Au_{25}(SR)_{18}$ cluster.

The bilayer structure of the core is characteristic of $[Cu_{32}Au_{12+n}(SR)_{30+n}]^{4-}$ ($R = C_6H_4CF_3$-4; $n = 0$, 2, 4, 6) clusters.[106] These systems differ in composition of the 'staple' units. At $n = 0$, the $Cu_{20}Au_{12}$ core is stabilized by six $Cu_2(SR)_5$ units (see Fig. 18 *b*); otherwise, the cluster contains $6-n$ $Cu_2(SR)_5$ units and n $Cu_2Au(SR)_6$ units. Among these clusters, only $[Cu_{32}Au_{12}(SR)_{30}]^{4-}$ is stable in a solution in dichloromethane at room temperature.

VIII. Properties and applications of $[L_sAu_nX_m]^q$ clusters in nanoelectronics, nanooptics and catalysis

VIII.1. The $[Au_n(SR)_m]^q$ clusters as quantum dots

Unusual properties of $[L_sAu_nX_m]^q$ clusters arise from quantum effects. Gold clusters have discrete electronic spectra in contrast to quasi-continuous spectrum of larger nanoparticles.[11,280] Quantum particles usually have complicated optical absorption spectra,[281] whereas spherical gold particles 200 nm in diameter exhibit one well-defined plasmon resonance peak at 520 nm.[282] Gold clusters exhibit fluorescent and magnetic properties as well as chirality.[283–285] Since the fluorescence intensity and lifetime depend on temperature, gold nanoparticles are used as a versatile nanothermometer in studies of biological systems.[283] In some cases, the onset of optical activity can be explained using the model for a disymmetric field produced in the presence of a chiral ligand.[286] The electronic and optical properties of a cluster can be significantly changed by varying the number of atoms. For gold nanoparticles, this quantum effect becomes noticeable as the particle size decreases to 2 nm.[11] Recently, nonlinear optical properties of the $Au_{15}(SG)_{20}$ cluster have been reported.[287] Understanding the origin of the optical properties of gold clusters requires taking account of the structure of the metal and ligand orbitals.

As mentioned above, the absorption spectrum of $[Au_{25}(SR)_{18}]^-$ exhibits three peaks at 670, 450 and 400 nm (see Fig. 4).[44] This spectral pattern was interpreted by comparing the experimental and theoretical spectra. The peak at $\lambda = 670$ nm corresponds to the HOMO → LUMO transition (interband D → SP transition). The peak at 400 nm is also an interband D → SP transition. Thus, discrete molecular-like character of the spectrum of $Au_{25}(SR)_{18}$ is due to one-electron transitions between quantum energy levels.

The influence of ligand configurations on the optical properties of gold clusters is still poorly studied.[286,288–290] As the size of the hydrocarbon fragment in the ligand increases, the octahedral ligand field is distorted and the low-energy band in the spectrum of $[Au_{25}(SCH_2Bn)_{18}]^-$ is split unlike the band in the spectrum of $[Au_{25}(SMe)_{18}]^-$. The interaction within the aromatic π-electron system leads to formation of a field of S_6 symmetry where P-orbitals are split into two sets, *viz*., a low-lying doubly degenerate orbital and a nondegenerate orbital which lies 0.13 eV higher. D-Orbitals are spilt into three sets, namely, two doubly degenerate orbitals and one nondegenerate orbital which lies 0.17 eV higher. Splitting of the P-orbitals causes the appearance of a double peak corresponding to the low-energy transition, as was observed for the $[Au_{25}(SPh)_{18}]^-$ and $[Au_{25}(SCH_2Bn)_{18}]^-$ clusters. The double peak can be reproduced theoretically by taking into account spin–orbit coupling.[291] Study of the optical properties of the $Au_n(SR)_m$ clusters is a complicated task because the ligand can be a source of Raman signal.[289]

Fluorescent gold clusters are of particular interest because of their application as sensors. To date, the reason for high yield of fluorescence in gold clusters remains unclear. Presumably, high yield of fluorescence is due to quantum effects in the metal atoms forming the cluster core. An alternative explanation is as follows: it is a consequence of the interaction between ligands and metal atoms on the core surface.[292] For instance, fluorescence of $Au_{25}(SR)_{18}$ clusters ($R = C_6H_{13}$, CH_2Bn, G) is governed by all constituent Au atoms. Stabilization of the cluster with ligands containing electron-rich atoms (N, O) or groups (CO_2H, NH_2) enhances the fluorescent properties. Fluorescence of the $Au_{25}(SG)_{18}$ cluster allows this system to be used as sensor for I^- anions[293] and silver ions.[294]

A characteristic feature of gold clusters protected by sulfur-containing ligands and proteins is luminescence.[85,295–299] Luminescence of metals is usually very weak owing to continuous spectrum of electronic states in the wide conduction band. The ability of small gold clusters 1–2 nm in size to luminesce arises from the existence of the HOMO–LUMO gap. Gold(I) compounds exhibit luminescent properties.[300–304] It seems reasonable to assume that the role of emitters in the $Au_n(SR)_m$ clusters is played by the $SR(AuSR)_x$ oligomeric structures in the shell. An important role in luminescence is also played by the nature of the ligand.[305,306] Recent experimental studies on the temperature dependence of luminescence in $Au_{38}(SR)_{24}$ showed that emission occurs at higher energies compared to the energy of the absorbed quantum.[118] However, the mechanism of filling of highly excited states is to be clarified. Luminescencnt properties of gold clusters allowed them to be used in microprinting,[307] in studies of cell structures,[308] in the design of metal ion sensors,[309] and in qualitative determination of amino acids.[310]

Individual gold atoms have an unpaired $6s^1$ electron and exhibit the paramagnetic properties. Probably, the loss of paramagnetism in individual atoms upon formation of diamagnetic metallic gold will be studied in the future. Paramagnetism in various $Au_n(SR)_m$ clusters was detected long ago,[311] but its origin remained unclear owing to the lack of information on the structure of these systems. Earlier, it was assumed that the magnetic properties of gold clusters arise from charge transfer from the Au atoms of the core surface to ligands. According to modern con-

cepts, the magnetic moment of a neutral cluster $Au_{25}(SR)_{18}$ is due to the spin of unpaired electron in the HOMO localized on the Au_{13} core. The magnetic properties of clusters can be reversibly switched by varying the charge of the cluster.[312] The $[Au_{25}(SR)_{18}]^-$ and $[Au_{25}(SR)_{18}]^+$ charged clusters have even numbers of electrons and behave as diamagnetics. Recently, the ferromagnetic properties were predicted for $Au_{55}(PPh_3)_{12}Cl_6$.[313]

Gold clusters stabilized by chiral ligands, L-glutathione and penicillamine, exhibit optical circular dichroism.[314, 315] Clusters stabilized by *N*-isobutyl-L-cysteine and *N*-isobutyl-D-cysteine behave analogously.[316] It should be noted that the $Au_{25}(SR)_{18}$ clusters with achiral ligand SCH_2Bn are optically inactive, whereas $Au_{25}(SG)_{18}$ exhibits a clearly seen circular dichroism signal.[314] There are three reasons for the appearance of chirality in gold clusters. First, this is intrinsic chirality of the cluster core;[11, 286] second, asymmetric coordination of ligands to the symmetric core leads to formation of optical isomers, as is the case for, *e.g.*, clusters $Au_{38}(SR)_{24}$ (Ref. 50) and $Au_{102}(SR)_{44}$.[51] Finally, chiral centres can exist in the ligands and thus influence the properties of the entire cluster. As was shown theoretically,[317] the optical activity is governed by the shell Au atoms surrounded by asymmtric ligands. Owing to their chiral properties gold nanoparticles are used as enantioselective catalysts.[89]

VIII.2. Application of $Au_n(SR)_m$ and $Au_n(PR_3)_m$ clusters in catalysis

Phosphine-protected gold clusters are widely used in homogeneous[268] and heterogeneous catalysis.[318–320] The catalytic properties of $Au_n(SR)_m$ clusters were discovered recently[321–338] and are rather surprising (Table 1).

It is commonly accepted that the sulfur atoms present in a cluster block the active sites and reduce the catalytic activity of the cluster. Therefore, it is surprising that the $Au_n(SR)_m$ clusters of different composition catalyze the oxidation and hydrogenation reactions.

Currently, the catalytic properties of gold particles are explained by the specific electronic properties of nanoparticles and by the presence of gold atoms with low coordination number in the gold particles. By varying the position of the centre of the density of d-electronic states for gold atoms in a cluster one can influence its catalytic properties. Thiol ligands possess electron-withdrawing properties and favour a shift of the centre of the electron density of Au d-levels in the cluster towards the Fermi level.[326] This can be a reason for the catalytic activity of $Au_n(SR)_m$.[322]

Gold clusters are used for catalysis in solution or as supported composites (Fig. 19). One can assume that the active sites of homogeneous systems containing $Au_n(SR)_m$ represent gold atoms from the cluster shell or gold atoms located on the core surface.

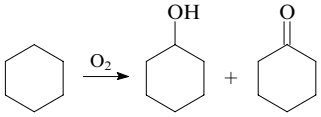
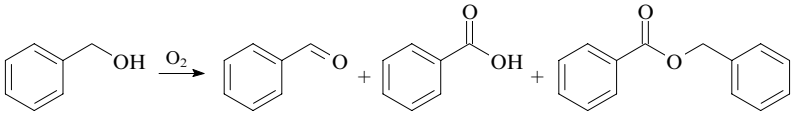
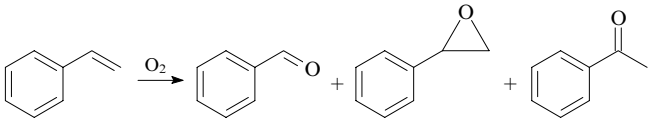
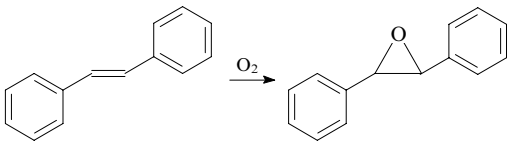
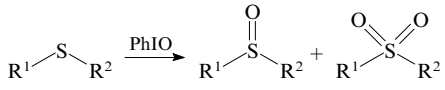
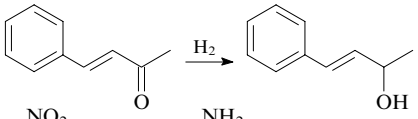
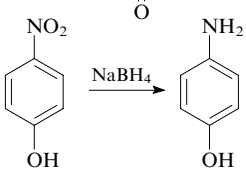
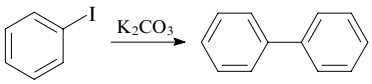
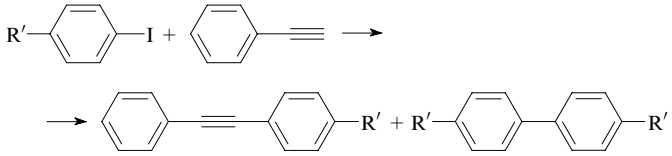
Besides, the catalytic properties of $Au_n(SR)_m$ clusters in solution are due to dynamic ligand exchange of the RS group with a substrate fragment. According to original studies,[325, 334] this is a key step in selective hydrogenation of unsaturated ketones and aldehydes.

The use of clusters as precursors of supported catalysts (see Fig. 19) appears to be a promising line of research. The advantages of supported systems include a higher stability compared to homogeneous systems and the possibility of multiple use owing to regeneration. Traditionally, supported catalysts are prepared by impregnating the surface of oxide supports with solutions containing $[L_sAu_nX_m]^q$ and subsequent calcination.[339] Removal of ligands from the cluster shell on heating makes the active sites more accessible. This is accompanied by changes in the number of filled electronic states of the metal that are responsible for the catalytic activity. Highly efficient catalysts were prepared by impregnating titania with a solution containing $[Au_6(PPh_3)_6][BF_4]_2$.[320]

The choice of the calcination temperature and reaction temperature specifies the extent of retention of the ligand shell. Ligands split off from the $Au_n(PPh_3)_m$ clusters at 200 °C.[340] Removal of the PR_3 ligands from the ligand shell enhances the catalytic activity in the oxidation of benzaldhyde.[319] A study of thiolate-capped gold clusters showed that ligand loss begins at 200 °C and the ligand shell no longer exists at 250 °C.[327] Also, heat treatment of $Au_{10}(SG)_{10}$/HAP, $Au_{18}(SG)_{14}$/HAP, $Au_{25}(SG)_{18}$/HAP and $Au_{39}(SG)_{24}$/HAP composites at 300 °C afforded catalysts containing ligand-free gold particles active in cyclohexane oxidation at 150 °C.[323] The gold particles thus formed retain the small cluster size due to strong interaction between Au atoms and phosphate groups. These catalysts are efficient in the oxidation of CO (at 60 °C)[321] and hydrocarbons (at 30–80 °C).[258, 323, 327–329] Probably, in this case the role of active sites is played by the type-D gold atoms with low coordination number or by the type-C gold atoms located near the particle–support interface (see Fig. 19). In other situations, calcination of supported gold clusters leads to reduction of their catalytic activity. For instance, the $Au_{25}(SCH_2Bn)/SiO_2$ and $Au_{25}(SC_6H_4NH_2\text{-}4)_{17}/SiO_2$ composites heat treated at 400 °C were characterized by the same particle size and reduced catalytic activity in selective oxidation of stilbene (80 °C).[330] This indicates an important role of ligands in the formation of active sites in the catalysts.

Like nanoparticles,[72, 73] gold clusters are active and selective catalysts of oxidation of many compounds including reactions involving molecular oxygen.[69] The oxidation of $[Au_{25}(SR)_{18}]^-$ ($R = CH_2Bn$) by oxygen takes a few days.[339] Surprisingly, the reaction includes photochemical steps.[341] The electron density transfer from the cluster to the oxygen molecule is a photoinitiated process whose rate is governed by the energy difference between the cluster LUMO and the energy of the acceptor level of O_2 molecule. Therefore, it seems quite natural that the maximum yield of H_2O_2 produced electrochemically from O_2 was observed in the presence of $[Au_{25}(SR)_{18}]^-$ (Ref. 332) owing to ready transfer of the electron density to the π-orbitals of O_2. The reaction of the Au_{32}–PVP complex with oxygen was studied using DFT calculations[342] assuming that O_2 can be activated owing to weak bond between PVP and the cluster core. When the supported clusters $[L_sAu_nX_m]^q$ are used, an important role in the activation of molecular oxygen is played by the nature of the support. For instance, $Au_{25}(SCH_2Bn)_{18}/CeO_2$[321] and $Au_{38}(SCH_2Bn)_{24}/CeO_2$[322] composites appeared to be the most active catalysts of CO oxidation at 60–80 °C. Calcination of the samples at 150 °C for 1.5–2 h causes the conversion to increase to 98%. It is believed that in this case ligands are retained in the cluster composition. A tentative reaction mechanism is as follows. Initially, the O_2 molecule is activated on the gold cluster through electron density transfer from the cluster to give active oxygen O_2^*.[321] Then O_2^* migrates to the cluster–

Table 1. Homogeneous and heterogeneous catalytic reactions with participation of gold clusters.

Reaction	Catalyst [a]	Ref.
$CO + O_2 \longrightarrow CO_2$	$Au_{25}(SR)_{18}/CeO_2$ $Au_{38}(SR)_{24}/CeO_2$	321 322
	$Au_{10}(SG)_{10}$/HAP, $Au_{18}(SG)_{14}$/HAP, $Au_{25}(SG)_{18}$/HAP, $Au_{39}(SG)_{24}$/HAP	323
	$Au_{25}(SR)_{18}$/CNT	324
	$Au_{25}(SR)_{18}$ $Au_{25}(SR)_{18}/SiO_2$ $Au_{25}(SG)_{18}$/HAP $Au_{38}(SR)_{24}/SiO_2$, $Au_{144}(SR)_{60}/SiO_2$ $Au_{55}(PPh_3)_{12}Cl_6$ $[Au_{25}(PPh_3)_{10}(SC_{12}H_{25})_5Cl_2]^{2+}$	325, 326 327 328 327 258, 329 330
	$Au_{25}(SR)_{18}/SiO_2$	327
 (R^1 = Ph, $C_6H_4NO_2$-2, C_6H_4Br-2, C_6H_4Me-2, C_6H_4CHO-2; R^2 = Me, $CH_2CH{=}CH_2$, C_8H_{17})	$Au_{25}(SR)_{18}/TiO_2$	331
$O_2 + 2H^+ + 2e^- \longrightarrow H_2O_2$	$[Au_{25}(SR)_{18}]^-$	332
$Ph{-}C{\equiv}CH + H_2 \longrightarrow Ph{-}CH{=}CH_2$	$Au_{25}(SR)_{18}/SiO_2$, $[Au_{25}(PPh_3)_{10}(C{\equiv}CPh)_5]^{2+}$	333
	$Au_{25}(SR)_{18}$	325, 334
	$Au_{25}(SG)_{18}$	335, 336
	$Au_{25}(SR)_{18}/TiO_2$	337
	$Au_{25}(SR)_{18}$/MgO	338

[a] HAP stands for hydroxyapatite $Ca_{10}(PO_4)_6(OH)_2$ and CNT stands for carbon nanotubes.

support contact region and undergoes transformation to the hydroperoxide intermediate OOH with participation of the surface OH groups from CeO_2. The intermediate oxidizes the adsorbed CO molecule. This mechanism of CO oxidation was proposed for the gold nanoparticles immobilized on CeO_2.[72, 73]

The oxidation of styrene was studied in homogeneous systems, *e.g.*, toluene in the presence of $Au_{25}(SR)_{18}$

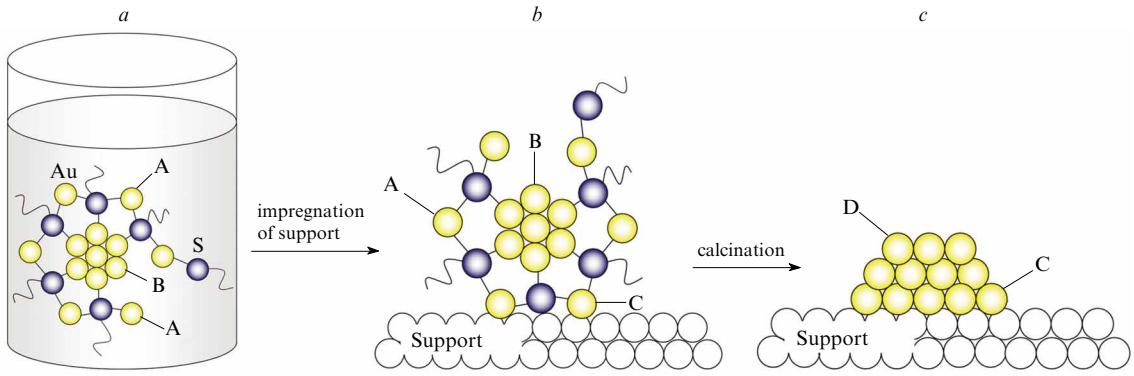


Figure 19. Catalytic systems based on $Au_n(SR)_m$ clusters.
Clusters in solution (*a*); clusters immobilized on support by impregnation with solution and characterized by partial retention of ligand environment (*b*); and ligand-free clusters immobilized on support and prepared by calcination of the catalyst *b* (*c*).
Capital letters denote possible types of active sites in the catalyst: A are gold atoms from the ligand shell; B are gold atoms on the surface of the cluster core; C are gold atoms in the region of cluster–support interface; and D are gold atoms belonging to the cluster and having low coordination number.

(R = CH_2Bn, C_6H_{13}, $C_{12}H_{25}$)[325] and using heterogeneous catalysts $Au_{25}(SCH_2Bn)_{18}/SiO_2$,[327] $Au_{25}(SR)_{18}$/HAP (R = G, CH_2Bn)[328] and $Au_{55}(PPh_3)_{12}Cl_6$/HAP.[258, 329] It was found that the $Au_{55}(PPh_3)_{12}Cl_6$ cluster exhibits catalytic activity in styrene oxidation resulting in benzaldhyde, styrene epoxide and acetophenone.[329] Low reaction temperature (80 °C) suggests retention of the ligand shell in the clusters. Theoretical studies of the structure of the active site in this cluster and of the mechanism of oxidation showed that the catalytic properties of $Au_{55}(PPh_3)_{12}Cl_6$ arise from specific arrangement of ligands on the surface of the quasi-icosahedral Au_{55} core.[258] The active site represents a centred Au_6 pentagon surrounded by PR_3 ligands. Catalytic oxidation of styrene on thiolate-protected gold clusters depends on the catalyst preparation procedure, on the type of support and on the nature of oxidizing agent. A 100% yield of benzaldhyde was obtained using $Au_{25}(SCH_2Bn)_{18}/SiO_2$ as the catalyst (without calcination) and *tert*-butyl hydroperoxide (TBHP) as the oxidizing agent.[327] Similar results were obtained using the $Au_{38}(SR)_{24}/SiO_2$ and $Au_{144}(SR)_{60}/SiO_2$ systems. It was found that the cluster shell is retained under experimental conditions. The mechanism of styrene oxidation was studied theoretically taking ligand-free Au_n clusters (n = 16–35) as examples. It involves the formation of a cyclic intermediate CCOO*.[343] But the key step in styrene oxidation represents activation of the oxidizing agent (O_2 or TBHP). One can assume that activation is as a result of the shift of the electron density from the metallic cluster core to the adsorbed oxidant. Activation of the double bond in the hydrocarbon molecule occurs on the $Au^{\delta+}$ sites from the cluster shell. The activity of such cationic sites in activation of unsaturated hydrocarbons was predicted theoretically for ligand-free gold clusters.[144, 146] Establishment of the mechanism of catalytic selective oxidation of styrene in the presence of gold clusters with certainty requires an additional theoretical research.

Studies on the catalytic properties of HAP-supported $Au_{10}(SG)_{10}$, $Au_{18}(SG)_{14}$, $Au_{25}(SG)_{18}$ and $Au_{39}(SG)_{24}$ clusters stored at 300 °C for 2 h in aerobic oxidation of cyclohexane at 150 °C revealed a correlation between the catalyst activity and the cluster size.[323] The authors of that study believe that the samples contain supported ligand-free atomic gold clusters. The maximum activity [TOF = 2×10^{-4} h^{-1} (Au atom)$^{-1}$] was observed for the Au_{39} cluster. Further increase in the Au_n particle size reduced the catalytic activity. The size effects of gold nanoparticles in the oxidation reaction are well known and can be explained by different structure of the particle–support interface at different particle size values.[72]

The thiolate cluster $Au_{25}(SCH_2Bn)_{18}$ supported on TiO_2, CeO_2, MgO and Fe_2O_3 exhibits high activity and selectivity (92%) in the oxidation of sulfides to sulfoxides using PhIO as the oxidizing agent.[331] The activity and selectivity of the supported catalyst are significantly influenced by the electronic properties and geometry of substituents. For instance, the oxidation of sulfides containing electron-donating groups [4-bromophenyl(methyl) sulfide, 4-methylphenyl(methyl) sulfide] proceeds with a higher yield compared to the oxidation of sulfides containing electron-withdrawing groups [methyl(4-nitrophenyl) sulfide]. The nature of support also significantly influences the catalytic activity, which enhances in the order $MgO < CeO_2 < Fe_2O_3 < TiO_2$. Low reaction temperature (40 °C) suggests retention of the ligand shell and possible involvement of the 'staple' units in the activation. It was assumed that owing to the reversible transition $Au_{25}(SR)_{18} \rightleftharpoons [Au_{25}(SR)_{18}]^-$ the cluster can act as acceptor and as oxygen carrier from PhIO to the sulfide molecule coordinated to the gold atom in the 'staple' unit. However, since the catalyst activity depends on the support nature, the role of the cluster/support interface in the activation of substrates and in the reaction itself cannot be ruled out.

Among other processes catalyzed by the $[L_sAu_nX_m]^q$ clusters, mention may be made of low-temperature (25 °C) catalytic hydrogenation of unsaturated ketones[325, 334] and reduction of nitro compounds.[335, 336] Cross-coupling reactions in the presence of gold clusters are carried out at higher temperatures. The oxide-supported cluster $Au_{25}(SCH_2Bn)_{18}$ catalyzes cross-coupling of aryl iodide resulting in diphenyl (130 °C).[337] The product yield can be as high as 99.8% using CeO_2 as support. The same cluster, $Au_{25}(SCH_2Bn)_{18}$, supported on SiO_2, Al_2O_3, CeO_2, and MgO catalyzes the Sonogashira cross-coupling reaction,

which involves the reaction of phenylacetylene with 4-iodomethoxybenzene at 160 °C to give 4,4′-dimethoxy-1,1′-biphenyl with a selectivity of 88%.[338] At this temperature, type-B sites (see Fig. 19) forming the Au_3 unit in the cluster core may be accessible. A theoretical simulation revealed activation of phenylacetylene on the Au_3 unit; the calculated adsorption energy for this coordination was 0.40 eV.[338]

The $Au_{25}(SCH_2Bn)_{18}$ and $Au_{25}(PPh_3)_{10}(C{\equiv}CPh)_5X_2$ (X = Br, Cl) clusters on oxide supports (TiO_2, CeO_2, SiO_2, Al_2O_3) exhibit high activity and selectivity in partial hydrogenation of alkynes $RC{\equiv}CH$ to alkenes $RCH{=}CH_2$ at 100 °C (R = Ph, CH_2Bn, C_5H_{11}, C_7H_{15}, C_9H_{19}).[333] Hydrogenation of terminal alkynes does not require calcination of catalysts, therefore, the ligand shell does not preclude the process. The reaction mechanism involves deprotonation of hydrocarbon and the formation of an intermediate, $R-C{\equiv}C-Au_nL_m$. For $Au_{25}(PPh_3)_{10}(C{\equiv}CPh)_5X_2$, the existence of such an intermediate was detected by FT-IR spectroscopy. Thus, the activity of the catalyst in this reaction is due to the peculiar structure of the cluster, namely, the presence of the Au_3 centres that are necessary for activation of the alkyne. This is a common feature of gold clusters and gold nanoparticles in selective hydrogenation of alkynes.[144, 145, 344, 345]

Concluding this Section, the use of $[L_sAu_nX_m]^q$ atomic clusters as catalysts allows catalytic reactions to be studied at the molecular level and thus the measured property of the catalyst (activity, selectivity and stability) can be related to a particular composition and structure of the cluster; this can hardly be done for most heterogeneous catalytic systems. The type of the active site in the heterogeneous systems based on ligand-protected gold clusters is governed by the annealing temperature and reaction temperature. Emphasize that the mechanisms of most catalytic reactions involving the $Au_n(SR)_m$ and $Au_n(PR_3)_m$ clusters are still to be clarified, so quantum chemical simulation seems to have great prospects in this field.

IX. Conclusion

Advances in experimental and theoretical research on the synthesis and structure of individual ligand-protected gold clusters revealed the possibility for the structure and properties of stable systems to be described within the framework of the superatom theory. The observed deviations from theory mainly concern aspherical clusters containing subunits obeying the superatom theory. Magic number of metal atoms in small clusters arises from the electronic effects due to the need to complete the electron shells in the cluster core. At the same time, as the cluster size increases, structural effects related to the formation of metal – metal bonds begin to dominate the electronic effects; this, in particular, leads to the stable non-magic open-shell cluster $Au_{55}(PPh_3)_{12}Cl_6$. The decisive role in the formation of large clusters is played by geometric effects, *i.e.*, the possibility for a highly symmetric structure (icosahedron, a Marks polyhedron, truncated octahedron) to exist. Selenols seem to be promising ligands for stabilizing atomic gold clusters.

At present, quantum chemical simulation is a reliable method for determination of the structure of stable gold nanoclusters; it underlies theoretical research into novel interesting systems. The variety of structures predicted theoretically for the $Au_{38}(SR)_{24}$ clusters helped to develop universal concepts and rules aimed at determinng the structure of these species.

The synthesis and studies on the structure of bimetallic clusters $M@Au_nL_m$ represent a novel trend of research in cluster chemistry. All the available doped clusters obey the electron count rule for 'magic' number of valence electrons. The $M@Au_nL_m$ structural motif is governed by the nature of the metal. In the case of platinum and palladium, (i) the initial structure of the Au_nL_m cluster is retained, (ii) the dopant occupies the central position and (iii) singly doped clusters are mainly formed in contrast to the variable-composition clusters for M = Cu, Ag. Atoms of these elements replace gold atoms on the surface of the cluster core or in the cluster shell.

Research into the structure and properties of atomic clusters allows one to disclose the characteristic features of the structure and properties of gold nanoparticles of arbitrary size, because atomic clusters are their constituents. Therefore, studies on the properties of atomic clusters give the key to understanding the chemical and physical properties of nano-sized gold, including the influence of size and morphology of gold nanoparticles on the catalytic properties. Better insight into the properties and structure of ligand-protected gold clusters opens prospects for targeted design of systems for applications in electronics, medicine and catalysis. Great potential of small gold clusters in catalysis is clearly seen now.

The authors express their gratitude to Professor E K Beloglazkina and Assistant Professor A G Majouga (both from M V Lomonosov Moscow State University) for advice in organic synthesis and nomenclature of organic compounds. The review has been written with the financial support from the Russian Foundation for Basic Research (Project Nos 14-01-00310, 13-03-00320) and the Ministry of Education and Science of the Russian Federation (Grant NSh-3171.2014.3).

References

1. *Nanoscale Materials in Chemistry* (Eds K J Klabunde, R M Richards) (New York: Wiley, 2009)
2. C P Poole Jr, F J Owens *Introduction to Nanotechnology* (New York: Wiley, 2005)
3. *Nanocrystals — Synthesis Characterization and Applications* (Ed. S Neralla) (Rijeka, Croatia: InTech, 2012)
4. K G Nikolaev, S S Ermakov, A Offenhäusser, Yu Mourzina *Mendeleev Commun.* **24** 145 (2014)
5. M Yu Ziangirova, M S Kotelev, G S Skorikova, E V Ivanov, L T Perelman, V A Vinokurov *Mendeleev Commun.* **24** 53 (2014)
6. A Müller, S Roy *Russ. Chem. Rev.* **71** 981 (2002)
7. Y Lu, W Chen *Chem. Soc. Rev.* **41** 3594 (2012)
8. D-e Jiang *Nanoscale* **5** 7149 (2013)
9. R Jin, Y Zhu, H Qian *Chem. – Eur. J.* **17** 6584 (2011)
10. T Tsukuda *Bull. Chem. Soc. Jpn.* **85** 151 (2012)
11. H Qian, M Zhu, Z Wu, R Jin *Acc. Chem. Res.* **45** 1470 (2012)
12. M Laupp, J Strihle *Angew. Chem., Int. Ed. Engl.* **33** 207 (1994)
13. J W A van der Velden, J J Bour, W P Bosman, J H Noordik *J. Chem. Soc., Chem. Commun.* 1218 (1981)
14. P L Bellon, F Cariati, M Manassero, L Naldini, M Sansoni *J. Chem. Soc., Chem. Commun.* 1423 (1971)
15. C E Briant, K P Hall, A C Wheeler, D M P Mingos *J. Chem. Soc., Chem. Commun.* 248 (1984)

16. M McPartlin, R Mason, L Malatesta *J. Chem. Soc., Chem. Commun*. 334 (1969)
17. B K Teo, X Shi, H Zhang *J. Am. Chem. Soc*. **114** 2743 (1992)
18. D M P Mingos *J. Chem. Soc., Dalton Trans*. 1163 (1976)
19. Y Pei, X C Zeng *Nanoscale* **4** 4054 (2012)
20. H Häkkinen, in *Metal Nanoparticles and Nanoalloys (Frontiers of Nanoscience* Vol. 3) (Eds R Johnston, J Wilcoxon) (Amsterdam: Elsevier, 2012) p. 129
21. G Schmid *Chem. Soc. Rev*. **37** 1909 (2008)
22. W Kurashige, M Yamaguchi, K Nobusada, Y Negishi *J. Phys. Chem. Lett*. **3** 2649 (2012)
23. C K Yee, A Ulman, J D Ruiz, A Parikh, H White, M Rafailovich *Langmuir* **19** 9450 (2003)
24. X Meng, Q Xu, S Wang, M Zhu *Nanoscale* **4** 4161 (2012)
25. W Kurashige, S Yamazoe, K Kanehira, T Tsukuda, Y Negishi *J. Phys. Chem. Lett*. **4** 3181 (2013)
26. P Maity, H Tsunoyama, M Yamauchi, S Xie, T Tsukuda *J. Am. Chem. Soc*. **133** 20123 (2011)
27. P Maity, T Wakabayashi, N Ichikuni, H Tsunoyama, S Xie, M Yamauchi, T Tsukuda *Chem. Commun*. **48** 6085 (2012)
28. H Hikkinen *Nat. Chem*. **4** 443 (2012)
29. M Askerka, D Pichugina, N Kuz'menko, A Shestakov *J. Phys. Chem. A* **116** 7686 (2012)
30. F Furche, R Ahlrichs, P Weis, C Jacob, S Gilb, T Bierweiler, M M Kappes *J. Chem. Phys*. **117** 6982 (2002)
31. F Remacle, E S Kryachko *J. Chem. Phys*. **122** 044304 (2005)
32. R F Höckendorf, Y Cao, M K Beyer *Organometallics* **29** 3001 (2010)
33. A A Herzing, C J Kiely, A F Carley, P Landon, G J Hutchings *Science* **321** 1331 (2008)
34. Z W Wang, R E Palmer *Nanoscale* **4** 4947 (2012)
35. M A Habeeb Muhammed, T Pradeep *Small* **7** 204 (2011)
36. K Okumura, K Yoshino, K Kato, M Niwa *J. Phys. Chem. B* **109** 12380 (2005)
37. G Schmid, R Pfeil, R Boese, F Bandermann, S Meyer, G H M Calis, J W A van der Velden *Chem. Ber*. **114** 3634 (1981)
38. M Brust, M Walker, D Bethell, D J Schiffrin, R Whyman *J. Chem. Soc., Chem. Commun*. 801 (1994)
39. C Zeng, C Liu, Y Chen, N L Rosi, R Jin *J. Am. Chem. Soc*. **136** 11922 (2014)
40. A Das, T Li, K Nobusada, C Zeng, N L Rosi, R Jin *J. Am. Chem. Soc*. **135** 18264 (2013)
41. D Crasto, G Barcaro, M Stener, L Sementa, A Fortunelli, A Dass *J. Am. Chem. Soc*. **136** 14933 (2014)
42. A Das, T Li, G Li, K Nobusada, C Zeng, N L Rosi, R Jin *Nanoscale* **6** 6458 (2014)
43. M W Heaven, A Dass, P S White, K M Holt, R W Murray *J. Am. Chem. Soc*. **130** 3754 (2008)
44. M Zhu, C M Aikens, F J Hollander, G C Schatz, R Jin *J. Am. Chem. Soc*. **130** 5883 (2008)
45. T Dainese, S Antonello, J A Gascón, F Pan, N V Perera, M Ruzzi, A Venzo, A Zoleo, K Rissanen, F Maran *ACS Nano* **8** 3904 (2014)
46. C Zeng, T Li, A Das, N L Rosi, R Jin *J. Am. Chem. Soc*. **135** 10011 (2013)
47. H Yang, Y Wang, A J Edwards, J Yan, N Zheng *Chem. Commun*. **50** 14325 (2014)
48. D Crasto, S Malola, G Brosofsky, A Dass, H Häkkinen *J. Am. Chem. Soc*. **136** 5000 (2014)
49. C Zeng, H Qian, T Li, G Li, N L Rosi, B Yoon, R N Barnett, R L Whetten, U Landman, R C Jin *Angew. Chem., Int. Ed*. **51** 13114 (2012)
50. H Qian, W T Eckenhoff, Y Zhu, T Pintauer, R Jin *J. Am. Chem. Soc*. **132** 8280 (2010)
51. P D Jadzinsky, G Calero, C J Ackerson, D A Bushnell, R D Kornberg *Science* **318** 430 (2007)
52. J W A van der Velden, J J Bour, J J Steggerda, P T Beurskens, M Roseboom, J H Noordik *Inorg. Chem*. **21** 4321 (1982)
53. Y Shichibu, M Zhang, Y Kamei, K Konishi *J. Am. Chem. Soc*. **136** 12892 (2014)
54. Y Kamei, Y Shichibu, K Konishi *Angew. Chem., Int. Ed*. **50** 7442 (2011)
55. K Nunokawa, S Onaka, M Ito, M Horibe, T Yonezawa, H Nishihara, T Ozeki, H Chiba, S Watase, M Nakamoto *J. Organomet. Chem*. **691** 638 (2006)
56. C E Briant, B R C Theobald, J W White, L K Bell, D M P Mingos, A J Welch *J. Chem. Soc., Chem. Commun*. 201 (1981)
57. B S Gutrath, I M Oppel, O Presly, I Beljakov, V Meded, W Wenzel, U Simon *Angew. Chem., Int. Ed*. **52** 3529 (2013)
58. X-K Wan, Z-W Lin, Q-M Wang *J. Am. Chem. Soc*. **134** 14750 (2012)
59. J Chen, Q-F Zhang, P G Williard, L-S Wang *Inorg. Chem*. **53** 3932 (2014)
60. X-K Wan, S-F Yuan, Z-W Lin, Q-M Wang *Angew. Chem., Int. Ed*. **53** 2923 (2014)
61. J Chen, Q-F Zhang, T A Bonaccorso, P G Williard, L-S Wang *J. Am. Chem. Soc*. **136** 92 (2014)
62. A Das, T Li, K Nobusada, Q Zeng, N L Rosi, R Jin *J. Am. Chem. Soc*. **134** 20286 (2012)
63. Y Shichibu, Y Negishi, T Watanabe, N K Chaki, H Kawaguchi, T Tsukuda *J. Phys. Chem. C* **111** 7845 (2007)
64. P Maity, S Xie, M Yamauchi, T Tsukuda *Nanoscale* **4** 4027 (2012)
65. H Häkkinen, M Walter, H Grönbeck *J. Phys. Chem. B* **110** 9927 (2006)
66. M Walter, J Akola, O Lopez-Acevedo, P D Jadzinsky, G Calero, C J Ackerson, R L Whetten, H Grönbeck, H Häkkinen *Proc. Natl. Acad. Sci. USA* **105** 9157 (2008)
67. N K Chaki, Y Negishi, H Tsunoyama, Y Shichibu, T Tsukuda *J. Am. Chem. Soc*. **130** 8608 (2008)
68. Y Pei, Y Gao, X C Zeng *J. Am. Chem. Soc*. **130** 7830 (2008)
69. M Jin, G Hao, X Sun, W Chen *Rev. Nanosci. Nanotechnol*. **1** 3 (2012)
70. D A Pichugina, A G Mazhuga, A F Shestakov, in *Organicheskie i Gibridnye Nanomaterialy: Tendentsii i Perspektivy* (Organic and Hybrid Nanomaterials: Trends and Prospects) (Eds V F Razumov, M V Klyuev) (Ivanovo: Ivanovo State University, 2013) p. 147
71. G Guan, S Liu, Y Cai, M Low, M S Bharathi, S Zhang, S Bai, Y-W Zhang, M-Y Han *Adv. Mater*. **26** 3427 (2014)
72. G C Bond, C Louis, D T Thompson *Catalysis by Gold (Catal. Sci. Ser. Vol. 6)* (London: Imperial College Press, 2006)
73. M Haruta *Magazine Catal. Sci. Technol. Innov. (CATTECH)* **6** 102 (2002)
74. L McEwan, M Julius, S Roberts, J C Q Fletcher *Gold Bull*. **43** 298 (2010)
75. Y Zhang, R W Cattrall, I D McKelvie, S D Kolev *Gold Bull*. **44** 145 (2011)
76. V I Bukhtiyarov, M G Slin'ko *Russ. Chem. Rev*. **70** 147 (2001)
77. M Boronat, A Leyva-Pérez, A Corma *Acc. Chem. Res*. **47** 834 (2014)
78. R Philip, P Chantharasupawong, H Qian, R Jin, J Thomas *Nano Lett*. **12** 4661 (2012)
79. X Huang, P K Jain, I H El-Sayed, M A El-Sayed *Nanomedicine* **2** 681 (2007)
80. K Park, G Liang, X Ji, Z -P Luo, C Li, M C Croft, J T Markert *J. Phys. Chem. C* **111** 18512 (2007)
81. W Luo, S J Pennycook, S T Pantelides *Nano Lett*. **7** 3134 (2007)
82. L A Dykman, V A Bogatyrev *Russ. Chem. Rev*. **76** 181 (2007)
83. R A Sperling, P R Gil, F Zhang, M Zanella, W J Parak *Chem. Soc. Rev*. **37** 1896 (2008)
84. P Pyykkö *Angew. Chem., Int. Ed*. **43** 4412 (2004)

85. D M Chevrier, A Chatt, P Zhang *J. Nanophoton.* **6** Art. No. 064504 (2012)
86. Y Mikami, A Dhakshinamoorthy, M Alvaro, H García *Catal. Sci. Technol.* **3** 58 (2013)
87. Y Zhu, H Qian, R Jin *J. Mater. Chem.* **21** 6793 (2011)
88. I Cano, M A Huertos, A M Chapman, G Buntkowsky, T Gutmann, P B Groszewicz, P W N M van Leeuwen *J. Am. Chem. Soc.* **137** 7718 (2015)
89. G Li, R Jin *Acc. Chem. Res.* **46** 1749 (2013)
90. Y Negishi *Bull. Chem. Soc. Jpn.* **87** 375 (2014)
91. K G Stamplecoskie, P V Kamat *J. Am. Chem. Soc.* **136** 11093 (2014)
92. Y Negishi, W Kurashige, Y Niihori, K Nobusada *Phys. Chem. Chem. Phys.* **15** 18736 (2013)
93. D-e Jiang, R L Whetten *Phys. Rev. B* **80** 115402 (2009)
94. K A Kacprzak, L Lehtovaara, J Akola, O Lopez-Acevedo, H Häkkinen *Phys. Chem. Chem. Phys.* **11** 7123 (2009)
95. Y Negishi, W Kurashige, Y Niihori, T Iwasa, K Nobusada *Phys. Chem. Chem. Phys.* **12** 6219 (2010)
96. H Qian, E Barry, Y Zhu, R Jin *Acta Phys. Chim. Sin.* **27** 513 (2011)
97. Y Negishi, K Igarashi, K Munakata, W Ohgake, K Nobusada *Chem. Commun.* **48** 660 (2012)
98. B K Teo, H Zhang *J. Organomet. Chem.* **614** – **615** 66 (2000)
99. C Kumara, A Dass *Nanoscale* **3** 3064 (2011)
100. C Kumara, A Dass *Nanoscale* **4** 4084 (2012)
101. C Yao, J Chen, M-B Li, L Liu, J Yang, Z Wu *Nano Lett.* **15** 1281 (2015)
102. Y Negishi, K Munakata, W Ohgake, K Nobusada *J. Phys. Chem. Lett.* **3** 2209 (2012)
103. C Kumara, C M Aikens, A Dass *J. Phys. Chem. Lett.* **5** 461 (2014)
104. H Yang, Y Wang, H Huang, L Gell, L Lehtovaara, S Malola, H Häkkinen, N Zheng *Nat. Commun.* **4** Art. No. 2422 (2013)
105. H Yang, Y Wang, J Lei, L Shi, X Wu, V Mäkinen, S Lin, Z Tang, J He, H Häkkinen, L Zheng, N Zheng *J. Am. Chem. Soc.* **135** 9568 (2013)
106. H Yang, Y Wang, J Yan, X Chen, X Zhang, H Häkkinen, N Zheng *J. Am. Chem. Soc.* **136** 7197 (2014)
107. H Häkkinen *Chem. Soc. Rev.* **37** 1847 (2008)
108. K Clemenger *Phys. Rev. B* **32** 1359 (1985)
109. J Turkevich *Gold Bull.* **18** 125 (1985)
110. R J Bau *J. Am. Chem. Soc.* **120** 9380 (1998)
111. R Jin, H Qian, Z Wu, Y Zhu, M Zhu, A Mohanty, N Garg *J. Phys. Chem. Lett.* **1** 2903 (2010)
112. C Liu, G Li, G Pang, R Jin *RSC Adv.* **3** 9778 (2013)
113. Y Negishi, K Nobusada, T Tsukuda *J. Am. Chem. Soc.* **127** 5261 (2005)
114. Yong Yu, Z Luo, Yue Yu, J Y Lee, J Xie *ACS Nano* **6** 7920 (2012)
115. Yong Yu, X Chen, Q Yao, Yue Yu, N Yan, J Xie *Chem. Mater.* **25** 946 (2013)
116. G H Woehrle, L O Brown, J E Hutchison *J. Am. Chem. Soc.* **127** 2172 (2005)
117. D Stellwagen, A Weber, G L Bovenkamp, R Jin, J H Bitter, C S S R Kumar *RSC Adv.* **2** 2276 (2012)
118. H Qian, Y Zhu, R Jin *ACS Nano* **3** 3795 (2009)
119. Q Yao, Yong Yu, X Yuan, Yue Yu, J Xie, J Y Lee *Small* **9** 2696 (2013)
120. X Yuan, Y Yu, Q Yao, Q Zhang, J Xie *J. Phys. Chem. Lett.* **3** 2310 (2012)
121. Z Wu, M A MacDonald, J Chen, P Zhang, R Jin *J. Am. Chem. Soc.* **133** 9670 (2011)
122. J W A van der Velden, F A Vollenbroek, J J Bour, P T Beurskens, J M M Smits, W P Bosnian *Recl. Trav. Chim. Pays-Bas (J.R. Neth. Chem. Soc.)* **100** 148 (1981)
123. G Schmid, N Klein, L Korste, U Kreibig, D Schönauer *Polyhedron* **7** 605 (1988)
124. G Schmid, R Pugin, W Meyer-Zaika, U Simon *Eur. J. Inorg. Chem.* 2051 (1999)
125. G Schmid, R Pugin, J-O Malm, J -O Bovin *Eur. J. Inorg. Chem.* 813 (1998)
126. J W Hudgens, J M Pettibone, T P Senftle, R N Bratton *Inorg. Chem.* **50** 10178 (2011)
127. R L Whetten, J T Khoury, M M Alvarez, S Murthy, I Vezmar, Z L Wang, P W Stephens, C L Cleveland, W D Luedtke, U Landman *Adv. Mater.* **8** 428 (1996)
128. Y Yanagimoto, Y Negishi, H Fujihara, T Tsukuda *J. Phys. Chem. B* **110** 11611 (2006)
129. Ren Jin, C Liu, S Zhao, A Das, H Xing, C Gayathri, Y Xing, N L Rosi, R R Gil, Ron Jin *ACS Nano* **9** 8530 (2015)
130. E S Shibu, T Pradeep *Chem. Mater.* **23** 989 (2011)
131. A Mathew, G Natarajan, L Lehtovaara, H Häkkinen, R M Kumar, V Subramanian, A Jaleel, T Pradeep *ACS Nano* **8** 139 (2014)
132. J P Hermes, F Sander, T Peterle, R Urbani, T Pfohl, D Thompson, M Mayor *Chem. – Eur. J.* **17** 13473 (2011)
133. J Hassinen, P Pulkkinen, E Kalenius, T Pradeep, H Tenhu, H Häkkinen, R H A Ras *J. Phys. Chem. Lett.* **5** 585 (2014)
134. D Thompson, J P Hermes, A J Quinn, M Mayor *ACS Nano* **6** 3007 (2012)
135. J Z Sexton, C J Ackerson *J. Phys. Chem. C* **114** 16037 (2010)
136. J Xie, Y Zheng, J Y Ying *J. Am. Chem. Soc.* **131** 888 (2009)
137. A Baksi, P Lourdu Xavier, K Chaudhari, N Goswami, S K Pal, T Pradeep *Nanoscale* **5** 2009 (2013)
138. A Baksi, T Pradeep, B Yoon, C Yannouleas, U Landman *ChemPhysChem* **14** 1272 (2013)
139. Z Li, C V Ciobanu, J Hu, J-P Palomares-Báez, J-L Rodríguez-López, R Richards *Phys. Chem. Chem. Phys.* **13** 2582 (2011)
140. C Zhang, A Michaelides, S J Jenkins *Phys. Chem. Chem. Phys.* **13** 22 (2011)
141. J Li, X Li, H-J Zhai, L-S Wang *Science* **299** 864 (2003)
142. S N Lanin, D A Pichugina, A F Shestakov, V V Smirnov, S A Nikolaev, K S Lanina, A Yu Vasil'kov, Fam Tien Zung, A V Beletskaya *Russ. J. Phys. Chem. A* **84** 2133 (2010) [*Zh. Fiz. Khim.* **84** 2330 (2010)]
143. D F Mukhamedzyanova, N K Ratmanova, D A Pichugina, N E Kuz'menko *J. Phys. Chem. C* **116** 11507 (2012)
144. D A Pichugina, S A Nikolaev, D F Mukhamedzyanova, N E Kuz'menko *Russ. J. Phys. Chem. A* **88** 959 (2014) [*Zh. Fiz. Khim.* **88** 991 (2014)]
145. S A Nikolaev, D A Pichugina, D F Mukhamedzyanova *Gold Bull.* **45** 221 (2012)
146. D A Pichugina, S N Lanin, N V Kovaleva, K S Lanina, A F Shestakov, N E Kuz'menko *Russ. Chem. Bull., Int. Ed.* **59** 2039 (2010) [*Izv. Akad. Nauk, Ser. Khim.* 1987 (2010)]
147. E V Golubina, D A Pichugina, A G Majouga, S A Aytekenov *Stud. Surf. Sci. Catal.* **175** 297 (2010)
148. S Chrétien, S K Buratto, H Metiu *Curr. Opin. Solid State Mater. Sci.* **11** 62 (2007)
149. T Udayabhaskararao, T Pradeep *J. Phys. Chem. Lett.* **4** 1553 (2013)
150. P Zhang *J. Phys. Chem. C* **118** 25291 (2014)
151. T G Schaaff, G Knight, M N Shafigullin, R F Borkman, R L Whetten *J. Phys. Chem. B* **102** 10643 (1998)
152. M Farrag, M Tschurl, A Dass, U Heiz *Phys. Chem. Chem. Phys.* **15** 12539 (2013)
153. S Knoppe, M Vanbel, S van Cleuvenbergen, L Vanpraet, T Bürgi, T Verbiest *J. Phys. Chem. C,* **119** 6221 (2015)
154. Z Wu, C Gayathri, R R Gil, R Jin *J. Am. Chem. Soc.* **131** 6535 (2009)
155. Z Liu, M Zhu, X Meng, G Xu, R Jin *J. Phys. Chem. Lett.* **2** 2104 (2011)
156. C L Cleveland, U Landman, T G Schaaff, M N Shafigullin, P W Stephens, R L Whetten *Phys. Rev. Lett.* **79** 1873 (1997)

157. J C Love, L A Estroff, J K Kriebel, R G Nuzzo, G M Whitesides *Chem. Rev.* **105** 1103 (2005)
158. C Vericat, M E Vela, R C Salvarezza *Phys. Chem. Chem. Phys.* **7** 3258 (2005)
159. N Shao, Y Pei, Y Gao, X C Zeng *J. Phys. Chem. A* **113** 629 (2009)
160. D-e Jiang, R L Whetten, W Luo, S Dai *J. Phys. Chem. C* **113** 17291 (2009)
161. D-e Jiang, S H Overbury, S Dai *J. Am. Chem. Soc.* **135** 8786 (2013)
162. A Tlahuice-Flores, M Jose-Yacamán, R L Whetten *Phys. Chem. Chem. Phys.* **15** 19557 (2013)
163. A Tlahuice, I L Garzón *Phys. Chem. Chem. Phys.* **14** 3737 (2012)
164. H Qian, Y Zhu, R Jin *J. Am. Chem. Soc.* **132** 4583 (2010)
165. D-e Jiang, M Walter, J Akola *J. Phys. Chem. C* **114** 15883 (2010)
166. P R Nimmala, B Yoon, R L Whetten, U Landman, A Dass *J. Phys. Chem. A* **117** 504 (2013)
167. A Tlahuice-Flores, U Santiago, D Bahena, E Vinogradova, C V Conroy, T Ahuja, S B H Bach, A Ponce, G Wang, M José-Yacamán, R L Whetten *J. Phys. Chem. A* **117** 10470 (2013)
168. X-G Xiong, W-H Xu, J Li, P Pyykkö *Int. J. Mass Spectrom.* **354 – 355** 15 (2013)
169. J A Hansen, P Piecuch, B G Levine *J. Chem. Phys.* **139** 091101 (2013)
170. K Balasubramanian, D-W Liao *J. Chem. Phys.* **94** 5233 (1991)
171. K G Dyall *J. Chem. Phys.* **100** 2118 (1994)
172. P J Hay, W R Wadt *J. Chem. Phys.* **82** 270 (1985)
173. B Assadollahzadeh, P Schwerdtfeger *J. Chem. Phys.* **131** 064306 (2009)
174. F Muniz-Miranda, M C Menziani, A Pedone *J. Phys. Chem. C* **118** 7532 (2014)
175. B S Gutrath, U Englert, Y Wang, U Simon *Eur. J. Inorg. Chem.* 2002 (2013)
176. B Chan, W-L Yim *J. Chem. Theory Comput.* **9** 1964 (2013)
177. D Mollenhauer, N Gaston *J. Comput. Chem.* **35** 986 (2014)
178. S Grimme, J Antony, S Ehrlich, H Krieg *J. Chem. Phys.* **132** 154104 (2010)
179. S Moncho, E N Brothers, B G Janesko *J. Phys. Chem. C* **117** 7487 (2013)
180. S A Ivanov, I Arachchige, C M Aikens *J. Phys. Chem. A* **115** 8017 (2011)
181. M Dubecký, R Derian, P Jurečka, L Mitas, P Hobza, M Otyepka *Phys. Chem. Chem. Phys.* **16** 20915 (2014)
182. T T Järvi, A C T van Duin, K Nordlund, W A Goddard III *J. Phys. Chem. A* **115** 10315 (2011)
183. G-T Bae, C M Aikens *J. Phys. Chem. A* **117** 10438 (2013)
184. S Banerjee, J A Montgomery Jr, J A Gascón *J. Mater. Sci.* **47** 7686 (2012)
185. S M Reilly, T Krick, A Dass *J. Phys. Chem. C* **114** 741 (2010)
186. R Hamouda, F Bertorelle, D Rayane, R Antoine, M Broyer, P Dugourd *Int. J. Mass Spectrom.* **335** 1 (2013)
187. A Tlahuice, I L Garzón *Phys. Chem. Chem. Phys.* **14** 7321 (2012)
188. D M Chevrier, M A MacDonald, A Chatt, P Zhang, Z Wu, R Jin *J. Phys. Chem. C* **116** 25137 (2012)
189. M Zhu, H Qian, R Jin *J. Phys. Chem. Lett.* **1** 1003 (2010)
190. Y Pei, R Pal, C Liu, Y Gao, Z Zhang, X C Zeng *J. Am. Chem. Soc.* **134** 3015 (2012)
191. M R Wiseman, P A Marsh, P T Bishop, B J Brisdon, M F Mahon *J. Am. Chem. Soc.* **122** 12598 (2000)
192. J Akola, M Walter, R L Whetten, H Häkkinen, H Grönbeck *J. Am. Chem. Soc.* **130** 3756 (2008)
193. A Tlahuice-Flores, R L Whetten, M Jose-Yacamán *J. Phys. Chem. C* **117** 20867 (2013)
194. Y Negishi, N K Chaki, Y Shichibu, R L Whetten, T Tsukuda *J. Am. Chem. Soc.* **129** 11322 (2007)
195. M A Tofanelli, C J Ackerson *J. Am. Chem. Soc.* **134** 16937 (2012)
196. S Antonello, N V Perera, M Ruzzi, J A Gascón, F Maran *J. Am. Chem. Soc.* **135** 15585 (2013)
197. M Dijksma, B Kamp, J C Hoogvliet, W P van Bennekom *Langmuir* **16** 3852 (2000)
198. R L Donkers, D Lee, R W Murray *Langmuir* **20** 1945 (2004)
199. P R Nimmala, V R Jupally, A Dass *Langmuir* **30** 2490 (2014)
200. L Garzón, C Rovira, K Michaelian, M R Beltran, P Ordejórn, J Junquera, D Sánchez-Portal, E Artacho, J M Soler *Phys. Rev. Lett.* **85** 5250 (2000)
201. D-e Jiang, M L Tiago, W Luo, S Dai *J. Am. Chem. Soc.* **130** 2777 (2008)
202. S Knoppe, I Dolamic, T Bürgi *J. Am. Chem. Soc.* **134** 13114 (2012)
203. S Knoppe, S Michalet, T Bürgi *J. Phys. Chem. C* **117** 15354 (2013)
204. S Malola, L Lehtovaara, S Knoppe, K-J Hu, R E Palmer, T Bürgi, H Häkkinen *J. Am. Chem. Soc.* **134** 19560 (2012)
205. R C Price, R L Whetten *J. Am. Chem. Soc.* **127** 13750 (2005)
206. Y Pei, S Lin, J Su, C Liu *J. Am. Chem. Soc.* **135** 19060 (2013)
207. Y Gao, N Shao, X C Zeng *ACS Nano* **2** 1497 (2008)
208. Y Li, G Galli, F Gygi *ACS Nano* **2** 1896 (2008)
209. Y-K Han, H Kim, J Jung, Y C Choi *J. Phys. Chem. C* **114** 7548 (2010)
210. D Schooss, P Weis, O Hampe, M M Kappes *Philos. Trans. R. Soc. London, Ser. A* **368** 1211 (2010)
211. C L Heinecke, T W Ni, S Malola, V Mäkinen, O A Wong, H Häkkinen, C J Ackerson *J. Am. Chem. Soc.* **134** 13316 (2012)
212. Z Tang, D A Robinson, N Bokossa, B Xu, S Wang, G Wang *J. Am. Chem. Soc.* **133** 16037 (2011)
213. V R Jupally, A Dass *Phys. Chem. Chem. Phys.* **16** 10473 (2014)
214. H Qian, R Jin *Nano Lett.* **9** 4083 (2009)
215. H Qian, R Jin *Chem. Mater.* **23** 2209 (2011)
216. O Lopez-Acevedo, J Akola, R L Whetten, H Grönbeck, H Häkkinen *J. Phys. Chem. C* **113** 5035 (2009)
217. J Koivisto, K Salorinne, S Mustalahti, T Lahtinen, S Malola, H Häkkinen, M Pettersson *J. Phys. Chem. Lett.* **5** 387 (2014)
218. S Mustalahti, P Myllyperkiö, T Lahtinen, K Salorinne, S Malola, J Koivisto, H Häkkinen, M Pettersson *J. Phys. Chem. C* **118** 18233 (2014)
219. E Heikkilä, A A Gurtovenko, H Martinez-Seara, H Häkkinen, I Vattulainen, J Akola *J. Phys. Chem. C* **116** 9805 (2012)
220. A A Bagatur'yants, A A Safonov, H Stool, H-J Werner *J. Chem. Phys.* **109** 3096 (1998)
221. D A Pichugina, A F Shestakov, N E Kuz'menko *Russ. J. Phys. Chem. A* **81** 883 (2007) [*Zh. Fiz. Khim.* **81** 1015 (2007)]
222. C Vericat, M E Vela, G A Benitez, J A Martin Gago, X Torrelles, R C Salvarezza *J. Phys.: Condens. Matter* **18** R867 (2006)
223. F Ma, R B Lennox *Langmuir* **16** 6188 (2000)
224. L Zhang, W A Goddard III, S Jiang *J. Chem. Phys.* **117** 7342 (2002)
225. G Poirier *Chem. Rev.* **97** 1117 (1997)
226. C Masens, M J Ford, M Cortie *Surf. Sci.* **580** 19 (2005)
227. Ya A Elfimova, D A Pichugina, I A Anan'eva, A G Mazhuga, O A Shpigun *Russ. J. Phys. Chem. A* **86** 1623 (2012) [*Zh. Fiz. Khim.* **86** 1739 (2012)]
228. A Majouga, D Pichugina, I Ananieva, S Kurilova, O Shpigun, N Kuz'menko, N Zyk *J. Manufact. Technol. Manag.* **21** 950 (2010)
229. P Maksymovych, D C Sorescu, J T Yates Jr *J. Phys. Chem. B* **110** 21161 (2006)

230. P Maksymovych, D C Sorescu, J T Yates Jr *Phys. Rev. Lett.* **97** 146103 (2006)
231. G Rajaraman, A Caneschi, D Gatteschi, F Totti *Phys. Chem. Chem. Phys.* **13** 3886 (2011)
232. D P Woodruff *Phys. Chem. Chem. Phys.* **10** 7211 (2008)
233. H Grönbeck, H Häkkinen, R L Whetten *J. Phys. Chem. C* **112** 15940 (2008)
234. R Mazzarello, A Cossaro, A Verdini, R Rousseau, L Casalis, M F Danisman, L Floreano, S Scandolo, A Morgante, G Scoles *Phys. Rev. Lett.* **98** 016102 (2007)
235. E Pensa, E Cortés, G Corthey, P Carro, C Vericat, M H Fonticelli, G Benítez, A A Rubert, R C Salvarezza *Acc. Chem. Res.* **45** 1183 (2012)
236. A Cossaro, R Mazzarello, R Rousseau, L Casalis, A Verdini, A Kohlmeyer, L Floreano, S Scandolo, A Morgante, M L Klein, G Scoles *Science* **321** 943 (2008)
237. B M Barngrover, C M Aikens *J. Phys. Chem. Lett.* **2** 990 (2011)
238. B M Barngrover, C M Aikens *J. Phys. Chem. A* **117** 5377 (2013)
239. I Chakraborty, W Kurashige, K Kanehira, L Gell, H Häkkinen, Y Negishi, T Pradeep *J. Phys. Chem. Lett.* **4** 3351 (2013)
240. W Kurashige, S Yamazoe, M Yamaguchi, K Nishido, K Nobusada, T Tsukuda, Y Negishi *J. Phys. Chem. Lett.* **5** 2072 (2014)
241. H Zhang, P Yin, T You, T Sun, X Lang, E Tan, X Liang, L Guo *Spectrochim. Acta, Part A: Mol. Biomol. Spectrosc.* **134** 96 (2015)
242. D M P Mingos *Chem. Soc. Rev.* **15** 31 (1986)
243. S Goel, K A Velizhanin, A Piryatinski, S Tretiak, S A Ivanov *J. Phys. Chem. Lett.* **1** 927 (2010)
244. N Kobayashi, Y Kamei, Y Shichibu, K Konishi *J. Am. Chem. Soc.* **135** 16078 (2013)
245. W Bos, R P F Kanters, C J van Halen, W P Bosman, H Behm, J M M Smits, P T Beurskens, J J Bour, L H Pignolet *J. Organomet. Chem.* **307** 385 (1986)
246. B Fresch, E Hanozin, F Dufour, F Remacle *Eur. Phys. J. D* **66** 326 (2012)
247. Y Shichibu, K Konishi *Small* **6** 1216 (2010)
248. Y Yuan, L Cheng, J Yang *J. Phys. Chem. C* **117** 13276 (2013)
249. S Knoppe, L Lehtovaara, H Häkkinen *J. Phys. Chem. A* **118** 4214 (2014)
250. H-F Zhang, M Stender, R Zhang, C Wang, J Li, L-S Wang *J. Phys. Chem. B* **108** 12259 (2004)
251. J-Q Goh, S Malola, H Häkkinen, J Akola *J. Phys. Chem. C* **117** 22079 (2013)
252. T Iwasa, K Nobusada, A Nakajima *J. Phys. Chem. C* **117** 24586 (2013)
253. D H Rapoport, W Vogel, H Cölfen, R Schlögl *J. Phys. Chem. V* **101** 4175 (1997)
254. W W Weare, S M Reed, M G Warner, J E Hutchison *J. Am. Chem. Soc.* **122** 12890 (2000)
255. R Sharma, G P Holland, V C Solomon, H Zimmermann, S Schiffenhaus, S A Amin, D A Buttry, J L Yarger *J. Phys. Chem. C* **113** 16387 (2009)
256. J P Fackler Jr, C J McNeal, L H Pignolet, R E P Winpenny *J. Am. Chem. Soc.* **111** 6434 (1989)
257. W Chen, S Chen *Angew. Chem., Int. Ed.* **48** 4386 (2009)
258. Y Pei, N Shao, Y Gao, X C Zeng *ACS Nano* **4** 2009 (2010)
259. A Genest, S Krüger, N Rösch *Z. Naturforsch., B* **64** 1246 (2009)
260. G Periyasamy, F Remacle *Nano Lett.* **9** 3007 (2009)
261. M Walter, M Moseler, R L Whetten, H Häkkinen *Chem. Sci.* **2** 1583 (2011)
262. D-e Jiang, S Dai *Inorg. Chem.* **48** 2720 (2009)
263. C A Fields-Zinna, M C Crowe, A Dass, J E F Weaver, R W Murray *Langmuir* **25** 7704 (2009)
264. Y Niihori, M Matsuzaki, T Pradeep, Y Negishi *J. Am. Chem. Soc.* **135** 4946 (2013)
265. Y Negishi, W Kurashige, Y Kobayashi, S Yamazoe, N Kojima, M Seto, T Tsukuda *J. Phys. Chem. Lett.* **4** 3579 (2013)
266. M Walter, M Moseler *J. Phys. Chem. C* **113** 15834 (2009)
267. O G Ellert, M V Tsodikov, S A Nikolaev, V M Novotortsev *Russ. Chem. Rev.* **83** 718 (2014)
268. L H Pignolet, M A Aubart, K L Craighead, R A T Gould, D A Krogstad, J S Wiley *Coord. Chem. Rev.* **143** 219 (1995)
269. H Qian, D-e Jiang, G Li, C Gayathri, A Das, R R Gil, R Jin *J. Am. Chem. Soc.* **134** 16159 (2012)
270. S L Christensen, M A MacDonald, A Chatt, P Zhang, H Qian, R Jin *J. Phys. Chem. C* **116** 26932 (2012)
271. N de Silva, L F Dahl *Inorg. Chem.* **44** 9604 (2005)
272. Y Negishi, T Iwai, M Ide *Chem. Commun.* **46** 4713 (2010)
273. E Gottlieb, H Qian, R Jin *Chem. – Eur. J.* **19** 4238 (2013)
274. S Wang, X Meng, A Das, T Li, Y Song, T Cao, X Zhu, M Zhu, R Jin *Angew. Chem., Int. Ed.* **53** 2376 (2014)
275. E B Guidez, V Mäkinen, H Häkkinen, C M Aikens *J. Phys. Chem. C* **116** 20617 (2012)
276. S Malola, L Lehtovaara, H Häkkinen *J. Phys. Chem. C* **118** 20002 (2014)
277. A Tlahuice-Flores *J. Nanopart. Res.* **15** 1771 (2013)
278. T Udayabhaskararao, Y Sun, N Goswami, S K Pal, K Balasubramanian, T Pradeep *Angew. Chem., Int. Ed.* **51** 2155 (2012)
279. A Tlahuice-Flores *Phys. Chem. Chem. Phys.* **16** 18083 (2014)
280. T G Schaaff, M N Shafigullin, J T Khoury, I Vezmar, R L Whetten, W G Cullen, P N First, C Gutiérrez-Wing, J Ascensio, M J Jose-Yacamán *J. Phys. Chem. B* **101** 7885 (1997)
281. H-Ch Weissker, H Barron Escobar, V D Thanthirige, K Kwak, D Lee, G Ramakrishna, R L Whetten, X López-Lozano *Nat. Commun.* **5** Art. No. 3785 (2014)
282. A Dass *J. Am. Chem. Soc.* **133** 19259 (2011)
283. L Shang, F Stockmar, N Azadfar, G U Nienhaus *Angew. Chem., Int. Ed.* **52** 11154 (2013)
284. Y Liu, X Han, L He, Y Yin *Angew. Chem., Int. Ed.* **51** 6373 (2012)
285. L Zhang, E Wang *Nano Today* **9** 132 (2014)
286. C M Aikens *J. Phys. Chem. Lett.* **2** 99 (2011)
287. I Russier-Antoine, F Bertorelle, M Vojkovic, D Rayane, E Salmon, C Jonin, P Dugourd, R Antoine, P-F Brevet *Nanoscale* **6** 13572 (2014)
288. J Akola, K A Kacprzak, O Lopez-Acevedo, M Walter, H Grönbeck, H Häkkinen *J. Phys. Chem. C* **114** 15986 (2010)
289. N Pazos-Perez, C S Wagner, J M Romo-Herrera, L M Liz-Marzán, F J García de Abajo, A Wittemann, A Fery, R A Alvarez-Puebla *Angew. Chem., Int. Ed.* **51** 12688 (2012)
290. S Knoppe, T Bürgi *Acc. Chem. Res.* **47** 1318 (2014)
291. D-e Jiang, M Kühn, Q Tang, F Weigend *J. Phys. Chem. Lett.* **5** 3286 (2014)
292. Z Wu, R Jin *Nano Lett.* **10** 2568 (2010)
293. M Wang, Z Wu, J Yang, G Wang, H Wang, W Cai *Nanoscale* **4** 4087 (2012)
294. Z Wu, M Wang, J Yang, X Zheng, W Cai, G Meng, H Qian, H Wang, R Jin *Small* **8** 2028 (2012)
295. Z Luo, X Yuan, Y Yu, Q Zhang, D T Leong, J Y Lee, J Xie *J. Am. Chem. Soc.* **134** 16662 (2012)
296. I O Koshevoy, Y-C Lin, A J Karttunen, P-T Chou, P Vainiotalo, S P Tunik, M Haukka, T A Pakkanen *Inorg. Chem.* **48** 2094 (2009)
297. I Sakanaga, M Inada, T Saitoh, H Kawasaki, Y Iwasaki, T Yamada, I Umezu, A Sugimura *Appl. Phys. Express* **4** 095001 (2011)
298. T Huang, R W Murray *J. Phys. Chem. B* **105** 12498 (2001)

299. Y Yu, Z Luo, D M Chevrier, D T Leong, P Zhang, D-e Jiang, J Xie *J. Am. Chem. Soc.* **136** 1246 (2014)
300. L H Gade *Angew. Chem., Int. Ed. Engl.* **36** 1171 (1997)
301. X He, V W-W Yam *Coord. Chem. Rev.* **255** 2111 (2011)
302. V W-W Yam, K M-C Wong *Chem. Commun.* **47** 11579 (2011)
303. C-M Che, S-W Lai, in *Gold Chemistry: Applications and Future Directions in the Life Sciences* (Ed. F Mohr) (Weinheim: Wiley, 2009) p. 249
304. M C Gimeno, A Laguna *Chem. Soc. Rev.* **37** 1952 (2008)
305. R Jin *Nanoscale* **2** 343 (2010)
306. C-Y Ke, T-H Chen, L-C Lu, W-L Tseng *RSC Adv.* **4** 26050 (2014)
307. E S Shibu, B Radha, P K Verma, P Bhyrappa, G U Kulkarni, S K Pal, T Pradeep *ACS Appl. Mater. Interfaces* **1** 2199 (2009)
308. C-A J Lin, T-Y Yang, C-H Lee, S H Huang, R A Sperling, M Zanella, J K Li, J-L Shen, H-H Wang, H-I Yeh, W J Parak, W H Chang *ACS Nano* **3** 395 (2009)
309. M A H Muhammed, P K Verma, S K Pal, R C A Kumar, S Paul, R V Omkumar, T Pradeep *Chem. – Eur. J.* **15** 10110 (2009)
310. M A H Muhammed, P K Verma, S K Pal, A Retnakumari, M Koyakutty, S Nair, T Pradeep *Chem. – Eur. J.* **16** 10103 (2010)
311. Y Negishi, H Tsunoyama, M Suzuki, N Kawamura, M M Matsushita, K Maruyama, T Sugawara, T Yokoyama, T Tsukuda *J. Am. Chem. Soc.* **128** 12034 (2006)
312. M Zhu, C M Aikens, M P Hendrich, R Gupta, H Qian, G C Schatz, R Jin *J. Am. Chem. Soc.* **131** 2490 (2009)
313. K S Krishna, P Tarakeshwar, V Mujica, C S S R Kumar *Small* **10** 907 (2014)
314. T G Schaaff, R L Whetten *J. Phys. Chem. B* **104** 2630 (2000)
315. H Yao, K Miki, N Nishida, A Sasaki, K Kimura *J. Am. Chem. Soc.* **127** 15536 (2005)
316. C Gautier, T Bürgi *J. Am. Chem. Soc.***128** 11079 (2006)
317. A Sánchez-Castillo, C Noguez, I L Garzón *J. Am. Chem. Soc.* **132** 1504 (2010)
318. A I Kozlov, A P Kozlova, H Liu, Y Iwasawa *Appl. Catal., A: Gen.* **182** 9 (1999)
319. J Kilmartin, R Sarip, R Grau-Crespo, D D Tommaso, G Hogarth, C Prestipino, G Sankar *ACS Catal.* **2** 957 (2012)
320. C C Chusuei, X Lai, K A Davis, E K Bowers, J P Fackler, D W Goodman *Langmuir* **17** 4113 (2001)
321. X Nie, H Qian, Q Ge, H Xu, R Jin *ACS Nano* **6** 6014 (2012)
322. X Nie, C Zeng, X Ma, H Qian, Q Ge, H Xu, R Jin *Nanoscale* **5** 5912 (2013)
323. Y Liu, H Tsunoyama, T Akita, S Xie, T Tsukuda *ACS Catal.* **1** 2 (2011)
324. S Xie, H Tsunoyama, W Kurashige, Y Negishi, T Tsukuda *ACS Catal.* **2** 1519 (2012)
325. Y Zhu, H Qian, M Zhu, R Jin *Adv. Mater.* **22** 1915 (2010)
326. J Liu, K S Krishna, Y B Losovyj, S Chattopadhyay, N Lozova, J T Miller, J J Spivey, C S S R Kumar *Chem. – Eur. J.* **19** 10201 (2013)
327. Y Zhu, H Qian, R Jin *Chem. – Eur. J.* **16** 11455 (2010)
328. Y Liu, H Tsunoyama, T Akita, T Tsukuda *Chem. Commun.* **46** 550 (2010)
329. M Turner, V B Golovko, O P H Vaughan, P Abdulkin, A Berenguer-Murcia, M S Tikhov, B F G Johnson, R M Lambert *Nature (London)* **454** 981 (2008)
330. C Lavenn, A Demessence, A Tuel *Catal. Today* **235** 72 (2014)
331. G Li, H Qian, R Jin *Nanoscale* **4** 6714 (2012)
332. Y Lu, Y Jiang, X Gao, W Chen *Chem. Commun.* **50** 8464 (2014)
333. G Li, R Jin *J. Am. Chem. Soc.* **136** 11347 (2014)
334. Y Zhu, H Qian, B A Drake, R Jin *Angew. Chem., Int. Ed.* **49** 1295 (2010)
335. H Yamamoto, H Yano, H Kouchi, Y Obora, R Arakawa, H Kawasaki *Nanoscale* **4** 4148 (2012)
336. A Shivhare, S J Ambrose, H Zhang, R W Purves, R W J Scott *Chem. Commun.* **49** 276 (2013)
337. G Li, C Liu, Y Lei, R Jin *Chem. Commun.* **48** 12005 (2012)
338. G Li, D-e Jiang, C Liu, C Yu, R Jin *J. Catal.* **306** 177 (2013)
339. M Zhu, W T Eckenhoff, T Pintauer, R Jin *J. Phys. Chem. C* **112** 14221 (2008)
340. D P Anderson, J F Alvino, A Gentleman, H Al Qahtani, L Thomsen, M I J Polson, G F Metha, V B Golovko, G G Andersson *Phys. Chem. Chem. Phys.* **15** 3917 (2013)
341. D R Kauffman, D Alfonso, C Matranga, G Li, R Jin *J. Phys. Chem. Lett.* **4** 195 (2013)
342. S Yu, Q Zeng, Z Lou, M Yang, D Wu *Phys. Chem. Chem. Phys.* **15** 9742 (2013)
343. S Lin, Y Pei *J. Phys. Chem. C* **118** 20346 (2014)
344. S A Nikolaev, V V Smirnov, A Yu Vasil'kov, V L Podshibikhin *Kinet. Catal.* **51** 375 (2010) [*Kinet. Katal.* **51** 396 (2010)]
345. S A Nikolaev, N A Permyakov, V V Smirnov, A Yu Vasil'kov, S N Lanin *Kinet. Catal.* **51** 288 (2010) [*Kinet. Katal.* **51** 305 (2010)]